The Thesis Committee for Amroo Essam Mukhliss
Certifies that this is the approved version of the following thesis:

Simulation of Inorganic Scales Using UTCHEM Reservoir Simulator

APPROVED BY
SUPERVISING COMMITTEE:

Supervisor:

Kamy Sepehrnoori

Co-Supervisor:

Paul Bommer

Simulation of Inorganic Scales Using UTCHEM Reservoir Simulator

by

Amroo Essam Mukhliss, B.S. Petro. E.

Thesis

Presented to the Faculty of the Graduate School of

The University of Texas at Austin

in Partial Fulfillment

of the Requirements

for the Degree of

Master of Science in Engineering

The University of Texas at Austin

August 2011

Dedicated to my parents,

my wife

and our kids Layan and Abdullah

Acknowledgments

I would like to express my appreciation to my supervisors, Dr. Kamy Sepehrnoori and Dr. Paul Bommer for guiding me throughout this thesis. Their knowledge and expertise have inspired and enriched this work. I also would like to extend my appreciation to my colleague Mahdy Shirdel for his help in setting up some of the cases presented in this study. This work depended heavily on the UTCHEM simulator at the Center for Petroleum and Geosystems Engineering of The University of Texas at Austin.

I want to thank Saudi Aramco for giving me the opportunity to pursue my Master's degree in this particular field. And finally, I wish to thank my wife and parents for their encouragement and patience.

Abstract

Simulation of Inorganic Scales Using UTCHEM Reservoir Simulator

Amroo Essam Mukhliss, M.S.E.

The University of Texas at Austin, 2011

Supervisors: Kamy Sepehrnoori and Paul Bommer

Scale deposition, either in the formation or inside the tubing, is a serious problem that can affect the productivity of oil fields. Production sustainability depends on the successful implementation of scale management strategies prior to developing new fields. Such strategies should involve tools capable of addressing the risks of developing scales during the production stage as well as determining the outcomes of possible remediation jobs in the future. UTCHEM, a multi-compositional flow model, was used in this work to present a comprehensive study that includes both precipitation and remediation scenarios.

Although there are different mechanisms prompting the deposition of mineral scales, barite and calcite were selected primarily to simulate the effect of mixing incompatible water compositions; an issue that is usually associated with seawater injection. Equilibrium state calculations were carried out using a geochemical model

(EQBATCH) to verify the incompatibility of the injection water with the formation water.

In this work, we show the evolution, distribution, and remediation of solids over time for several hypothetical cases. The quantity of deposits in the near-wellbore region was found to be less at a highly heterogeneous reservoir model in contrast to the amount precipitated in homogenous reservoirs. This could be critical to wells productivity in the long-run since much of the drop in reservoir pressure occurs near the wellbore. The predictive ability of UTCHEM was extended to include simulating the removal of carbonate scales using a chelating chemical. The optimization of the injected treatment can be achieved mechanically through adjusting the well spacing (during the initial stages of field development) or through adjusting the concentrations of active components in the remediation fluids.

The model provides a valuable tool that helps planners to predict scaling-related issues ahead of time, and subsequently to determine the economic viability of the project. This work serves as an opportunity to re-assess this simulator and allows for further work to enhance its capabilities.

TABLE OF CONTENTS

Acknowledgments ..... **v**

Abstract ..... **vi**

Table of Contents ..... **viii**

List of Tables ..... **xi**

List of Figures ..... **xiii**

Chapter 1: Introduction **1**

Chapter 2: Literature Survey **4**

2.1 The Formation of Scales 4

2.1.1 The Process of Nucleation 5

2.2 Formation Mechanisms 6

2.2.1 Carbonate Scales 6

2.2.2 Sulfate Scales 6

2.2.3 Iron Sulfide Scales 7

2.2.4 Iron Oxide Scales 8

2.3 Scale Inhibition 9

2.3.1 Crystal Growth Retarders 10

2.3.1.1 Effect of pH 11

2.3.1.2 Effect of Temperature 11

2.3.1.3 Effect of Calcium and Magnesium 12

2.3.2 Nucleation Retarders 14

2.3.2.1 Effect of pH 14

2.3.2.2 Effect of Temperature 14

2.3.2.3 Effect of Calcium and Magnesium 15

2.4 The Performance of Scale Inhibitors at HP/HT 15

2.5 Scale Inhibition Placement 19
2.5.1 Placement by the Squeeze Technique.....19
2.5.2 Pumping the Inhibitor with the Stimulation 21
2.5.3 Pumping the Inhibitor with Fracturing Fluid.....23
2.5.4 Inhibitor Impregnated into Proppant 24
2.6 The Effect of Adding Hydrate Inhibitors to SI Efficiency 24

Chapter 3: Description of UTCHEM.....27
3.1 Assumptions.....27
3.2 Flow Equations 29
3.3 EQBATCH Description 31
3.4 Equilibrium Equations 31
3.5 Example of Equilibrium Calculations 33

Chapter 4: Precipitation Simulation Runs 38
4.1 Quarter 5-Spot Model Including One Injector and One Producer with Only $BaSO_4$ Being Precipitated.....38
4.2 Quarter 5-Spot Model Including One Injector and One Producer with Both $CaCO_3$ and $BaSO_4$ Being Precipitated 41
4.3 Quarter 5-Spot Model Including One Injector and One Producer with ($CaCO_3$, $BaSO_4$, FeS) Being Precipitated 42
4.4 5-Spot Homogeneous Model (1 Producer + 4 Injectors) with Only $BaSO_4$ Being Precipitated 44
4.5 5-Spot Heterogeneous Model (1 Producer + 4 Injectors) with Only $BaSO_4$ Being Precipitated 46

Chapter 5: Remediation Simulation Runs.....85
5.1 Description of EDTA Reaction with Calcite 85
5.2 Simulating Calcite Remediation with EDTA Using Quarter 5-Spot Reservoir Model 86

5.3 Simulating Calcite Precipitation/Remediation Using a Two 5-Spot Well Spacing and a Real Geological Model 88

5.4 Simulating Calcite Precipitation/Remediation (with a Higher EDTA Dose) Using a Two 5-Spot Well Spacing and a Real Geological Model.....90

5.5 Simulating the Effect of Precipitation/Remediation on Permeability and Porosity Using a Quarter 5-Spot Model.....91

Chapter 6: Summary, Conclusions, and Recommendations 119

6.1 Summary and Conclusions 119

6.2 Recommendations 121

References.....123

LIST OF TABLES

Table 4-1 List of UTCHEM input data used in Runs 4.1, 4.2, and 4.3 49

Table 4-2 Relative permeability data used in Runs 4.1, 4.2, and 4.3 49

Table 4-3 List of initial concentrations written in the input section for Run 4.1.. 50

Table 4-4 List of elements and reactive species for Run 4.1 50

Table 4-5 List of components and their corresponding numbers in the UTCHEM for this reaction equilibrium (Run 4.1) 51

Table 4-6 List of elements and reactive species for Run 4.2 51

Table 4-7 List of initial concentrations written in the input section (Run 4.2)..... 52

Table 4-8 List of elements and reactive species for Run 4.2 53

Table 4-9 List of cations and anions included in the input file (Run 4.3) 54

Table 4-10 List of UTCHEM input data used in runs 4.4 and 4.5.....55

Table 4-11 Relative permeability data used in Runs 4.4, 4.5 55

Table 4-12 List of cations and anions with their respective concentrations used in Runs 4.4 and 4.5 56

Table 4-13 Summary of the results in Runs 4.4 and 4.5.....57

Table 5-1 List of UTCHEM input data used in Run 5.1.....94

Table 5-2 Relative permeability data used in Run 5.1.....94

Table 5-3 Chemical composition for formation and injection waters used in Run 5.1.....95

Table 5-4 Chemical composition for formation and injection waters used in Runs 5.2 and 5.3.....96

Table 5-5 Relative permeability data used in Runs 5.2 and 5.3 96
Table 5-6 Chemical composition for formation and injection waters used in Runs 5.2 and 5.3 (for the pre-treatment scenario).....97
Table 5-7 Chemical composition for formation and injection waters used in Run 5.4.....98
Table 5-8 Relative permeability data used in Run 5.4.....98
Table 5-9 Chemical composition for formation and injection waters used in Run 5.4.....99

LIST OF FIGURES

Figure 1-1 The effect of scale build-up on the performance of a gas well in Saudi Arabia.....2

Figure 2-1 Effect on $BaSO_4$ inhibition efficiency for various types of inhibitors when using a) pH=2 b) pH=7 11

Figure 2-2 Effect of temperature on $BaSO_4$ inhibition efficiency for various types of inhibitors 12

Figure 2-3 Effect of (Ca^{+2}) and (Mg^{+2}) on $BaSO_4$ inhibition efficiency for various types of inhibitors 13

Figure 2-4 $BaSO_4$ inhibition efficiency for different types of inhibitors comparing the effect of thermal degradation (under 200C for 14 days) vs. the same chemicals, but not degraded.....17

Figure 2-5 Return profile for PVS vs. Vs-Co after pumping at low concentrations (<10 ppm) 18

Figure 2-6 An ideal adsorption isotherm curve of an inhibitor 'A' on silica sand. 20

Figure 2-7 Static adsorption.....21

Figure 2-8a The polymer-based inhibitor (SI-6) precipitates less iron compared to other inhibitor samples.....23

Figure 2-8b The compatibility of polymer-based inhibitors after spending the acid system with calcium carbonate 23

Figure 2-9 $BaSO_4$ solubility in a brine when mixed with different concentrations of methanol, glycol and triethylene glycol at 25°C with their respective scale indices (SI).....25

Figure 2-10 Measured nucleation time at different amounts of methylene phosphonic acid with the presence of a) 0% cosolvent, b) 20% methanol, c) 40% methanol, and d) 40% ethylene glycol.....26

Figure 4-1 Reservoir model used in Run 4.1 58

Figure 4-2 2-D Pressure Contour map after 365 days of production (psi) in Run 4.1 58

Figure 4-3 a) 2-D Pressure contour map after 7000 days of production (psi) in Run 4.1 b) Average reservoir pressure throughout the life of the field in Run 4.1.....59

Figure 4-4 Bottomhole pressure profile at both producer and injector wells throughout the simulation time in Run 4.1 60

Figure 4-5 Average water and oil saturations vs. time in Run 4.1.....60

Figure 4-6 Cumulative oil recovery vs. time in bbls and as a percentage of original oil in place in Run 4.1.....61

Figure 4-7 Initial Ba^{++} concentration before beginning the injection in Run 4.1 61

Figure 4-8 Ba^{++} concentration profile at (a) T=1460, (b) T=4016, and (c) T=7000 days in Run 4.1 62

Figure 4-9 Injection front shape at (a) T=1460 and (b) T=4015 days using a smaller grid size (20') in Run 4.1 63

Figure 4-10 $BaSO_4$ concentration in the reservoir at (a) T= 4016 days and (b) T=7000 days with more solids accumulated near the wellbore toward the end of the simulation (Run 4.1) 63

Figure 4-11 (a) BaSO4 concentration profile in the producer well vs. time in Run 4.1 (b) Water and Oil Production rates vs. time in Run 4.1 64
Figure 4-12 CO_3 concentration distribution after (a) T=146 days (b) T= 5840 days of continuous injection in Run 4.2 64
Figure 4-13 CO_3 dominates the majority of the field at almost the end of the simulation Run 4.2 65
Figure 4-14 $CaCO_3$ at (a) T=0 and (b) T=1460 days (Run 4.2) 65
Figure 4-15 $CaCO_3$ concentration profiles at (a) T=5110, (b) T=6569, and (c) T=7000 days (Run 4.2) 66
Figure 4-16 $BaSO_4$ concentration profiles at (a) T=0, (b) T=3651, and (c) T=7000 days (Run 4.2) 67
Figure 4-17 Reservoir pressure in 2-D map (T=365 days) (in Run 4.2) 68
Figure 4-18 Reservoir pressure in 2-D map at the end of the simulation in Run 4.2 68
Figure 4-19 Iron sulfide profile at (a) T= 0, (b) T=3651, (c) T=7000 days (Run 4.3) 69
Figure 4-20 Barite at (a) T=0, (b) T=5110, and (c) T=7000 days (Run 4.3) 70
Figure 4-21 Calcite concentration profiles at (a) T=0, and (b) T=7000 days (Run 4.3) 71
Figure 4-22 Iron [Fe^{++}] initially at equilibrium, [Fe^{++}] = 0.097 mol/l. Note: Here, we consider the reservoir as the iron source in this process (Run 4.3)..... 71
Figure 4-23 Iron [Fe^{++}] at (a) T=3651, and (b) T=7000 days (Run 4.3) 72
Figure 4-24 Reservoir pressure 2-D map (T=365 days) for Run 4.3 72

Figure 4-25 Reservoir pressure 2-D map at the end of the simulation for Run 4.3.....73
Figure 4-26 Sulfate-rich injection water front in (a) T=730 days (using a 100' grid blocks) compared to (b) T= 730 days (using a 50' grid block) (Run 4.4) 73
Figure 4-27 Sulfate concentration profile in the water fronts at (a) T= 2190, (b) T=3284, and (c) T=4000 days (Run 4.4) 74
Figure 4-28 $BaSO_4$ precipitation progress at (a) T=1825, (b) T= 2555, and (c) T=2919 and (d) T=3649 days (Run 4.4) 75
Figure 4-29 $BaSO_4$ concentration profile at T=4000 days (Run 4.4) 76
Figure 4-30 Ba and SO_4 concentration profile in the producer well vs. time (Run 4.4) 76
Figure 4-31 Permeability map used in Run 4.5 77
Figure 4-32 Porosity map used in Run 4.5 77
Figure 4-33 Sulfate-rich injection water fronts in (a) T= 730, (b) T= 1460, (c) T=2190, and (d) T=4000 days (Run 4.5) 78
Figure 4-34 $BaSO_4$ concentration profiles in (a) T= 730, (b) T=1460, (c) T=2190, and (d) T=2920 days (Run 4.5).....79
Figure 4-35 $BaSO_4$ concentration profile in T=4000 days (Run 4.5).....80
Figure 4-36 Ba and SO_4 Concentration profile in the producer well vs. time (Run 4.5) 80
Figure 4-37 Cumulative oil recovery as a percentage of original oil in place and in bbls (Run 4.4).....81

Figure 4-38 (a) Oil and water production rates and (b) Overall production rate (Run 4.4) 81
Figure 4-39 Reservoir average pressure for Run 4.4 82
Figure 4-40 Oil and water saturation profiles for Run 4.4.....82
Figure 4-41 Cumulative oil recovery as a percentage of original oil in place and in bbls (Run 4.5).....83
Figure 4-42 (a) Oil and water production rates and (b) Overall production rate (Run 4.5) 83
Figure 4-43 Reservoir average pressure for Run 4.5 84
Figure 4-44 Oil and water saturation profiles for Run 4.5.....84
Figure 5-1 Ca^{++} concentration profiles at (a) T=0, (b) T=100, (c) T=300, and (d) T=1600 days 100
Figure 5-2 CO_3^{--} concentration profiles at (a) T=0, (b) T=100, (c) T=300, and (d) T=600 days 101
Figure 5-3 CO_3^{--} concentration profile at T=1600 days (Run 5.2).....102
Figure 5-4 EDTA injection progress at (a) T=100 and (b) T=1600 days (Run 5.2).....102
Figure 5-5 Calcite concentration profiles at (a) T=200, and (b) T=1600 days (Run 5.2)..... 103
Figure 5-6 Permeability map used in Runs 5.3 and 5.4..... 104
Figure 5-7 Porosity map used in Runs 5.3 and 5.4.....104

Figure 5-8 Initial water saturation map of the system (used in Runs 5.3 and 5.4) 105

Figure 5-9 Calcite exists initially at 0.1 mol/l pv prior to remediation (Run 5.3).....105

Figure 5-10 Calcite accumulates at .12 mol/l pv in the absence of EDTA injection (Run 5.3).....106

Figure 5-11 Calcite removal as EDTA is injected at 0.025 mol/l pv after 2500 days (Run 5.3).....106

Figure 5-12 Calcium concentration at the end of the remediation (T=2500 days) for the two 5-spot Spacing (Run 5.3) 107

Figure 5-13 Carbonate is accumulated around the treated area at 0.03 mol/l pv after 2500 days following the successful dissolution and chelating of calcite (Run 5.3).....107

Figure 5-14 EDTA distribution in the two 5-spot reservoirs at T=2500 days (Run 5.3).....108

Figure 5-15 (a) Cumulative oil recovered (both as percentage of original oil in place and in bbls) vs. time (Runs 5.3 and 5.4) (b) Overall production rate (left) along with water and oil production rates (right) vs. time (Runs 5.3 and 5.4) (c) Reservoir average pressure in (Psi) (Runs 5.3 and 5.4).....108

Figure 5-16 Calcite removal as EDTA is injected at 0.2 mol/l pv after 2500 days (Run5.4).....110

Figure 5-17 Calcium concentration at the end of the remediation (T=2500 days) as EDTA is injected at 0.2 mol/l pv (Run 5.4).....110

Figure 5-18 (a) Calcite profile at the end of the 1st injection period at T=400 days, (b) The modified porosity map and (c) The modified permeability map (Run 5.5).....111

Figure 5-19 (a) Calcite concentration profile at T=420 days (b) Permability and (c) Porosity are shown post-treatment are shown as well (Run 5.5).....112

Figure 5-20 (a) Calcite concentration profile at T=920 days at the end of the simulation, (b) Permeability map at the end of the simulation and (c) porosity map at the end of the simulation (Run 5.5).....113

Figure 5-21 Comparison between two flooding cases one with EDTA remediation in terms of cumulative oil recovery as the percentage of original oil in place (Run 5.5).....114

Figure 5-22 (a) water and oil production rates for 900 days and (b) overall production rate profile for 900 days (Run 5.5).....115

Figure 5-23 Reservoir average pressure for the flooding case with EDTA (psi) (Run 5.5).....116

Figure 5-24 (a) Water and oil production rate profiles for 1000 days without EDTA treatment. (b) overall production rate profile for 1000 days without EDTA treatment (Run5.5).....117

Figure 5-25 Reservoir average pressure for the flooding case without EDTA (psi) (Run 5.5).....118

Chapter 1 Introduction

Inorganic (mineral) scaling deposition is a serious problem that can significantly shorten the oil/gas well's life by reducing production. Underground fluids (water, hydrocarbons, and dissolved gases) and solids (metals) are found initially in equilibrium. However, after drilling and producing the well, the equilibrium state changes and the process of scaling begins in response to that. The thermodynamics and kinetics of the dissolved molecules govern the formation of a specific type of scale. In addition, the geology (mineralogy) of the formation could be of importance to the scaling process as it controls the type and abundance of the ions dissolved. The typical mineral scales found in the oilfield can be classified under two major generic families: carbonates or sulfates. However, there are other complex iron salts such as sulfides, oxides, and carbonates that can pose similar or more difficult challenges when removing or inhibiting them.

Once the scaling process is initiated in the wellbore, an array of problems emerges such as plugging of the tubular and pore spaces inside the formation. The scale build-up in the formation contributes significantly to the total skin value by restricting the flow channels (paths) in the formation as well as increasing the pressure drop in the near-wellbore area. For example, it is believed that 4 million bbl per year is being lost from the North Sea oil producers because of the sulfate scales in the near-wellbore region (Graham and Mackay, 2004). Similarly, the deposition inside the wellbore will reduce the inner diameter of the tubing which restricts the flow to the surface. Figure 1-1 illustrates the impact of scales deposition in the production string on well productivity for one of the wells in Saudi Arabia.

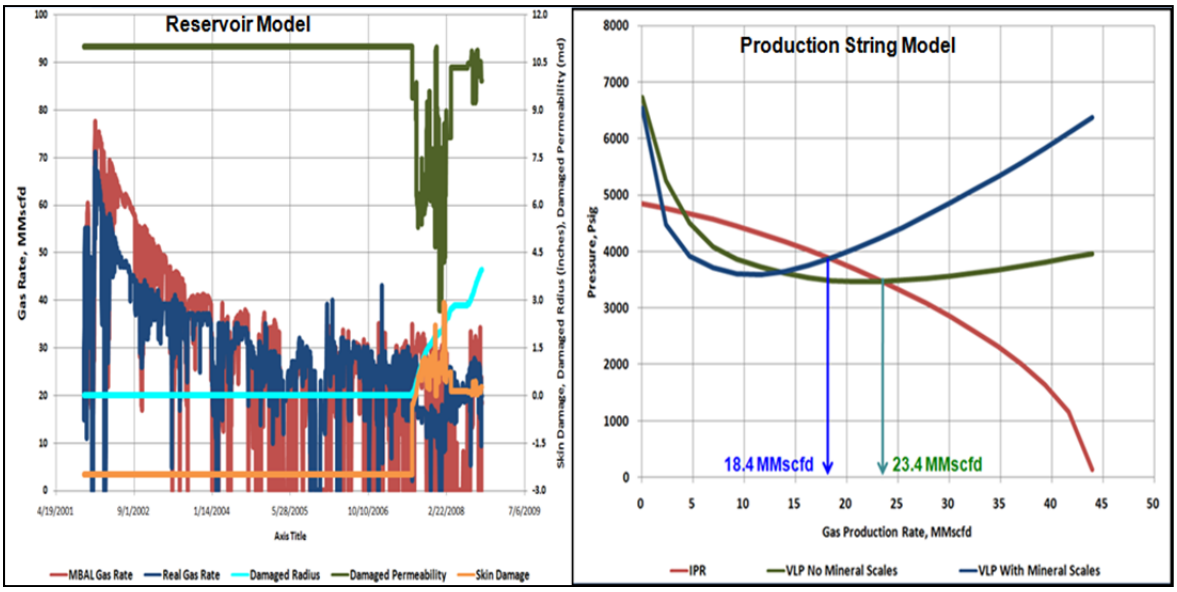

Figure 1-1 The effect of scale build-up on the performance of a gas well in Saudi Arabia. (Left side) the well history data is showing deterioration in the daily gas rate associated with a sudden increase in the skin damage. (Right side) The scale build-up is responsible for losing nearly 5 mmscfd of gas production from the same well as illustrated by the intersection of IPR and VLP curves (Franco et al., 2009)

That can be well explained by the Hagen-Poiseuille law, where the drop in pressure (ΔP) is inversely proportional to the flow diameter to the fourth power (D^4). In addition, running tools inside the wellbore might pose a risk as there is always the potential of getting stuck across these scales. The total estimate of global scale costs is near $1.4 billion annually with more than 35% of the total costs coming from North and South America according to (Frenier, 2002). The costs include ones associated with lost production as well as the ones associated to removing/treating these scales. This highlights the economic impact of scales on the oil industry. The loss of productivity caused by scaling leads to a large number of costly remediation work each year in both

production and injection wells. Furthermore, some of the oil and gas fields have been abandoned prematurely because of scaling.

Chapter 2 Literature Survey

Most of the literature in this field has been focusing primarily on understanding the main drivers of the scaling process as well as testing and analyzing chemicals used for remedial/inhibition operations to mitigate the serious impact of these depositions. This section will present a review of the significant papers presented by both academic institutions as well as industry experts to help establish a solid background on the scaling problem.

2.1 The Formation of Scales

As mentioned previously, the change in the equilibrium state of the solution or the deposition environment will trigger the process of deposition. This change can occur either by varying bottom hole pressure and temperature (i.e., when reservoir pressure is depleted), salinity, or pH, which measures the solution acidity. The degree of agitation of the solution plays an important role during the crystallization phase as it may destabilize the crystals. Generally, the deposition of minerals starts when the formation brine becomes over-saturated by the ions dissolved in the brine (when the ion concentrations are above the solubility limit). However, the degree of super-saturation dictates how fast the deposition will take.

In general, scales mainly form by changing the pressure and temperature of the formation water as in case of the carbonate. On other hand, changing the salinity of formation water can promote sulfate as in the case when incompatible brines are mixed together.

2.1.1 The Process of Nucleation

Many researchers have focused on understanding the mechanism by which the scale crystals evolve from the solution. Crabtree (1999) described how the scale first grows from unstable clusters of atoms to then become a perfect crystal; a process called homogenous nucleation. When the solution reaches the super-saturation stage, small ion clusters or sub-particles start growing as more ions attach to it. The increase in the radius is associated with a reduction in the free energy level at the surface of the cluster, which leads to more stability. Eventually, the cluster begins taking shape and growing along crystal planes. The crystal now becomes difficult to break apart and large enough to fall out of suspension. In heterogeneous nucleation, the mechanism is similar but with the difference that the process takes place over a substrate such as a sand particle or metallic surface (e.g., tubing walls). A subsequent stage called secondary nucleation occurs when the scale crystals act as a substrate for new particles (Crabtree et al., 1999). According to Ramastad (2004), the formation of scales can occur in a shorter induction time once crystallites form. Any delay in crystallites formation will delay the process of depositing minerals. This concept is very important when dealing with inhibitors (Ramastad et al., 2004).

The turbulent nature of the flow and severity of the agitation can disrupt the process of deposition. However, the influence of this factor is minimal and is only limited to delaying the process.

2.2 Formation Mechanisms

2.2.1 Carbonate Scales

When carbon dioxide (CO_2) gases are dissolved in water, the pH is lowered because aqueous carbonic acid is formed. The dissociation of CO_2 to carbonate and bicarbonate makes the water acidic, which leads to the solubility of carbonate anions increasing. As the reservoir pressure depletes, CO_2 starts coming out of the solution and carbonate scales precipitate. The general equation is as follows:

$$Ca^{++} + 2HCO^{---} \rightleftarrows CaCO_3 + H_2O + CO_2 .$$

Precipitation of $CaCO_3$ in the formation or inside the perforations will add to the drop in pressure and cause further deposition. The solubility of ions is increased by higher temperatures along with the salinity effect. The influence of salinity varies depending on the type of salts and the type of deposited scales. For example, brine containing Mg^{++} and SO_4^{--} ions most likely will retard the $CaCO_3$ formation because the inclusion of these ions disrupts the crystal growth by attaching to the lattice or crystal surface. This will increase the induction time required to form scaling particles (Sorbie, 2004).

2.2.2 Sulfate Scales

The mixing of formation water and injected seawater inside the reservoir is the main driver of sulfate scales in general. While it is very scarce in the formation, the sulfate can be found in significant concentrations in seawater (around 2,960 ppm). On the other hand, the formation water may have high amounts of barium or calcium unlike the

seawater, which leads to precipitation as the two waters are incompatible. More precipitation occurs when mixed water is produced into the wellbore and pressure and temperature decrease. However, barium sulfate, one of the common oilfield scales, has a temperature-dependent solubility. The $BaSO_4$ solubility increases with temperatures from 25-100°C by a factor of two and then decreases when it goes beyond 200°C (Langmuir, 1997).

2.2.3 Iron Sulfide Scales

Generally, corrosion of the metal tubular provides the ideal source for iron to begin scaling deposition. This occurs mostly in sour wells where H_2S gas is produced along with hydrocarbons. The net corrosion reaction appears after a series of partial sub-reactions as follows: $Fe+H_2S \Longrightarrow FeS + H_2$. In the case of sweet wells, there is always a potential to form iron scales with the help of sulfate-reducing bacteria (SRB). SRB provide the enzymes required to oxidize the hydrocarbons by sulfate ions as detailed in the following equation (Przybylinski, 2001):

$$CH_4+SO_4^{--} \Longrightarrow HCO_3^- +HS^- +H_2O$$

The bisulfide ion then is reduced to form the H_2S gas.

Initially, the iron sulfide builds up around the tubing wall and ends up cracking and flaking to the bottom of the well. The remaining attached portion of the scale becomes exposed and immersed in the brine, which allows it to seep in underneath the scaling. The oxygen/H_2S-rich water will become trapped between the scale and the wall, which leads to under-deposit corrosion of the tubing, a phenomena called "crevice corrosion" or "pitting" (Claassen, 1989). This mechanism is valid to describe the

formation of iron chloride when reservoir water contains a high percentage of chloride anions (measures up to 250-300 mg/l at surface conditions).

In practice, iron sulfide exists in different forms (species). Depending on the sulfur/iron ratio in the molecular composition, the solubility of the scale is significantly affected. The iron sulfide ages with time and converts to a species like pyrite and marcasite with the (FeS_2) chemical composition (which is slow and difficult to react). Mackinawite (FeS) represents the most reduced and less stable form, which is very soluble in HCl acid. Normally, the scale side facing the flow has more sulfur such as pyrite or marcasite because it is exposed to the stream containing the dissolved HS^- ions. Scales usually deposit simultaneously with hydrocarbons to make them hard to treat (Ford et al., 1992).

2.2.4 Iron Oxide Scales

Iron oxide is the typical product from the corrosion of iron-based metals dissolved in solutions or gases that contain oxygen. When the rust (FeOOH) starts to develop on the surface, which exists either in oxidation state Fe (II) (ferrous) or the more stable, Fe (III) (ferric), iron comes in equilibrium with oxygen to form Fe_2O_3 (hematite). Other types of oxides like Fe_3O_4 (magnetite) can be generated by the decomposition of the unstable (FeO) at high temperatures as can be shown from the following chemical equation (Talbot, 1997):

$4FeO \rightleftarrows Fe+Fe_3O_4$ (precipitation).

In the field, it is important to remove the air from the fluids being pumped into the well, because of the hazard of accelerating the corrosion of the tubular.

2.3 Scale Inhibition

Inhibitors are chemically engineered to reduce the rate of formation of a particular scale by acting on crustal surfaces and scaling nuclei. Chemicals that are used to target the nucleation process (early stage of scale formation) are called nucleation inhibitors. They act by covering the scale proto-crystal and increasing the surface tension between the growing nuclei and the solution to disrupt the nucleation and re-dissolve it in the solution.

Crystal growth inhibitors, on the other hand, retard any further growth in the crystal. According to Nancollas (1979), the adsorbed inhibitor agent onto the nuclei can change the lattice structure and distort its orientation and ability to attract other ions. In other words, the crystal surface (the active site for deposition) is blocked and solids will no longer be able to attach to it. He also proposed another possible scenario where the inhibitor itself acts as a nucleation center which will lower the super-saturation state of the solution and decrease the scaling tendency to deposit minerals (Nancollas et al., 1979).

Dispersants are another type of inhibitors that use the concept of electrostatic repulsion (dispersion) to keep the crystal from adhering to pipe walls or other substrates.

A minimum concentration or (threshold level) of the inhibitor is required to react with scale clusters. Most of the papers that address the inhibition issue agreed that a successful inhibitor product must meet the following general criteria:

- Must exhibit high tolerance to calcium, iron and other impurities that could reduce its effectiveness.
- Must show high stability in acid formulation and high temperature oil wells.

The observed effects of pH, temperature, and ion levels were described in many papers as highlighted in the literature survey below.

2.3.1 Crystal Growth Retarders

Scale inhibitors, functioning as crystal growth retarders, undergo repetitive dissociations (speciations), illustrated in this sequence (Sorbie and Laing, 2004):

If we assume that $H_nA \rightleftarrows H^+ + H_{n-1}A$ represents the general composition of scale inhibitor molecules. Then,

$H_{n-1}A^- \rightleftarrows H^+ + H_{n-2}A^{2-}$

.....

.....

$H_{n-x}A^{x-} \rightleftarrows H^+ + H_{n-x-1}A^{(x+1)-}$

where *x* is the dissociation level and *A* is the scale inhibitor complex.

Each step represents a level of dissociation, while each level requires a specific reaction rate (Pka). Depending on the type of scale and type of inhibitor, a certain level of dissociation must be achieved for the inhibition to start. Thus, it is not the inhibitor molecule which adsorbs into the crystal. Instead, it is the active complex [$H_{n-x-1}A^{(x+1)-}$] generated from the speciation. Different types of phosphonate are categorized as crystal growth retarders.

2.3.1.1 Effect of pH on Crystal Growth Retarders

In most cases, a certain pH number should be maintained to inhibit a scale effectively and reach a certain level of dissociation. Sorbie (2004) has determined that a pH value of 5 or 6 is necessary for DETPMP (diethylene triamine penta methylene phosphonic acid) to inhibit barium sulphate (Sorbie and Laing, 2004). Refer to Figure 2-1 to compare the inhibition efficiency (IE) against $BaSO_4$ at PH=2 and PH=7. At PH=2, IE<=20% compared to 58% at PH=7. The inability to cope with high acidic environments is one of the deficiencies of phosphonate.

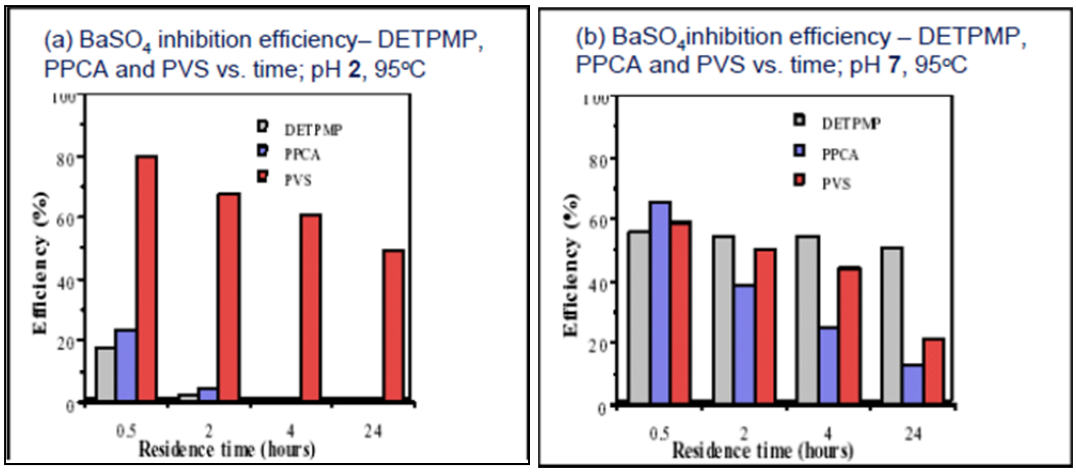

Figure 2-1 Effect on $BaSO_4$ inhibition efficiency for various types of inhibitors when using a) pH=2 and b) pH=7 (Sorbie and Laing, 2004)

2.3.1.2 Effect of Temperature on Crystal Growth Retarders

The temperature of the solution may not be as influential as the pH level on the inhibition mechanism. However, Sorbie (2004) detected a positive trend where the efficiency increases with temperature up to 95°C (Figure 2-2) as the brine becomes less super-

saturated. Although the study did not simulate high temperature wells, it is well known that phosphonates usually show poor thermal stability with time at high temperatures (up to 200°C).

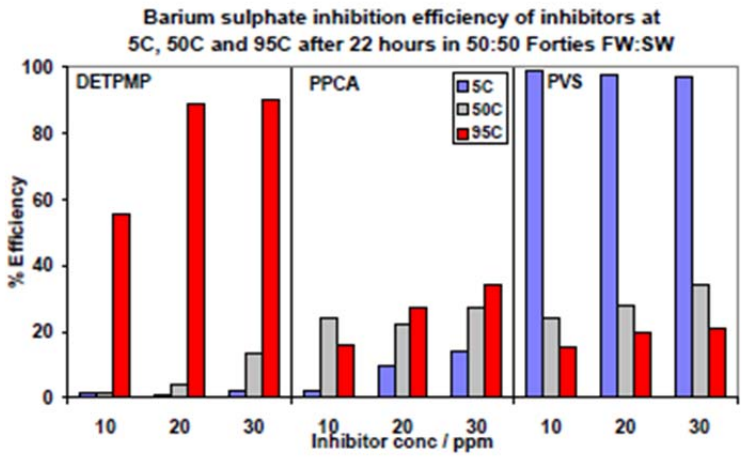

Figure 2-2 Effect of temperature on $BaSO_4$ inhibition efficiency for various types of inhibitors (Sorbie and Laing, 2004)

2.3.1.3 Effect of Calcium and Magnesium on Crystal Growth Retarders

The importance of calcium and magnesium varies based on the type of inhibitor as well as the scale. Calcium is believed to bond with the inhibitor to form an effective complex that can attach to the surface of the crystal as shown below:

$Ca^{++} + A^{(x+1)-} \Rightarrow$ Ca.A (calcium inhibitor complex).

The calcium inhibitor complex substitutes for the scales and molecules as well as distorts the morphology of the crystal or lattice. In general, a positive response occurs when increasing the calcium concentration in the mixture (Figure 2-3) (Sorbie, 2004). The performance of the DETPMP is impacted negatively by adding Mg^{++} when inhibiting

$BaSO_4$. The magnesium was found to interfere in the process by altering the calcium in the complex and making the inhibitor ineffective (Tantayakom et al., 2005).

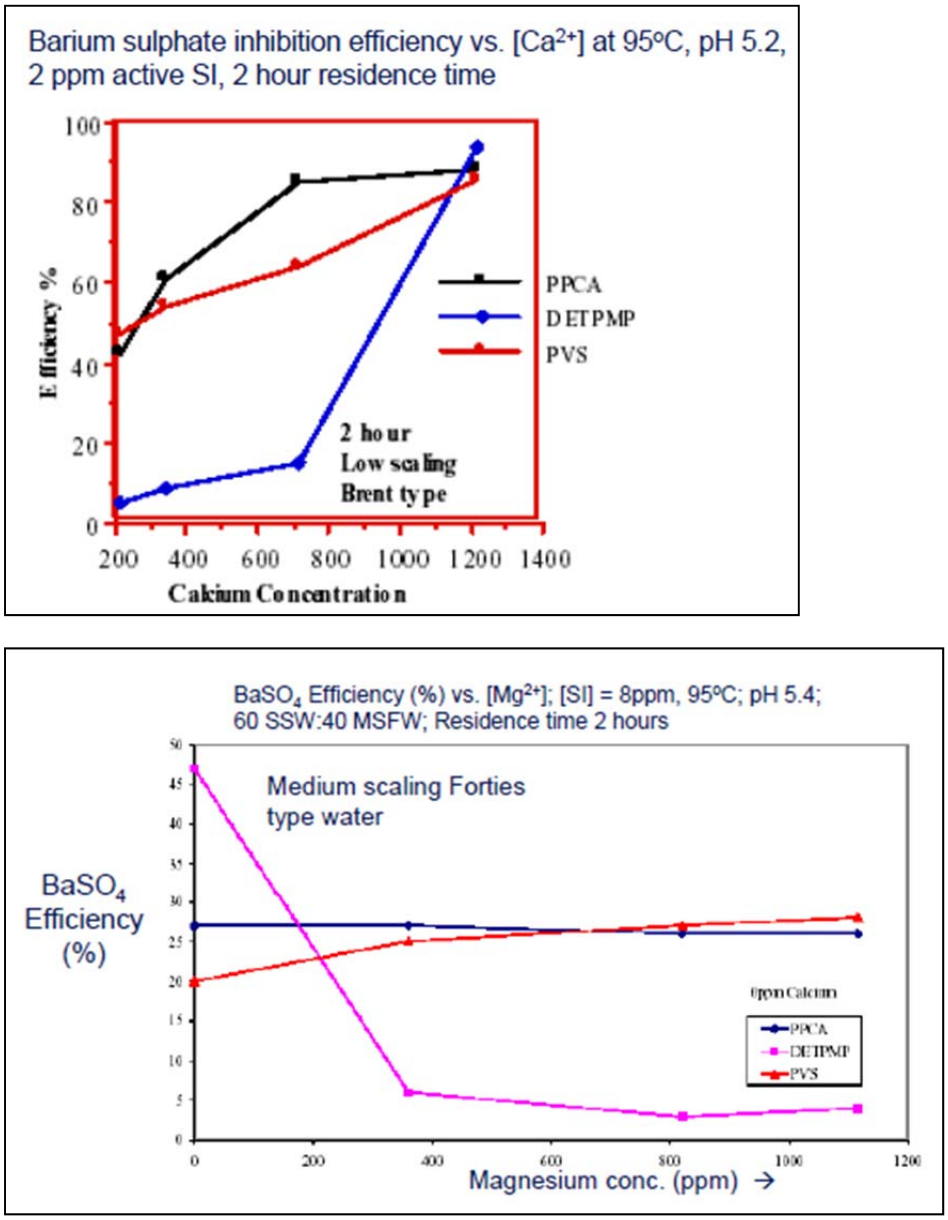

Figure 2-3 (Upper) Effect of (Ca^{+2}) on $BaSO_4$ inhibition efficiency for various types of inhibitors. (Lower) Effect of (Mg^{+2}) on $BaSO_4$ inhibition efficiency for various types of inhibitors (Sorbie, 2004)

2.3.2 Nucleation Retarders

This type of scale inhibitor interferes with the nucleation stage. The inhibitor's particles are small enough to diffuse in the bulk brine in order to get into the ion cluster. Polymers like poly vinyl sulphonate (PVS) coat the scale ion by a certain percentage to increase the surface tension between the growing nuclei and the solution and subsequently to re-dissolve it. The minimum inhibition concentration (MIC) is more critical in the case of nucleation inhibitors. For example, Thomson estimated that the MIC, that is required to inhibit the barite formation completely, is 16% of surface coverage based on an empirical model. This assumes that the inhibitor's effect is mainly to delay or extend the nucleation time (Thomson et al., 2002).

2.3.2.1 pH Effect on Nucleation Retarders

The nucleation inhibitor works principally through a totally different mechanism which does not involve dissociation of the inhibitor. That means the pH role is insignificant and the polymer still can function at pH values as low as 2 (as was proved experimentally with the PVS (see Figure 2-1).

2.3.2.2 Effect of Temperature on Nucleation Retarders

One of the striking features of Figure 2-2 is the good inhibition efficiency of PVS at 5°C. At such a low temperature, the polymer takes advantage of the slow kinetics and efficiency can increase to 100%. However, in much more ideal situations, efficiency remains reasonable at temperatures up to 95°C.

2.3.2.3 Effect of Calcium and Magnesium on Nucleation Retarders

The stability constant (pKa), which represents the measured bonding strength between cations like Ca, Mg, and the (SO_3H-) group in the PV (poly vinyl), is low in the PVS (poly vinyl sulphonate inhibitor) case. The (Pka) itself is an indicator of the strength of the complex interaction between them which might compromise the effectiveness of the inhibitor. Experiments in Figure 2-3 show that the inclusion of calcium increases the efficiency of the PVS although the increase is not as dramatic as displayed by DETPMP. Sorbie suggested that the increasing calcium content in the brine is being adsorbed into the lattice, making it softer or easier to inhibit (Sorbie, 2004). As for magnesium, the inhibition process is impacted positively if the brine is rich in Mg ions. The Mg indirectly inhibits the calcite. For instance, it incorporates onto deposited crystals and poisons the growth sites of the crystal. Reduction in calcite growth by 50% is achieved (induction time is higher) and solubility increases for calcite with Mg^{++}. This is completely in opposition to the effect of magnesium on the growth retarder-classified inhibitors as illustrated earlier.

2.4 The Performance of Scale Inhibitors at HP/HT Reservoirs

Graham (1998) performed extensive research on the implications of the harsh environment existing downhole in several North Sea reservoirs on typical scale inhibitors. The environment there is harsh either in terms of salinity ([ca]>40,000 ppm) or high pressures/temperatures. Graham conducted screening tests on four different inhibitors (that belong to the polymer family) to come up with the most promising chemical that can sustain its efficiency for a longer time. He began by excluding the

phosphonates because of their poor thermal stability (see Figure 2-4). Thermal degradation will destroy the parts of the molecules binding to the sulphate/carbonate scale lattice. As a result, this will reduce the adsorptive capacity of the inhibitor which will result in reducing the squeeze lifetime (Graham et al., 1998).

The conclusions of his lab work are summarized below:

1. PPCA (phosphino poly-carboaxylate) was dependent on the pH as well as on temperature. Reduction in performance was noted when pH was reduced to 3-4. The thermal ageing tests were conducted at a range of 180-200°C while the oxidative degradation environment was simulated by adding iron to act as a catalyst for the oxidization degradation process. Further reduction in performance was detected at 180°C in a severe oxidative degradation environment. On the other hand, the sodium and calcium ions are helpful in stabilizing the PPCA.

2. Sulphonated co-polymer (VS-Co) undergoes degradation at pH < 4.5 if thermally aged (heated for a long time).

3. PVS (poly vinyl sulphonate) showed thermal stability up to 200°C at pH ranging from 2 to 6. However, the polymer showed sensitivity to an oxidative environment but not to sodium or calcium cations (See Figure 2-4).

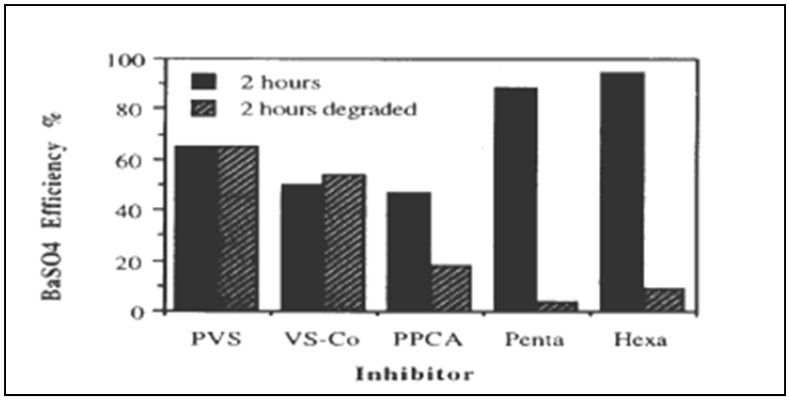

Figure 2-4 $BaSO_4$ inhibition efficiency for different types of inhibitors, comparing the effect of thermal degradation (under 200°C for 14 days) vs. the same chemicals but not degraded (Graham et al., 1998)

Initially, PVS and Vs-Co were selected to undergo an additional test to determine which one exhibits a longer squeeze time. A core flood test was prepared by pumping low concentrations of both inhibitors and monitoring the post flush return profile as shown in Figure 2-5. PVS outperformed the VS-Co in this area.

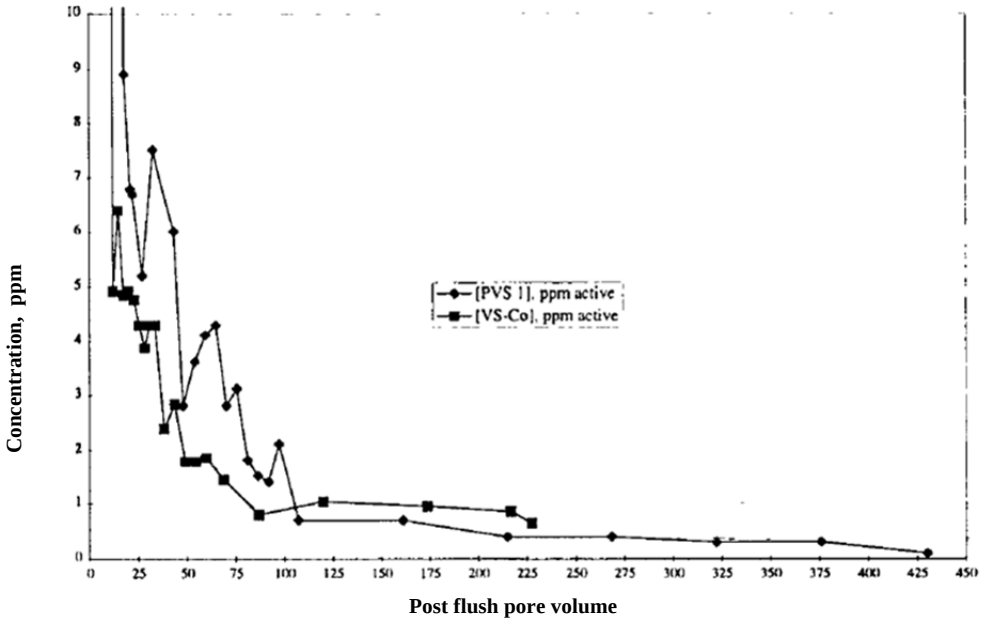

Figure 2-5 Return profile for PVS vs. Vs-Co after pumping at low concentrations (<10 ppm) (Graham et al., 1998)

In summary, PVS is recommended to inhibit against calcite as well as barite in High pressure/ High temperature (HP/HT) wells. However, some operators might refrain from using these expensive polymers and instead use HDMP (hexa phosphonate) in some HT wells where pH ≥ 5.5 at production conditions. HDMP shows high stability and could be appropriate as a cheaper option. The difference between HDMP and DETPMP, despite the fact that they belong to the same phosphonate family, is that amine groups in HDMP are linked together by $(CH_2)_6$ linkages in the molecular structure, which are believed to reduce the steric strain (repulsive interaction between methylene groups on non-neighboring carbons. On the other hand, DETPMP is less stable at high temperature because of the relatively weaker $(CH_2)_2$ linkages. Other operators may prefer blending both generic types to benefit from both working mechanisms such as PPCA and DETPMP. Together, PPCA begins taking action once the nucleation starts, while

DETMPM retards the growth of the crystal. This blend becomes more effective when inhibiting against the scale formation on metal surfaces in which large molecules of the PPCA and the small molecules of the DETMPM will form a much more dense film coating the surface.

2.5 Scale Inhibition Placement

2.5.1 Scale Inhibition Placement by the Squeeze Technique

The most widely used method to place the inhibitor into the formation is to inject at high pressures (without fracturing) into the water zone followed by a brief shut-in period. The chemical is adsorbed in the formation and then desorbs slowly into the produced water/fluids. Certain criteria will define the proper inhibitor to be squeezed: first, the efficiency of the chemical to inhibit at low or high concentrations; second, the ability of the fluid to be adsorbed by the rock's surface as well as the ability of that surface to retain the fluid; third, the fluid's ability to release (desorb) slowly from the rock to insure the minimum inhibitor concentration required for several months. Finally, the inhibitor must not risk well productivity by damaging the formation (Kerver and Heilhecker, 1969). Kerver and Heilhecker conducted laboratory tests to measure the amount of adsorbed inhibitor molecules into the formation at different concentrations in the bulk phase. Plotting both parameters generates the adsorption isotherm, which is useful to predict the behavior of the inhibitor. A desirable inhibitor should exhibit an isotherm rising at a fast rate and then leveling off with increasing inhibitor concentration. That means the inhibitor will remain adsorbed into the rock even at low concentrations of inhibitor. The

minimum inhibitor concentration (MIC) is defined as the point at which the curve changes its slope from flat to a steep one (see Figure 2-6).

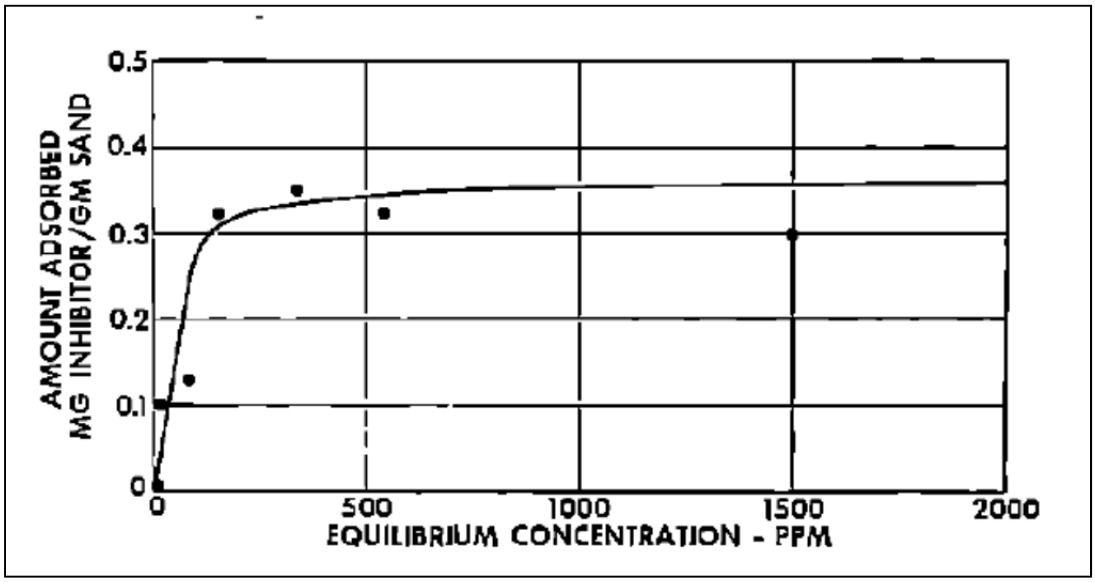

Figure 2-6 An ideal adsorption isotherm curve of an inhibitor 'A' on silica sand (Kerver and Heilhecker, 1969)

Precipitation is another theory that suggests calcium salt may precipitate and coat the reservoir rock. As a result, a number of calcium ions bind to a single scale inhibitor molecule in the following reaction:

INHIBITOR (SI) + Ca++ $\rightleftarrows$ SI_Ca "the inhibitor complex".

Recently, many researchers have come to believe that the two processes can happen simultaneously with some of the inhibitor being adsorbed and the remaining precipitating to form salts (refer to Figure 2-7). Kharwad and Sorbie (2009) conducted several lab experiments using DETPMP (methylphosphonic acid) on different types of surfaces including sand and minerals to monitor the mechanism by which inhibitor is retained

within the porous media. At low inhibitor concentrations, only pure adsorption is observed until reaching a certain threshold (equilibrium state), above which precipitates start forming. The coupled adsorption/precipitation mechanism is also observed at high pH values of 6 and above. Again, this is attributed to the dissociation level achieved under pH values of 5 or 6 as illustrated earlier when discussing the pH effect on the growth retarder inhibitor (Kahrwad, Sorbie, and Boak, 2009).

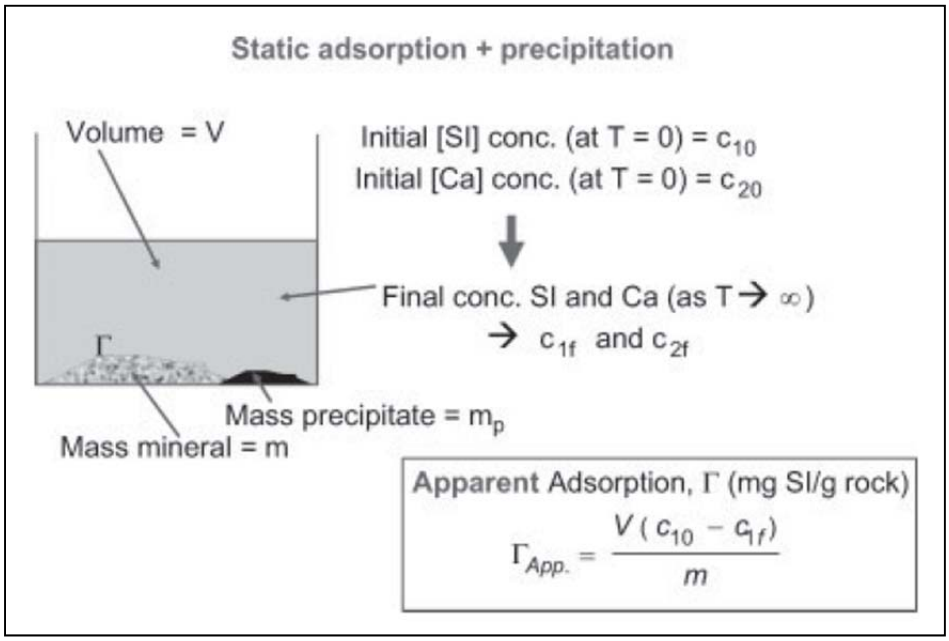

Figure 2-7 Static adsorption (Kahrwad, Sorbie, and Boak, 2009)

2.5.2 Pumping the Inhibitor with the Stimulation

This option has the advantage of using the same equipment to perform both stimulation and inhibition at the same time, which will be economical in terms of reducing the associated costs. Meyers (1984) suggested stimulating the formation with acid before injecting the inhibitor. A 24-hour period is required for soak-up prior to opening the well

for clean-up. However, the post-treatment production declines for some days before desirable performance is regained. Ethylenediaminetetraacetic acid (EDTA) or chelatant agent may be added to the acid to control any by-products resulting from acidizing the formation. This may reduce production decline associated with the acid treatment (Meyers, 1984). The economic viability of the treatment must be examined since EDTA is expensive. Furthermore, the study conducted by Meyers (1984) may not be applicable to all types of inhibitor/stimulation fluids. Therefore, compatibility studies using a series of core flooding tests are necessary. For instance, Smith et al. (2000) found that excessive amounts of scale inhibitors could affect the corrosion control agent in the HCl acid system. The formation damage can be an issue if the well has a low water cut and the used inhibitor happened to be water soluble (Smith et al., 2000). In a joint work supported by Schlumberger and Saudi Aramco, a single stage acid treatment which removes and inhibits $CaCO_3$ in sandstone and carbonate was tested. The polymer based inhibitor showed compatibility with different acid systems including HCl, mud acid (HF), and a chelating agent based system with a corrosion control agent. The polymer was chosen to be the optimum inhibitor after passing a series of rigorous tests. The following criteria qualified the polymer over five other inhibitors (Nasr El-Din et al., 2004):

1. It had no change in acid appearance, viscosity, and other rheological properties when heated to 150°C.
2. It produced a minimum precipitation of less than 5g/100 cm^3 when adding a high concentration of Ferric iron (>2000 ppm), which is considered a sign of high tolerance toward iron (see Figure 2-8a).
3. Its tolerance did not change much when spending the acid with calcium carbonate introduced to the test (pH reached 5) (see Figure 2-8b).
4. It did not interfere in the reaction of the acid with the reservoir rocks.

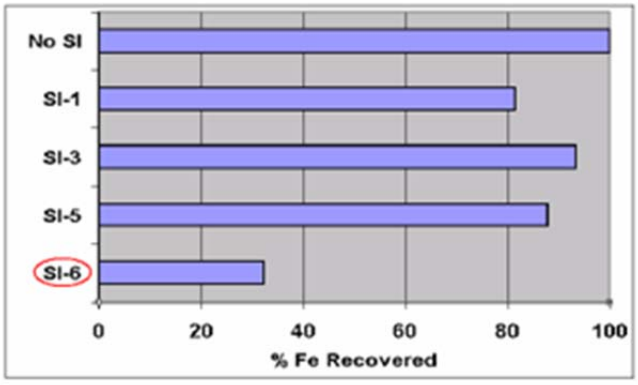

Figure 2-8a The polymer-based inhibitor (SI-6) precipitates less iron compared to other inhibitor samples (Nasr El-Din et al., 2004)

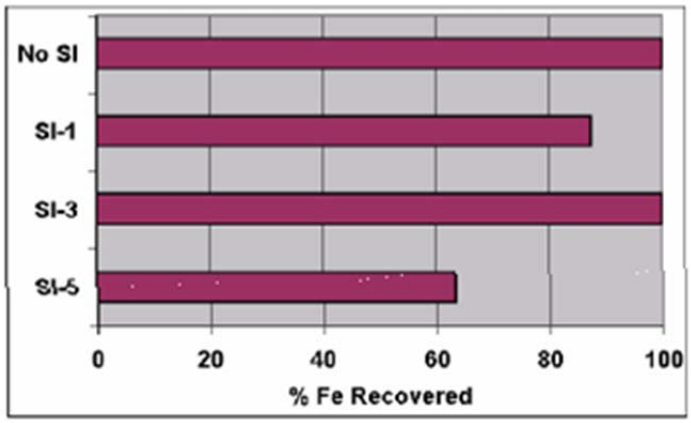

Figure 2-8b The compatibility of polymer based inhibitor after spending the acid system with calcium carbonate. The polymer-based inhibitor shows compatibility by precipitating less iron compared to other inhibitor samples (Nasr El-Din et al., 2004)

2.5.3 Pumping the Inhibitor with Fracturing Fluid

The main advantage when including the inhibitor in the fracturing fluid is the opportunity to place it in the entire fracture. Unless the inhibitor adversely affects the fracturing fluid reheology, this option proves effective in terms of cost and execution in the field. Similar

to acid squeeze techniques, compatibility issues must be investigated thoroughly. The significant pH contrast between the inhibitor system and cross-linked gel in the fracturing fluid may compromise the efficiency of the inhibitor or the carrier or both at the same time. The non-conventional inhibitors (i.e., polymer-based), which are effective against common oilfield carbonate and sulfate scales, showed high tolerance toward high levels of calcium or ferric iron that may be contained in the fracturing fluids (concentrations>50,000 mg/L) (Miller, 1999).

2.5.4 Inhibitor Impregnated into Proppant

This technique is implemented when the fracture is at risk of declining caused by the scale. The tiny cracks existing in proppant particles adsorb the inhibitor and slowly release it with produced water (Bourne et al., 1995).

2.6 The Effect of Adding Hydrate inhibitors to SI Efficiency

Tomson (2006) monitored the scale formation and prevention in the presence of three widely used hydrate inhibitors in the industry: methanol (MeOH), ethylene glycol, and triethylene glycol. He found that the solubility of the scales is adversely affected when the percentage of methanol added to the solution is increased. That effect is less with glycol and triethylene glycol (see Figure 2-9).

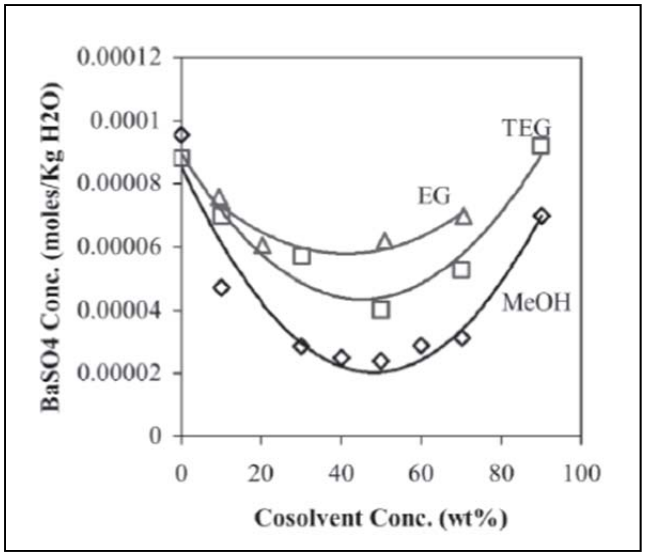

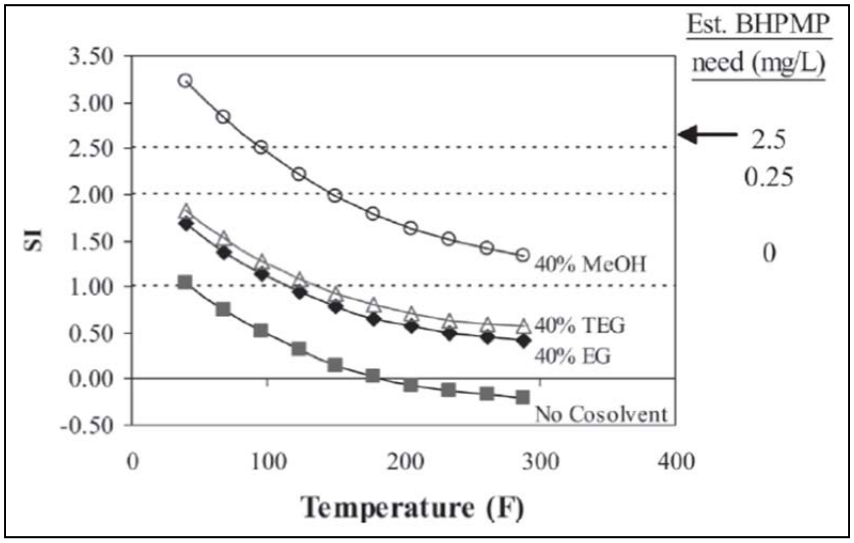

Figure 2-9 (Upper) $BaSO_4$ solublity in a brine when mixed with different concentrations of methanol, glycol, and triethylene glycol at 25°C. (Lower) The scale index (SI) for calcite in the presence of 40% methanol, glycol, and triethylene glycol at a temperature range from 25-300°F (Tomson, 2006)

In addition, Tomson investigated the nucleation time of a brine supersaturated with $BaSO_4$ with a scale index (SI=2) when mixed with various concentrations of BHPMP (bis-hexampethylene triamine-penta), a phosphonate scale inhibitor was considered to be the most effective barite inhibitor. These lab tests were repeated to account for the presence of methanol or glycol at similarly different percentages. It is clear that scale inhibition efficiency drops when a substantial amount of hydrate control is added to the brine (see Figure 2-10).

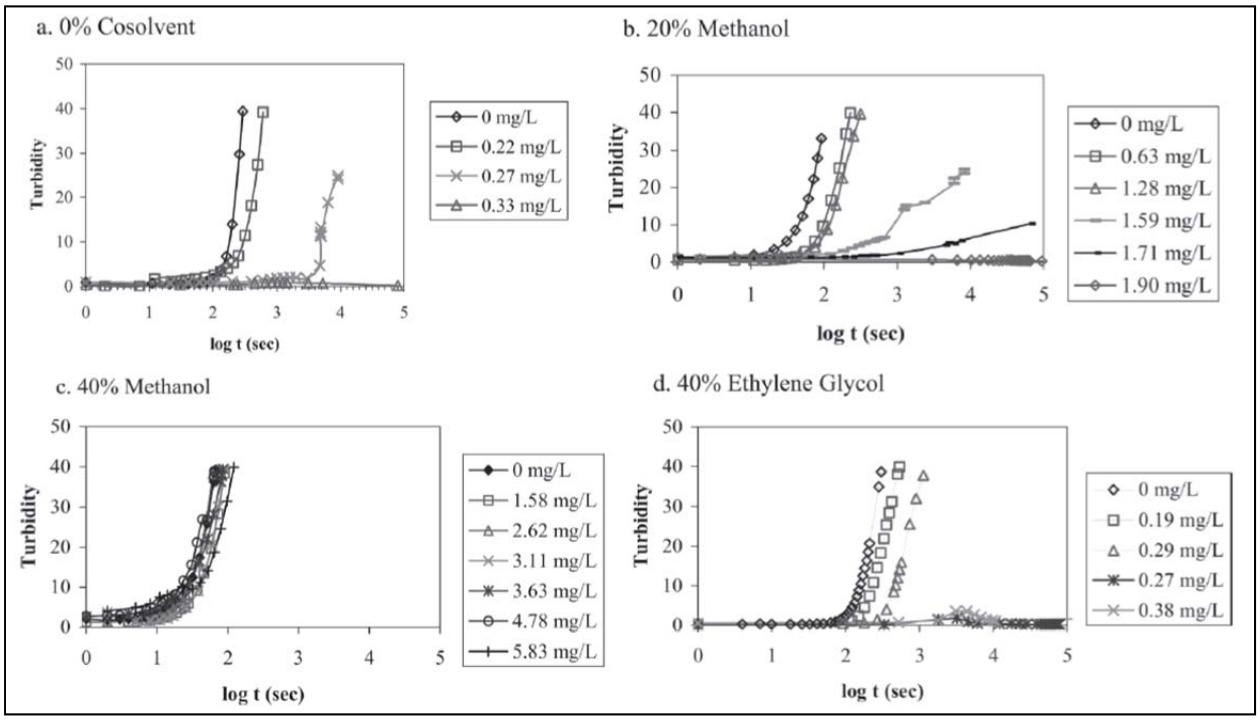

Figure 2-10 Measured nucleation time at different amounts of methylene phosphonic acid with the presence of a) 0% cosolvent b) 20% methanol, c) 40% methanol, and d) 40% ethylene glycol (Tomson, 2006)

Chapter 3 Description of UTCHEM

In order to monitor wells' tendency to produce mineral scales, UTCHEM, in-house developed software, was used primarily in this work. UTCHEM is a three-dimensional multi-phase simulator developed in the Center for Petroleum and Geosystems Engineering at the University of Texas at Austin. This tool, which went through a series of revisions and elaborations, was designed mainly for chemical flooding in the late 1970s by Pope and Nelson. Then, work was then extended further by Bhyan et al. in (1990) to include geochemical reactions between aqueous and solid pahses. The later work of Fathi (2005) and Delshad et al. (2006) added a model for wettability alterations in which a linear interpolation is performed for relative permeability, capillary pressure, and trapping to determine the current altered value for each of those three parameters. UTCHEM is also accounting for a variety of physical phenomena such as dispersion, diffusion, cation exchange, adsorption, capillary trapping, dissolution, precipitation, micro-emulsion phase behavior, tracer partitioning and reactions, shear-thinning polymer viscosity, temperature-dependent phase behavior among others. The simulator's other applications extend to include geochemical reactions between two phases.

This work serves as an opportunity to re-assess the limitations of this model and uses real reservoir inputs and production data to add more value to this study. The study is expanded further to investigate the formation of two or three simultaneous precipitations in one case.

3.1 Assumptions

User can specify any type of chemical components including geochemical ones such as (water, organic contaminants, surfactant, alcohols, polymer, chloride, calcium, other electrolytes, microbiological species, electron acceptors, etc.). Subsequently, the

simulator will solve the flow and mass-transport equations for these components. However, there are a few limitations related to both flow and equilibrium reaction models which are listed as follows (according to Delshad, 2003):

- Thermodynamic equilibrium has to be reached by all reactions.
- The reservoir is isothermal. Temperature changes due to chemical reactions are neglected.
- Activity coefficients of all reactive species are unity.
- The super-saturation of aqueous species is overlooked.
- Since temperature changes are neglected, changes in equilibrium constants and solubility products are assumed negligible and remain constant.
- A lack of kinetic reactions means UTCHEM can not accurately simulate for the near-wellbore region where fluid rates are high and equilibrium is difficult to establish.
- No permeability or porosity reduction is considered due to precipitates plugging the pores.
- Minimum pressure effect on the solubility product.
- Solids formed in the reservoir cannot migrate or flow.

These limitations can affect the quantity of the scaling simulated. For instance, the occurrence of scaling could plug the pores. Thus, the permeability/porosity is altered constantly throughout the simulation time. Further plugging increases the ΔP inside the pores in turn, promoting further scaling as a result. Therefore, scale volumes are underestimated if the permeability/porosity reduction is not considered. Moreover, the simulator restricts the solid movements within the reservoir, and thus, affects the real distribution of the scaling in the system.

Having said that, UTCHEM is still capable of predicting the extent of scaling/remediation processes in the reservoir.

3.2 Flow Equations

UTCHEM accommodates a set of partial differential mass conservation equations that were written to describe the multi-phase flow of *N* components based on the following general representation:

Number of moles in the outlet - Number of moles at the inlet = Accumulation + source/link

$$\frac{\delta \phi C_n^{Total}}{\delta t} + \frac{\delta}{\delta x}\sum_{j=1}^{np}[C_{nj}\, u_{xj} - \phi S_j\,(K_{xxnj}\frac{\delta C_{nj}}{\delta x} + K_{xynj}\frac{\delta C_{nj}}{\delta y} + K_{xznj}\frac{\delta C_{nj}}{\delta z})] + \frac{\delta}{\delta y}\sum_{j=1}^{np}[C_{nj}\, u_{yj} - \phi S_j\,(K_{yynj}\frac{\delta C_{nj}}{\delta y} + K_{yznj}\frac{\delta C_{nj}}{\delta z} + K_{yxnj}\frac{\delta C_{nj}}{\delta x})] + \frac{\delta}{\delta z}\sum_{j=1}^{np}[C_{nj}\, u_{zj} - \phi S_j\,(K_{zznj}\frac{\delta C_{nj}}{\delta z} + K_{zxnj}\frac{\delta C_{nj}}{\delta x} + K_{zynj}\frac{\delta C_{nj}}{\delta y})] = R_n\,, n = 1 \ldots . N. \quad \textbf{(3-1)}$$

C_n^{Total}	The total concentration of component *n* over all phases.
C_{nj}	The concentration of component n in phase *j*.
u_{xj}, u_{yj}, u_{zj}	The flux (convention rate) of component *n* in *x*, *y* and *z* direction and phase *j*.
S_j	The saturation of phase *j*.
K_{xxnj} , K_{xynj},.....	Elements of dispersion tensor (function of molecular diffusion)
R_n	Source term for component *n.*

The first term in **(Eq. 3-1)** represents the accumulation part (the change in total concentration of element n in respect to time). The second term represents the difference

between outlet and inlet concentrations at each of the three dimensions. To calculate the number of moles in the inlet, for example,

moles for element *n* at inlet/outlet= (convection rate for component *n* in a particular dimension) +(dispersion)

The *Rn* term deals with the reaction with the formation.

Similarly, the mass balance equation can be written in terms of Δp to come up with the following pressure equation **(eq. 3-2)**.

$$\varnothing C_t \frac{\partial P_1}{\partial t} + \vec{\nabla}.\vec{\vec{k}}.\lambda_{rT}\vec{\nabla}P_1 = -\vec{\nabla}.\sum_{\ell=1}^{np}\vec{\vec{k}}.\lambda_{r\ell c}\vec{\nabla}h + \vec{\nabla}.\sum_{\ell=1}^{np}\vec{\vec{k}}.\lambda_{r\ell c}\vec{\nabla}P_{c\ell 1} + \sum_{k=1}^{n_{cv}}Q_k \qquad \textbf{(3-2)}$$

Where

C_t	Total compressibility
$\vec{\vec{k}}$	Physical dispersion tensor
$\lambda_{r\ell c}$	Relative mobility ratio at a particular phase ℓ
λ_{rT}	Total relative mobility
Q_k	Injection rate for component k
$\vec{\nabla}P$	Pressure at particular phase ℓ
P_c	Capillary pressure at particular phase ℓ
h	Height

By solving for $\vec{\nabla}\boldsymbol{P}$ at each phase or (volume occupying component like oil and water), velocity terms (fluxes) used in **(Eq. 3-1)** can be computed using Darcy's law (Bhuyan, 1989).

3.3 EQBATCH Description

EQBATCH is a pre-processor for UTCHEM that was developed to do batch reaction equilibrium calculations. EQBATCH outcomes describe the initial equilibrium state of the reservoir which then can be fed into the geochemical input section in UTCHEM. Before running the geochemical model, the user first has to define the ions (elements) contained in the reservoir water. The ions that are regularly found in a sample of produced water include elements like sodium, calcium, magnesium, sulfate, carbonate and barium, etc. The equilibrium reactions of these electrolytes in the solution must be considered carefully when preparing the EQBATCH input file since it will determine the possibility of each precipitation.

The input file requires the stoichiometric coefficients of the elements in the solids which is included in the above reactions and the stoichiometric coefficients of the elements in the fluid species. The user must specify what type of solids expected to form in the future along with the fluid species.

3.4 Equilibrium Equations

The reactions covered by this model include aqueous electrolytes chemistry, precipitation/dissolution of minerals, ion-exchange reactions with the matrix, and reaction of acidic components of oil with the bases in the aqueous solution (Bhuyan 1989).

To determine the equilibrium state of the geo-system, the independent element balanced equations for the total number of components are to be solved. Usually, the components will be under two categories represented by the terms displayed below by the general formula **(Eq. 3-3):**

$$\boldsymbol{C_n^{Total} = \sum_{j=1}^{j} h_{nj} C_j + \sum_{K=1}^{K} g_{nk} C_K} \qquad \textbf{(3-3)}$$

where: n Total number of elements or components in the reactive system.

h_{nj} Denotes to stoichometric coeffecient of element n for fluid species j.

g_{nk} Denotes to stoichometric coeffecient of element n for solid species k

C_n^{Total} Total concentration of element n (in Kmol/ m3)

C_j Concentration of fluid species j (in Kmol/ m3)

C_K Concentration of solid species k (in Kmol/ m3)

Electric neutrality demands the sum of the charge and concentration to be zero **(Eq. 3-4)**:

$$\boldsymbol{0 = \sum_{J=1}^{J} Z_j C_j} \qquad \textbf{(3-4)}$$

where Zj denotes to charge of chemical species j.

The **solubility product** parameter is used to check if the solid is present or not. For each type of solid, the following equation is solved and compared to the left side (Ksp) that is

given by the user. If the right side is equal to the left one, the solid is assumed to be present **(Eq. 3-5)**:

$$\boldsymbol{K_K^{SP} \geq \prod_{j=1}^{N} C_j^w \, Kj \;\; , \;\; K = 1 \ldots\ldots\ldots n_k} \qquad \textbf{(3-5)}$$

3.5 Example of Equilibrium Calculations

In theory, the dilution of Na_2CO_3 and $CaCl_2$ in the water will yield a variety of fluid species. For instance, calcium can exist alone as an independent charged ion (Ca^{++}) or in an aqueous complex (dependent species) like calcium hydroxide $Ca(OH)^{+}$, calcium mono-hydroxide $Ca(HCO_3)^{-}$ or in a non-ionized calcium carbonate form $CaCO_3$. Below is a list of some of the reactions that were defined in EQBATCH for the next chapter's hypothetical cases:

$$Na_2CO_3(aq) \rightarrow 2Na^{+}(aq) + CO_3^{2-}(aq)$$
$$CaCl_2(aq) \rightarrow Ca^{2+}(aq) + 2Cl^{-}(aq)$$

$$Ca^{2+}(aq) + CO_3^{2-}(aq) \rightleftarrows CaCO_3(s) \qquad K1 = \frac{1}{KSP}$$

$$CaCO_3(aq) \rightleftarrows CaCO_3(s) \qquad K2 = \frac{1}{Keq}$$

$$H_2O \rightleftarrows H^{+}(aq) + OH^{-}(aq) \qquad Kw$$

$$H^{+}(aq) + CO_3^{2-}(aq) \rightleftarrows HCO_3^{-}(aq) \qquad K3 = \frac{1}{Ka_2}$$

$$H^{+}(aq) + HCO_3^{-}(aq) \rightleftarrows H_2CO_3(aq) \qquad K4 = \frac{1}{Ka_1}$$

The main elements in this case would be Ca, CO_3, Na, H, and Cl while the fluid species include independent species like H^+, Na^+, Ca^{2+}, CO_3^{2-}, and H_2O and dependent ones like HCO_3, $H2CO_3$ and $CaCO_3$.

By using **(Eq. 3-1)**, we write both **(Eq. 3- 6 and 3-7)**:

$$[Na2CO3]=[CO_3^{2-}(aq)]+[HCO_3^{-}(aq)]+[H_2CO_3(aq)\ ]+[CaCO_3(aq)]+\mathrm{n}CaCO_3(s) \quad \textbf{(3-6)}$$

$$[CaCl2]=[Ca^{2+}(aq)]+[CaCO_3(aq)]+\mathrm{n}CaCO_3(s) \quad \textbf{(3-7)}$$

We re-arrange **(Eq. 3-7)** and make a substitution back into **(Eq. 3-6)** to come up with **(Eq. 3-8)**:

$$[CaCO_3]+CaCO_{3(S)}=[CaCl_2]-[Ca^{2+}{}_{(aq)}]$$

$$[Na_2CO_3]=[CO_3^{2-}{}_{(aq)}]+[HCO_3^{-}]+[H_2CO_3]+[CaCl_2]-[Ca^{2+}{}_{(aq)}]$$

$$[Ca^{2+}(aq)]=([CaCl_2]-[Na_2CO_3])+[CO_3^{2-}(aq)]+[HCO_3^{-}(aq)]+[H_2CO_3(aq)\ ] \quad \textbf{(3-8)}$$

We also use electric neutrality to generate **(Eq. 3-9)** as follows:

$$2[Ca^{2+}(aq)]+[H^+(aq)]+[Na^+]=[OH^-(aq)\ ]+2[CO_3^{2-}(aq)]+[HCO_3^{-}(aq)]+[Cl^-]\ . \quad \textbf{(3-9)}$$

We can assume that the concentration values for Na and Cl will not change where [Na+]= 2[Na2CO3] & [Cl-]=2[CaCl2].

At equilibrium, we have **(Eq. 3-10)**:

$$[Ca^{2+}(aq)][CO_3^{2-}(aq)]=KSP\ . \quad \textbf{(3-10)}$$

For the aqueous reactions, the concentrations of dependent elements can be written in terms of the independent ones using the following general formula **(Eq. 3-11)**:

$$\boldsymbol{C_r = K_r^{eq} \prod_{j=1}^{N} C_j^{w_{rj}}} \quad \textbf{(3-11)}$$

The (Cr) denotes to concentration of dependent species *r*. So, for instance, the bicarbonate ion is one of the dependent fluid species for the calcite which can be written in terms of two independent ions based on the following aqueous reaction:

HCO3- = CO3-- + H+ → [HCO3-] = Ka1 [CO3--] [H+] ; where Ka1 is the equilibrium constant of this reaction that has to be provided by the user **(Eq. 3-12 through 3-15)**.

$$\frac{[H^+(aq)][CO_3^{2-}(aq)]}{[HCO_3^-(aq)]} = Ka1 \qquad \textbf{(3-12)}$$

Similarly, the following equations can be obtained

$$[CaCO_3(aq)] = Keq \qquad \textbf{(3-13)}$$

$$\frac{[H^+(aq)][HCO_3^-(aq)]}{[H_2CO_3(aq)]} = Ka2 \qquad \textbf{(3-14)}$$

$$[H^+(aq)][OH^-(aq)] = Kw \qquad \textbf{(3-15)}$$

Both **(Eq. 3-8)** and **(Eq. 3-9)** can be re-written using **(Eq. 3-10, 3-12 through 3-15)** to reduce the number of unknowns in the non-linear set of equations.

By substituting **(Eq. 3- 10)** & **(Eq. 3-12 to 3-15)** into **(Eq. 3-8)** results in **(Eq. 3-16)**:

$$\frac{KSP}{[CO_3^{2-}(aq)]} = ([CaCl_2] - [Na_2CO_3]) + [CO_3^{2-}(aq)] + \frac{[H^+(aq)][CO_3^{2-}(aq)]}{Ka_1} + \frac{[H^+(aq)]^2[CO_3^{2-}(aq)]}{Ka_1 Ka_2} \qquad \textbf{(3-16)}$$

And similarly, substituting into **(Eq. 3-9)** results in **(Eq. 3-17)**:

$$\frac{2KSP}{[CO_3^{2-}(aq)]}+[H^+(aq)]=2([CaCl_2]-[Na_2CO_3])+2[CO_3^{2-}(aq)] \\ +\frac{[H^+(aq)][CO_3^{2-}(aq)]}{Ka_1}+\frac{Kw}{[H^+(aq)]} \quad \textbf{(3-17)}$$

Now, we combine both **(Eq. 3-16 and Eq. 3-17)** to get **(Eq. 3-18)**

$$[CO_3^{2-}(aq)]^2(1+\frac{[H^+(aq)]}{Ka_1}+\frac{[H^+(aq)]^2}{Ka_1Ka_2})+([CaCl_2]-[Na_2CO_3])[CO_3^{2-}(aq)]-KSP=0 \quad \textbf{(3-18)}$$

Now, let's

$$(1+\frac{[H^+(aq)]}{Ka_1}+\frac{[H^+(aq)]^2}{Ka_1Ka_2})=f([H^+(aq)])$$

so **(Eq. 3-18)** becomes **(Eq. 3-19)**:

$$[CO_3^{2-}(aq)]^2\, f([H^+(aq)])+([CaCl2]-[Na2CO3])[CO_3^{2-}(aq)]-KSP=0 \quad \textbf{(3-19)}$$

The Second degree equation shown in **(Eq. 3-19)** can be solved using the quadratic equation $x=\frac{-b\pm\sqrt{b^2-4ac}}{2a}$ as shown in **(Eq. 3-20)**:

$$[CO_3^{2-}(aq)]=g([H^+(aq)])=\frac{([Na2CO3]-[CaCl2])+\sqrt{(([CaCl2]-[Na2CO3]))^2+4KSPf([H^+(aq)])}}{2f([H^+(aq)])} \quad \textbf{(3-20)}$$

By substituting **(Eq. 3-20)** into **(Eq. 3-17)**, we obtain **(Eq. 3-21)**:

$$F([H^+(aq)]) = 2g([H^+(aq)]) + \frac{[H^+(aq)]g([H^+(aq)])}{Ka_1} + \frac{Kw}{[H^+(aq)]}$$

$$+2([CaCl2] - [Na2CO3]) - [H^+(aq)] - \frac{2KSP}{g([H^+(aq)])} = 0 \qquad \textbf{(3-21)}$$

The next step would be using the Newton iteration method to calculate $[H^+(aq)]$. We start by assuming a hydrogen ion concentration and solve for the carbonate ion concentration in **(Eq. 3-20)**. Finally, from the equilibrium equation, we can obtain other species' concentrations.

Chapter 4 Precipitation Simulation Runs

In this section, a series of hypothetical cases (scenarios) is presented to simulate different types of mineral scales with different field geometries or injection/production conditions. S-3 graph-HDG Software (a property of ScienceSoft Limited) was used to display the results in this thesis. Most of the cases presented in the following sections are synthetic to suit the academic nature of this study and thus, some of the inputs that were used in this section are artificial and might not resemble the real field data. Nevertheless, the conclusions drawn from these studies are valid to understand the manner and the speed in which these precipitates develop.

4.1 Quarter 5-Spot Model Including One Injector and One Producer with Only $BaSO_4$ Being Precipitated

In this simulation, a hypothetical three-dimensional injection was simulated over a period of 7000 days. The chemical description and initial equilibrium state proposed in this simulation are given in Table 4-3 in which barium and sulfate are the only reactive species. The objective of this basic case is to study the precipitation of $BaSO_4$ in isolation considering there are initially no solids in the system. From Table 4-3, it is clear that the reservoir water is the only source of barium in this reactive system while the sulfate is provided by continuous injection. This condition is often found when seawater is injected into a formation containing barium in the pore fluid. The reservoir model used in this scenario (See Figure 4-1) has the assumptions listed in Tables 4-1 and 4-2.

This basic example assumes only barium and sulfate as elements, and one reaction that takes place during the injection as summarized in Table 4-4. The solubility

product constant of 1.4 x 10^{-15} is assumed insensitive to temperature changes associated with the reaction. The UTCHEM input file is set up such that the user has to define the existence of the following 8 components: water, oil, surfactant, polymer, anions, cations, alcohol 1, and alcohol 2 shown in Table 4-5, followed by the other geochemical components. Note that surfactant, polymer, and alcohol are not considered in this flooding case. The original reservoir pressure is set at 3120 psi while the constant 1000 ft^3/d injection rate helps maintaining that pressure. The producer is operated at a fixed pressure of 3000 psi and the injector has fixed operation conditions as well. However, with the consistent depletion in pore-occupying volumes, the overall average pressure will drop from 3120 psi to almost 3030 psi (only 30 psi above the minimum). Figure 4-2 shows the pressure profile after only 365 days. The average pressure starts at 5000 psi for a very short period because this closed system is being pressurized by the injection. However, the average pressure tends to equalize in the whole system very quickly once the drawdown from the producer takes effect. By the end of the simulation, the variation in pressures is at a minimum (see Figures 4-3a and 4-3b). The bottom hole pressure profile in both wells in Figure 4-4 shows a constant pressure in the producer well (as fixed in the input file) with a nearly flat trend for the injection pressure (about 3050 psi). Other profiles for water, oil saturations, and cumulative oil recovery (displayed in bbls and as a percentage of the original oil in place) are presented in Figures 4-5 and 4-6. The water saturation increases significantly to 0.65 when the oil saturation is lowered from 0.54 to 0.35, indicating an ideal recovery performance in a homogenous field. The cumulative oil produced by the end of the run is about 400,000 bbls which makes up nearly 40% of the original oil in place.

Figures 4-7 and 4-8 show the injection front shape with time and track the changes in barium concentration over time in a 3-D representation. The injection front

displays an upward curvature shape (Figure 4-8a), while it takes the most direct path toward the producer with some precipitation taking place at the moving front. The short contact time between Ba and SO_4 is dictated by the constantly advancing front which leads to a significant amount of barium being pushed or replaced by the sulfate-rich water; whereas only small amounts of barium are actually consumed in forming barite. By the time the injection water reaches the producer, the front will have a sharp-angled tip as illustrated in Figure 4-8b. It is clear that once the front gets closer to the producer, it tends to move faster because of the high drawdown and that explaining the variance in the front shape.

On the other hand, some of the barium is trapped in the flanks (sides) before reacting with the dominant sulfate and precipitating around the wellbore (Figure 4-8). It is possible that $BaSO_4$ is precipitated in low amounts (concentration of about 0.02-0.03 mol/l pore volume) before the breakthrough, but the majority of the precipitation occurs near the producer because of the trapped barium being depleted and converted to barite (Figure 4-10). Figure 4-11a shows that the well started producing barium in excessive amounts followed by sulfate. Most of the barium contained in the reservoir was swept effectively by the sulfate-rich water that was injected. When looking at the water and oil production rates in Figure 4-11b, we see that oil cut in the stream decreases, beginning at T=1500 days. The decrease in oil stream continues but is compensated by the formation water until the breakthrough occurs at T=4016 days then we see the injected water.

Although the injection pressure is expected to increase at the end of the simulation in response to the damaged near-wellbore, Figure 4-4 does not show that. This is mainly attributed to the fact that UTCHEM does not consider permeability reduction caused by scale damage.

Using smaller grid sizes as well as increasing the number of grids, used to simulate the front movement and solid distribution, yields better resolution for the 3D images. Figure 4-9 shows how different barium front shapes at T=1460 and T=4015 days using a smaller grid size (20') compares better than the ones when a 50' grid block was used (Figure 4-8a and 4-8b).

4.2 Quarter 5-Spot Model Including One Injector and One Producer with Both $CaCO_3$ and $BaSO_4$ Being Precipitated

In this section, the simultaneous precipitation of both barite ($BaSO_4$) and calcite ($CaCO_3$) is simulated. The calcite is challenging in terms of setting up the fluid species along with their corresponding exchange reactions. This run uses the same data and reservoir configuration as in the previous run. Table 4-6 and 4-7 present the geochemical reactions and the cations and anions concentrations in both formation and injection waters, respectively. As mentioned previously in Section 3.5, calcium bonds with water molecules to form different species in solution and calcite precipitation is controlled by the saturation state of the liquid. In the field, the majority of calcite formed in oil wells is driven by the changing pressures/pH rather than incompatible mixing of brines. In comparison with barite, calcite has a solubility product (Ksp) of 0.475×10^{-9} which is relatively higher than that of barium sulfate. Generally, high Ksp values indicate strong solubility, and thus a low potential to develop scales. Carbonate movement is presented at different time stages in Figures 4-12 and 4-13. Figures 4-14 to 4-16 show snapshots of the scaling distribution for both calcite and barite at different stages. The injected water, which provides the system with significant amounts carbonate, is moving in a similar way to the one displayed by sulfate in Run 4.1. The evolution of calcite continues after

the breakthrough, providing that there is a calcium supply lasting in the flanks. At the end of the simulation, some calcium remains in the system, but it should not alter the current calcite distribution in the near-wellbore region as well as in the majority of the field as shown in Figure 4-15. Figures 4-15b and 4-15c monitors the changes in scaling quantity around the wellbore for the last 500 days of the simulation.

Eventually, the generated calcite concentration ranges from 0.012 to a maximum of 0.09 mol/l PV, mostly around the wellbore. The quantity and distribution of generated barite (Figure 4-16) is exactly the same as that for calcite, despite the fact that the sulfate contained in the injection is half the carbonate's amount. The extremely low Ksp for $BaSO_4$ means little sulfate is needed to produce significant amounts of solids. Reservoir pressure contour maps in Figures 4-17 and 4-18 are for 365 and 7000 days, respectively. Since the same reservoir model and production conditions are used, production maps and oil recovery values will be the same as in Run 4.1.

4.3 Quarter 5-Spot Model Including One Injector and One Producer with ($CaCO_3$, $BaSO_4$, FeS) Being Precipitated

This run includes iron sulfide (FeS) to both calcite and barite with the purpose of introducing a more complicated scenario. Table 4-8 proposes 10 exchange reactions that take place between formation and injection water. Initially, ferrous ions (the second oxidation state of iron) are attracted to the hydroxide to form $Fe(OH)^+$ (iron monohydroxide) before reaching the non-ionized form $Fe(OH)_2$. The Iron(II) hydroxide in this case is assumed to be the most stable form. The iron is assumed to not oxidize to

produce Fe_3O_4 (iron oxide). On the other hand, it is assumed that sulfur will combine with hydrogen to form Hydrogen sulfide.

The mechanism of precipitating iron sulfide, as explained in the literature survey section, is related more to tubular corrosion rather than to the chemical incompatibility of two different brines. However, the formation's mineralogy in this case is assumed to have iron (about 0.3 mo/l PV) to carry out this reaction (see Table 4-9). The results of this simulation are presented in Figures 4-19 through 4-25. Iron sulfide exists initially at an equilibrium concentration of 0.096 mol/l PV (Figure 4-19) which represents the in-situ precipitation prior to the injection. Further precipitation occurs when injection begins and the solid concentration goes up to 0.105 mol/l PV at the tip of the front at lapsed time of T=3651 days. The final distribution for the iron sulfide is presented also in Figure 4-19 in which high volumes is anticipated to build up around the wellbore (up to 0.20 mol/l PV). The results for co-precipitation of calcite and barite are shown in Figures 4-20 and 4-21. The concentration profiles of iron as an aqueous species are shown in Figure 4-22. After 7000 days of continuous injection, some significant iron volumes remain un-swept in the flanks where there is no flux allowed across the boundaries (Figure 4-23). The remaining iron is expected to deplete gradually to supply the scaling process in the wellbore region. The slow consumption of these volumes is believed critical for the near-wellbore precipitation showing in Figure 4-19. This fact is also valid to explain the manner in which calcite and barite precipitates. Figures 4-24 and 4-25 track the changes in reservoir pressure in 365 and 7000 days respectively. This flooding scenario should yield saturation and oil recovery profiles similar to those in Figures 4-5 and 4-6.

4.4 5-Spot Homogeneous Model (1 Producer + 4 Injectors) with Only $BaSO_4$ Being Precipitated

In this run, a hypothetical three-dimensional case was simulated over a period of 4000 days. The chemical composition was kept simple with only barium and sulfate being the reactive elements (the chemical description for this run is given in Table 4-12). The purpose of running this case is to study the effect of heterogeneity on the magnitude and distribution of barite precipitated in the near-wellbore area. In order to perform the run, a 5-spot homogeneous reservoir model was built with the characteristics listed in Tables 4-10 and 4-11. The number of grid blocks used has a significant effect on the shape of the fronts. Using a smaller number of grid blocks or bigger grids may result in numerical errors that will be carried over the simulated time steps. Therefore, 50' grid size was selected in order to avoid the implications of such errors on the quality and accuracy of the front shapes. Figure 4-26 compares the sulfate injection front at T=730 days using 100' and 50' grid sizes. In terms of accuracy, there is a difference between sulfate concentrations calculated in both scenarios. The case with the bigger grids tends to overestimate the values. For example, in the 100' grid case, SO_4 exists at 0.003 mol/l pv in the injectors (it is supposed to be at 0.002 mol/l pv as described in Table 4-12).

The sulfated injection water progresses at different speeds because the injectors are pumping at different rates (Figure 4-26b). The water injection rate was set at 1000 bpd, 854 bpd, 534 bpd and 712 bpd for wells 1, 2, 3, and 4, respectively. As expected, the water from Injector 1 breaks through first, followed by that injected from well 2 (see Figure 4-27). Ideally, both progressing fronts will connect with each other at a certain point during the simulation time. In the beginning, the fronts' shapes start curving upward (Figure 4-26). However, as they get closer to the producer, the pressure effect from other

injectors defines the front shape. As a consequence, some of the barium were left isolated in the middle areas (see Figure 4-27), which later supplies the gradual precipitation action around the wellbore. Although instant formation of barite occurs at the (square-shaped) areas dominated by injection water, barite saturation decreases with time but increases at the constantly moving tips. The snapshots provided in Figures 4-28 and 4-29 show how the barite deposition rate has accelerated over time to take the solid concentration from .013 mol/l PV at T=1825 days to more than 0.075 mol/l PV at the end of the simulation. Figure 4-29 shows that the near-wellbore region is loaded with a high accumulation of barite as the solid concentration reaches a maximum of 0.1 mol/l PV in some blocks. The total volume precipitated in the near-wellbore region is calculated using **(Eq. 4-1)**:

$$\boldsymbol{Solid\ Volume\ per\ block\ (gm) = solid\ concentration\ \left(\frac{mol}{l}\right) \times \emptyset \times Sw \times 50^3\ (ft^3) \times MW\ for\ BaSO4\ (233)\ \left(\frac{gm}{mol}\right) \times 28.3\ \left(\frac{l}{ft^3}\right)} \qquad (4-1)$$

The near-wellbore region in this case is represented by a big sector, 150' long by 150' wide, with the wellbore in the center.

In the wellbore, Figure 4-30 shows the production of Ba vs. SO_4 over time. The decline in barium was sharp in the initial stages of the injection, but slowed down later. Before the breakthrough, the aqueous phase for sulfate in the production stream is significantly low compared to barium. After the breakthrough, both ions switch places and sulfate becomes dominant in the stream, which indicates the lack of sufficient mixing in both situations in order to deposit high quantities of barite inside the tubing. Additionally, the limited supply of barium (remained after the breakthrough) was precipitated along with sulfate in the near-wellbore region so there was not much left for mixing inside the tubing. The concentrations displayed in Figure 4-30 were used to

calculate the total solid volume precipitated inside the tubing, which was found to be only equal to 0.26 gm. The solid volume in the tubing is calculated by **(Eq. 4-2)**:

$$\boldsymbol{Barite\ volume\ in\ the\ tubing}\ (\boldsymbol{gm}) = \boldsymbol{solid\ concentration}\left(\frac{\boldsymbol{mol}}{\boldsymbol{l}}\right) \times \boldsymbol{rate}\left(\frac{\boldsymbol{ft^3}}{\boldsymbol{d}}\right) \times \boldsymbol{MW\ for\ BaSO4}\ (\mathbf{233})\left(\frac{\boldsymbol{gm}}{\boldsymbol{mol}}\right) \times \boldsymbol{\Delta t}\ (\boldsymbol{day}) \times \mathbf{28.3}\left(\frac{\boldsymbol{l}}{\boldsymbol{ft^3}}\right) \qquad (\mathbf{4-2})$$

In reality, any well that is supported by four injectors would have a strong lifting capacity to continuously flow any suspended solids out of the well. However, if the injection period were to extend beyond the 4000 day period, the effect of permeability reduction, caused by barite scales in the wellbore region, would be reflected in a high ΔP. A significant ΔP can minimize the lifting capacity by a significant amount.

4.5 5-Spot Heterogeneous Model (1 Producer + 4 Injectors) with Only $BaSO_4$ Being Precipitated

The reservoir model used in the last run was made highly heterogeneous by using a Dykstra-Parson coefficient of 0.7 and a correlation length of 100 ft. Then, the porosity was correlated by using the equation proposed in (Holtz, 2002):

$$K = 7 \times 10^7\, \emptyset^{9.61}$$

Figure 4-32 describes this highly heterogeneous reservoir in which porosity ranges from 10% to as high as 50%. The resulting permeability map will look like the one shown in Figure 4-31. The arithmetic average of all permeabilities and porosities should yield similar values to those used in the homogenous case; therefore, the comparison is representative. Once the injection has commenced, the water will follow a more tortuous path toward the producer because of the heterogeneity in the reservoir

(Figure 4-33). Some of the flow will pass through the low conductive channels, and as a result, it will become trapped in naturally formed deposition points that are scattered throughout the field. The evolution of barite over time is monitored in Figure 4-34. The solid precipitation looks more distributed in the reservoir at a concentration of 0.015 mol/l PV. However, considerable amounts of solids formed in the near wellbore region, especially in the side facing injector 1, whereby the concentration is about 0.045 mol/l PV. The injection rate at injector 1 (relative to other injectors) is high (1000 bpd), and thus more sulfates being supplied to form precipitates on that side.

The ions profile in Figure 4-36 behaves similarly to that in the homogeneous case. However, the calculated solids inside the tubing is .06 gm less than that in Run 4.4, indicating that relatively more barium was used during the heterogeneous reservoir flooding compared to that in the homogenous case. This is also reflected in the amount of solid precipitated in the near-wellbore zone. Figures 4-37 through 4-44 shows the oil recovery, water saturation, production rates and pressure profiles for Runs 4.4 and 4.5. Despite that the scaling magnitude and distribution was disturbed by the high level of heterogeneity, the effect on oil recovery is minimum. Again, the UTCHEM version used in this case does not consider changes in permeability inflicted by scaling in both cases. Table 4-13 summarizes the findings.

It worth mentioning that seawater injection, as an EOR mean, normally can achieve up to 20-50% of the original oil in place along with the traditional recovery. However, 67% was achieved in this synthetic case due to the type of well spacing arrangement and relative permeability and compressibility data used. The fact that selected residual saturation value for oil was relatively low and the rock and fluid compressibility were relatively high, the oil flow in the system has eased and made the

recovery efficient and fast. In addition, the oil volume in the reservoir is limited since the reservoir is assumed finite.

Table 4-1: List of UTCHEM input data used in Runs 4.1, 4.2, and 4.3

No. of Wells	2 (1 injector + 1 producer)
Reservoir Dimensions	1000' x1000' x50'
Grid Block Size	50'
Number of Grid Blocks	20 x 20 x 1
Reservoir Depth	7200'
Max. Simulation Time	7000 days
Initial Reservoir Pressure	3120 psia
Reservoir Permeability	Kx=1000 md, Ky=1000 md, Kz=250 md
Reservoir Porosity	20%
Initial Water Saturation	48%
Rock Compressibility	0.000005 1/psi
Reference (Stand) Pressure	3120 psia
Water Viscosity	0.65135 cp
Oil Viscosity	6.3 cp
Water Compressibility	4.7×10^{-7} 1/Psi
Oil Compressibility	0.000009 1/ Psi
Injection Rate	1000 ft^3/d
Well Flowing Pressure	3000 psi
Brine Salinity (C50)	1.7805 mol/l PV
Divalent Cation Conc. (c60)	0.248 mol/l PV

Note: C50 and C60 for Runs 4.2 and 4.3 are 1.26 mol/l PVand 0.08 mol/l PV respectively.

Table 4-2: Relative permeability data used in Runs 4.1, 4.2, and 4.3

	Water	**Oil**
Residual Saturation	0.25	0.15
End Point	0.5	0.7
Exponent	2.5	2

Table 4-3: List of initial concentrations written in the input section for Run 4.1

Initial Pore Water composition	**C (mol/l)**
Cl	0.14
Na	0.02
Ba	0.1
SO_4	0.02
Injected Water Composition	**C (mol/l)**
Cl	0.134
Ca	0.067
Na	0.4166
Ba	0
SO_4	0.21

Table 4-4: List of elements and reactive species for Run 4.1

Elements	Sodium (Na) , Barium (Ba), Sulfate (SO4)
Aqueous Species	Na^{+} , Ba^{++} , SO_4^{--}
Solid Species	$BaSO_4$ (Barite)
Dissolution Reaction	$BaSO_4 \rightleftarrows Ba^{+2} + SO_4^{--}$; $Ksp=[Ba^{++}]\ [SO4^{--}]=1.4x10^{-15}$

Table 4-5: List of components and their corresponding numbers in the UTCHEM for this reaction equilibrium (Run 4.1)

Component	Component Number	Considered?
WATER	1	Y
OIL	2	Y
Surfactant	3	N
Polymer	4	N
total ANION (chloride)	5	Y
total divalent (Calcium)	6	Y
Alcohol 1	7	N
Alcohol2	8	N
Na	9	Y
Ba	10	Y
SO_4	11	Y

Table 4-6: List of elements and reactive species for Run 4.2

Elements	Hydrogen (reactive), Sodium (Na) , Barium (Ba), Sulfate (SO_4) Calcium (Ca) , Carbonate (CO_3),
Aqueous Species	H^+, Ca^{++}, CO_3^{--}, Na^+ , Ba^{++} , SO_4^{--}, H_2O, OH^-, HCO_3^-, H_2CO_3, $CaCO_3^o$, $BaSO_4^o$
Solid Species	$BaSO_4$ (Barite), $CaCO_3$ (Calcite)
Dissolution Reaction	$BaSO_4 \rightleftarrows Ba^{+2} + SO_4^{--}$; $Ksp=[Ba^{++}]\,[SO_4^{--}]=1.4x10^{-15}$ $CaCO_3 \rightleftarrows Ca^{+2} + CO_3^{--}$; $Ksp=[Ca^{++}]\,[CO_3^{--}]= 0.475x10^{-9}$
Exchange reactions	$H_2O \rightleftarrows H^+ + OH^-$ $H^+ + CO_3^{--} \rightleftarrows HCO_3^-$ $HCO_3^- + {}_2H^+ \rightleftarrows H_2CO_3$ $Ca^{++} + CO_3^{--} \rightleftarrows CaCO_3^o$ $Ba^{++} + SO_4^{--} \rightleftarrows BaSO_4^o$

Table 4-7: List of initial concentrations written in the input section (Run 4.2)

Initial water composition	**C (mol/l)**
Cl	0.02
Na	0.02
Ba	0.1
SO_4	0.02
CO_3	0.01
Ca	0.1
Injected water	**C (mol/l)**
H	55
Ca	0
Na	0.15
Ba	0
SO_4	0.05
CO_3	0.1

Table 4-8: List of elements and reactive species for Run 4.3

Elements	Hydrogen (reactive), Sodium (Na) , Barium (Ba), Sulfate (SO_4) Calcium (Ca) , Carbonate (CO_3), Iron (Fe), Sulfur (S)
Aqueous Species	H^+, Ca^{++}, CO_3^{--}, Na^+ , Ba^{++} , Fe^{++}, S^{--}, SO_4^{--}, H_2O, OH^-, HCO_3^-, H_2CO_3, $FeOH^+$, $Fe(OH)_2$, HS^-, H_2S, $CaCO_3^o$, $BaSO_4^o$, FeS^o
Solid Species	$BaSO_4$ (Barite), $CaCO_3$ (Calcite), FeS (Iron Sulfide)
Dissolution Reaction	$BaSO_4 \rightleftarrows Ba^{+2} + SO_4^{--}$; $Ksp=[Ba^{++}]\,[SO_4^{--}]=1.4e^{-15}$ $CaCO_3 \rightleftarrows Ca^{+2} + CO_3^{--}$; $Ksp=[Ca^{++}]\,[CO_3^{--}]= 0.475e^{-9}$ $FeS \rightleftarrows Fe^{+2} + S^{--}$; $Ksp= [Fe^{++}]\,[S^{--}] = 8e^{-19}$
Exchange reactions	$H_2O \rightleftarrows H^+ + OH^-$ $H^+ + CO_3^{--} \rightleftarrows HCO_3^-$ $HCO_3^- + 2H^+ \rightleftarrows H_2CO_3$ $Fe^{2+} + OH^- \rightleftarrows Fe(OH)^+$ $Fe^{2+} + 2OH^- \rightleftarrows Fe(OH)_2$ $S2^- + H^+ \rightleftarrows HS^-$ $HS^- + H^+ \rightleftarrows H_2S$ $Ca^{++} + CO_3^{--} \rightleftarrows CaCO_3^o$ $Ba^{++} + SO_4^{--} \rightleftarrows BaSO_4^o$ $Fe^{2+} + S^{2-} \rightleftarrows FeS^o$

Table 4-9: List of cations and anions included in the input file (Run 4.3)

Initial water composition	**C (mol/l)**
Cl	0.6
Na	0.1
Ba	0.2
SO_4	0.1
CO_3	0.2
Ca	0.2
Fe	0.3
S	0.2
Injected water	**C (mol/l)**
H	55
Ca	0
Na	0.3
Ba	0
SO_4	0.05
CO_3	0.05
Fe	0
S	0.05

Table 4-10: List of UTCHEM input data used in Runs 4.4 and 4.5

No. of Wells	5 (4 injector + 1 producer)
Reservoir Dimensions	2000' x2000' x50'
Grid Block Size	50'
No. of Grid Block	40 x 40 x 1
Reservoir Depth	7200'
Max. Simulation Time	4000 days
Initial Reservoir Pressure	3120 psia
Reservoir Permeability	Kx=1000 md, Ky=1000 md, Kz=250 md
Reservoir Porosity	29%
Initial Water Saturaion	48%
Rock Compressibility	0.00002757 1/psi
Reference (Stand) Pressure	3888 psia
Water Viscosity	0.65135 cp
Oil Viscosity	6.3 cp
Water Compressibility	4.7 x10-7 1/Psi
Oil Compressibility	0.00005 1/ Psi
Injection Rate	5615, 4800, 3000, 4000 ft3/d
Well Flowing Pressure	3000 psi
Brine Salinity (C50)	1.7805 mol/l PV
Divalent Cation Conc. (C60)	0.2484 mol/l PV

Table 4-11: Relative permeability data used in Runs 4.4 and 4.5

	Water	**Oil**
Residual Saturation	0.35	0.25
End Point	0.51	1
Exponent	3.5	2.5

Table 4-12: List of cations and anions with their respective concentrations used in Runs 4.4 and 4.5

Initial water composition	**C (mol/l)**
Cl	0.6
Na	0.1
Ba	0.1
SO_4	0.004
Injected water	**C (mol/l)**
H	55
Ba	0
SO_4	0.002
Na	0.2

Table 4-13: Summary of the results in Runs 4.4 and 4.5

	Homogenous case	**Heterogeneous case**
Cumulative Oil Produced (OOIP%)	65.7%	64.4%
Cumulative Recovery	4,857,900 bbls	4,800,000 bbls
Injection Rate	3200 bpd	3200 bpd
Production Rate	3200 bpd	3100 bpd
So	0.32	0.34
Sw	0.68	0.66
Pwf	3120 psi	3120 psi
Solids in the Near-Wellbore Region	15.339 kg	2.863 kg

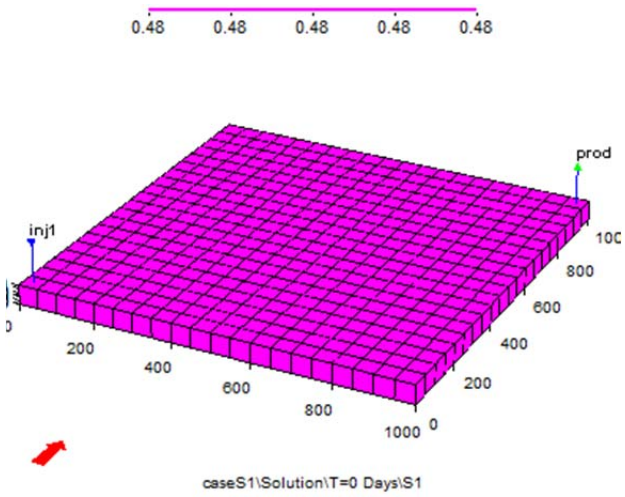

Figure 4-1 Reservoir model used in Run 4.1

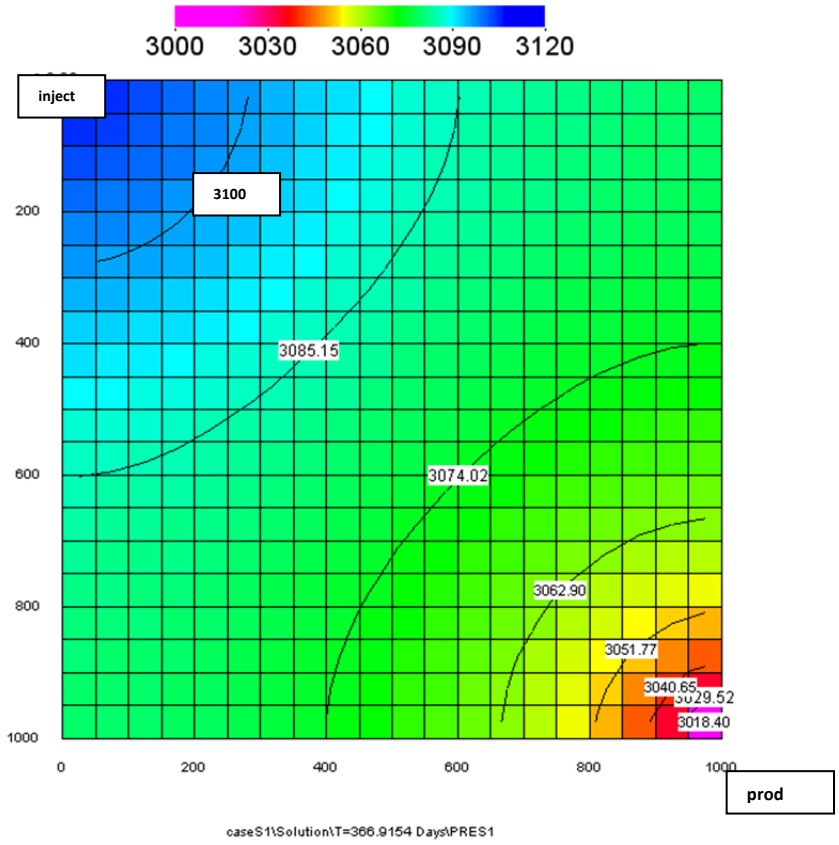

Figure 4-2 2-D pressure contour map after 365 days of production (psi) in Run 4.1

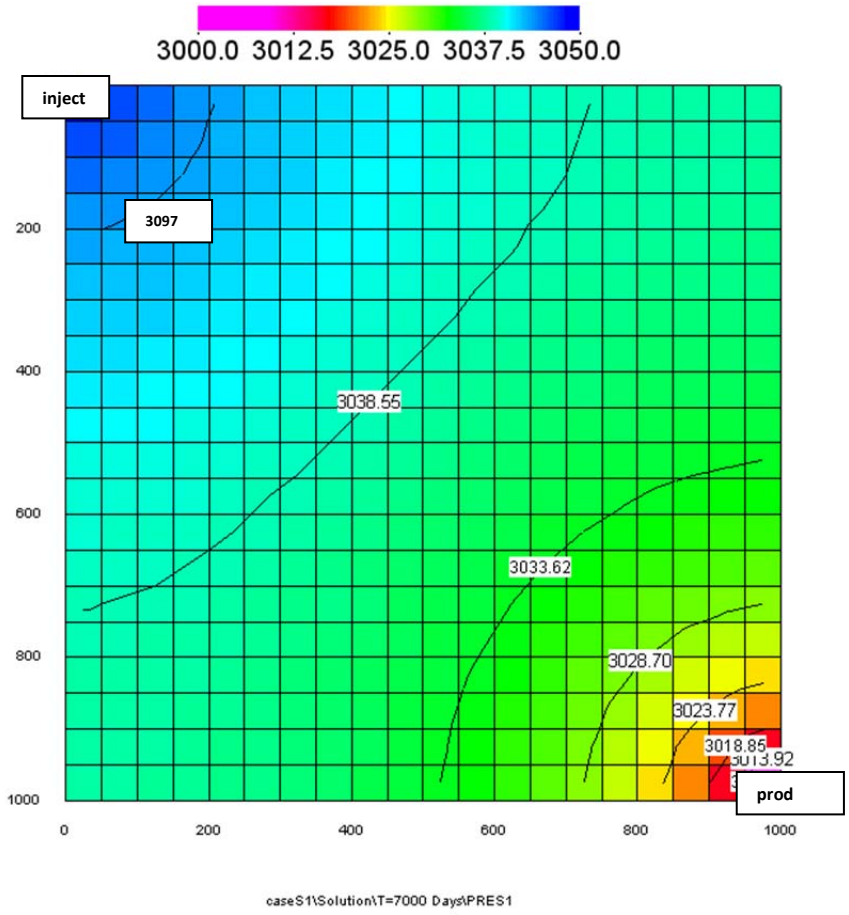

Figure 4-3a 2-D pressure contour map after 7000 days of injection (psi) in Run 4.1

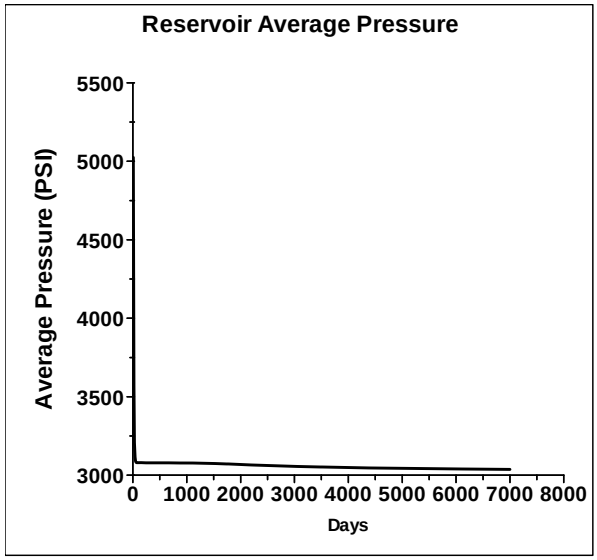

Figure 4-3b Average reservoir pressure throughout the life of the field in Run 4.1

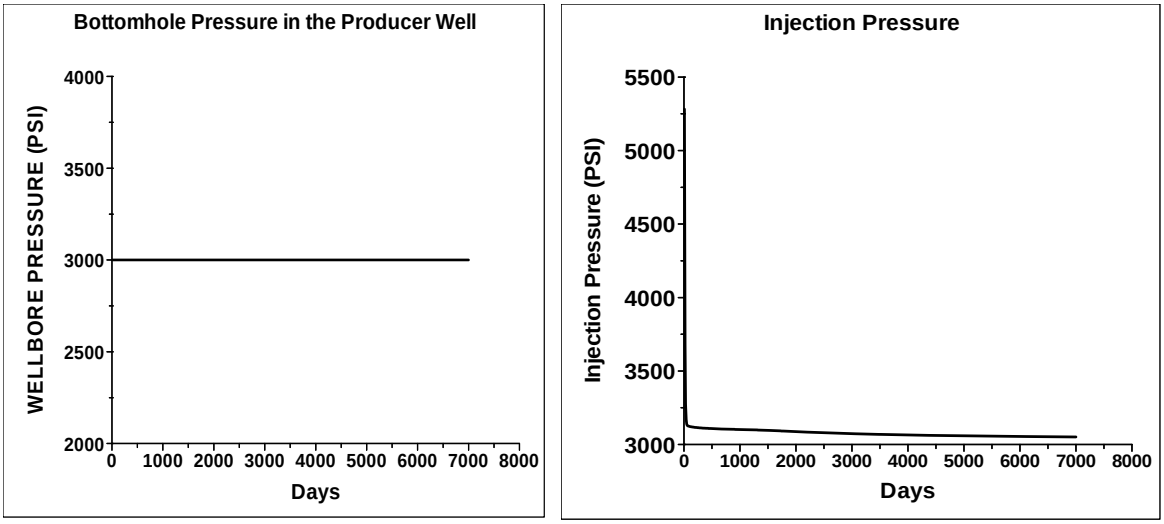

Figure 4-4 Bottomhole pressure profile at both producer and injector wells throughout the simulation time in Run 4.1

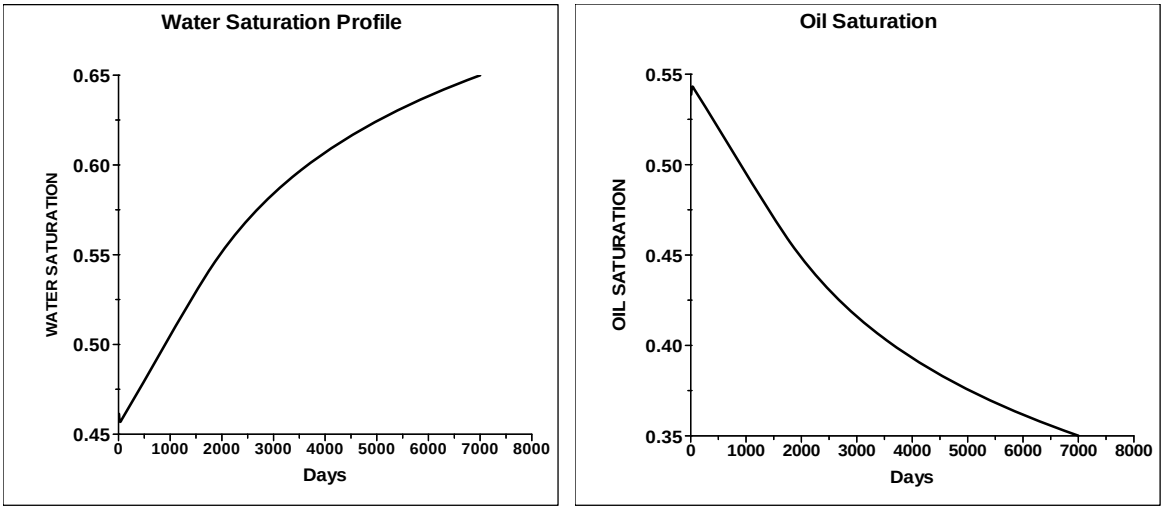

Figure 4-5 Average water and oil saturations vs. time in Run 4.1

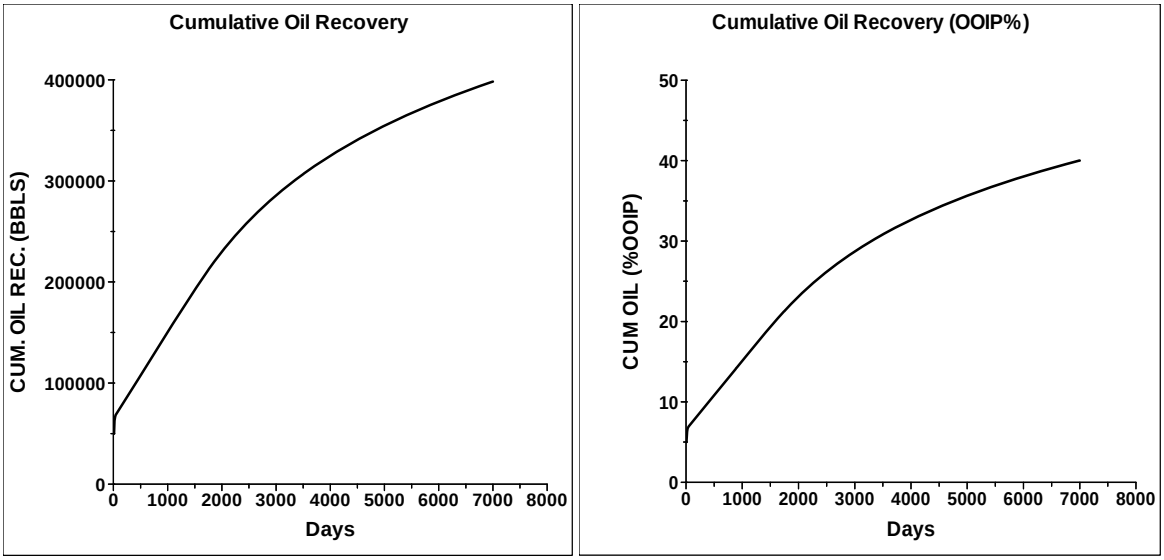

Figure 4-6 Cumulative oil recovery vs. time in bbls and as a percentage of original oil in place in Run 4.1

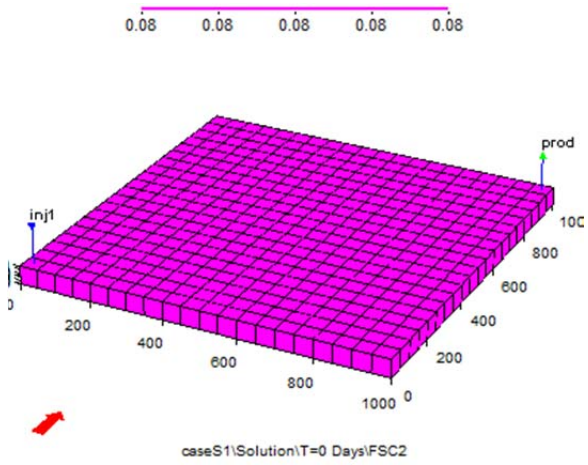

Figure 4-7 Initial Ba^{++} concentration before beginning the injection in Run 4.1

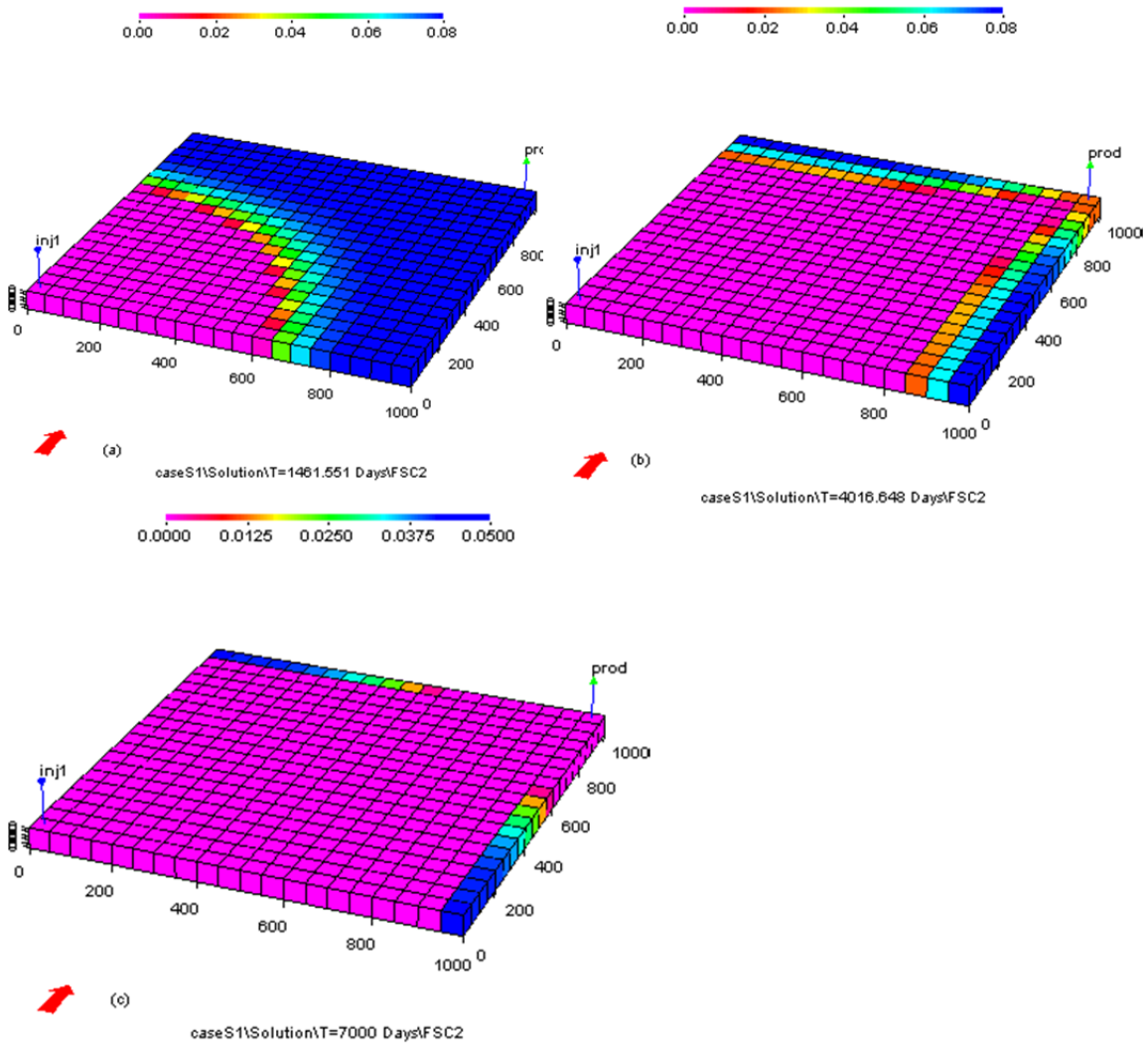

Figure 4-8 Ba^{++} concentration profile at (a) T=1460, (b) T=4016, and (c) T=7000 days in Run 4.1

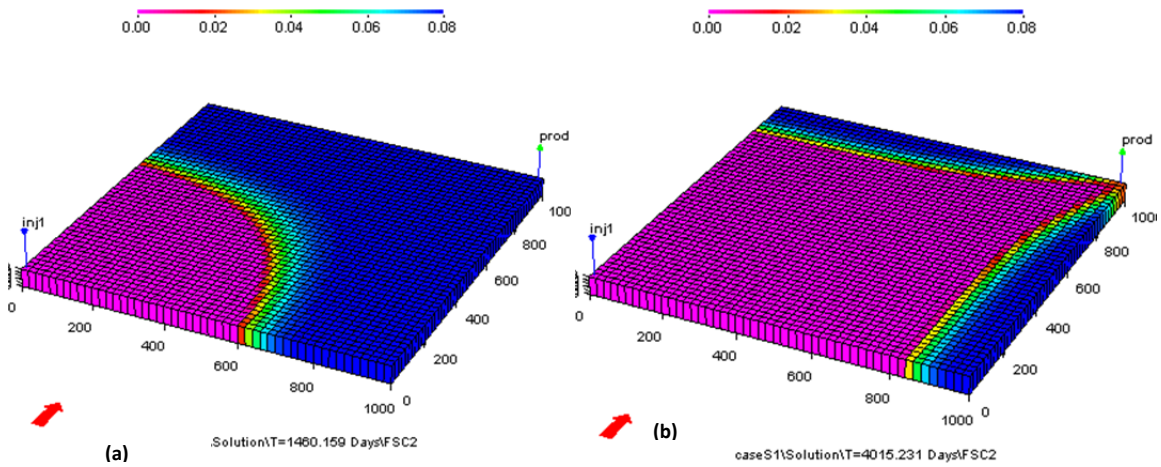

Figure 4-9 Injection front shape (Ba concentration) at (a) T=1460 and (b) T=4015 days using a smaller grid size (20') in Run 4.1

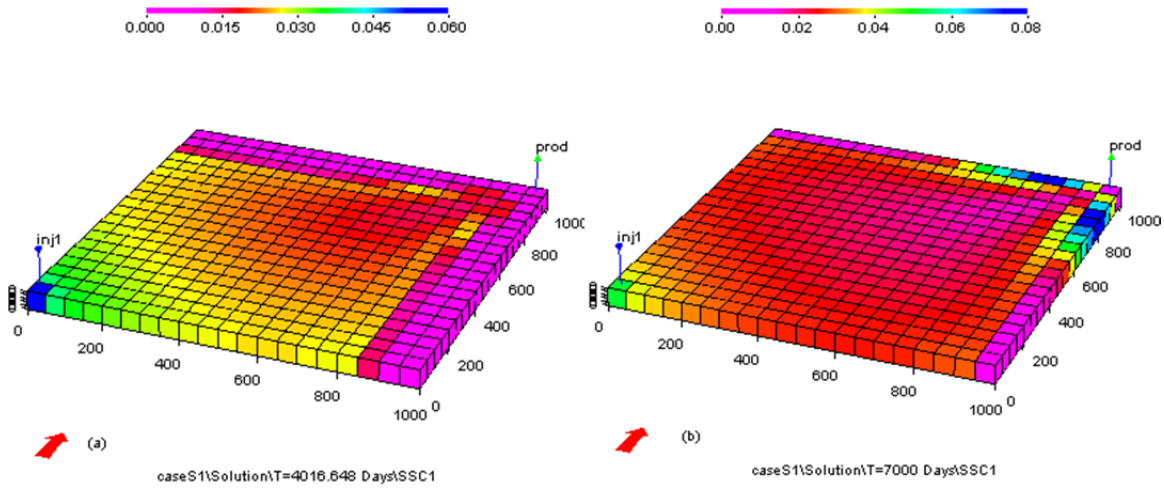

Figure 4-10 $BaSO_4$ concentration in the reservoir at (a) T= 4016 days and (b) T=7000 days with more solids accumulated at the near-wellbore toward the end of the simulation (in Run 4.1)

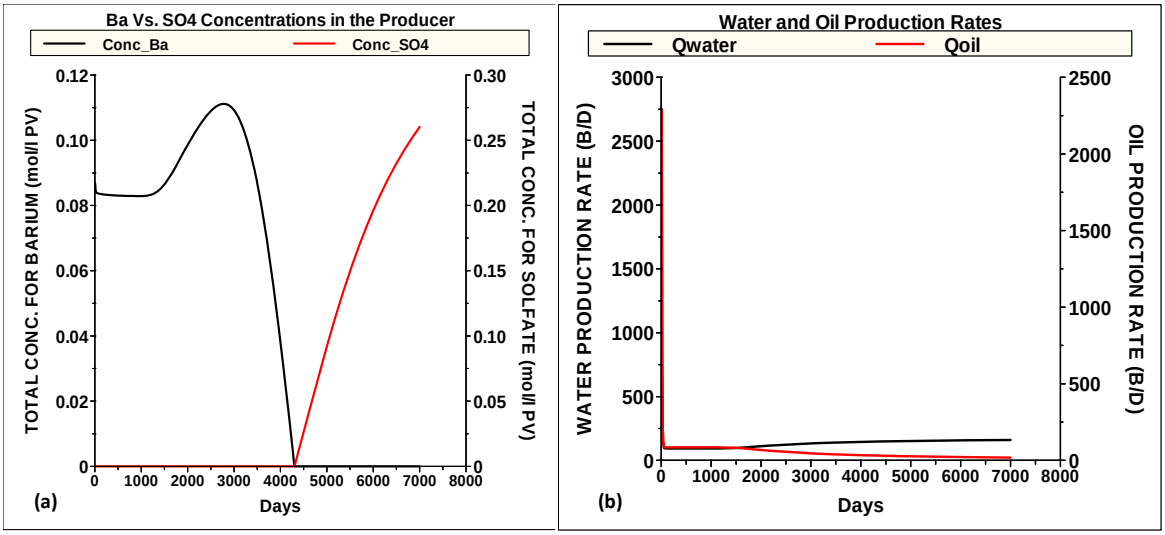

Figure 4-11 (a) $BaSO_4$ concentration profile in the producer well vs. time in Run 4.1. (b) Water and oil production rates vs. time in Run 4.1

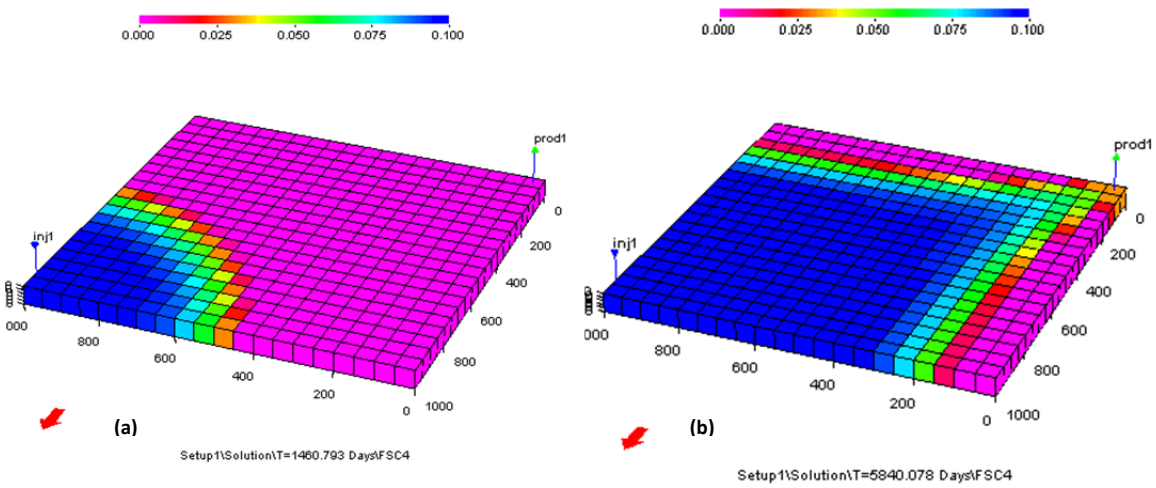

Figure 4-12 CO_3 concentration distribution after (a) T=1460 days and (b) T= 5840 days of continuous injection in Run 4.2

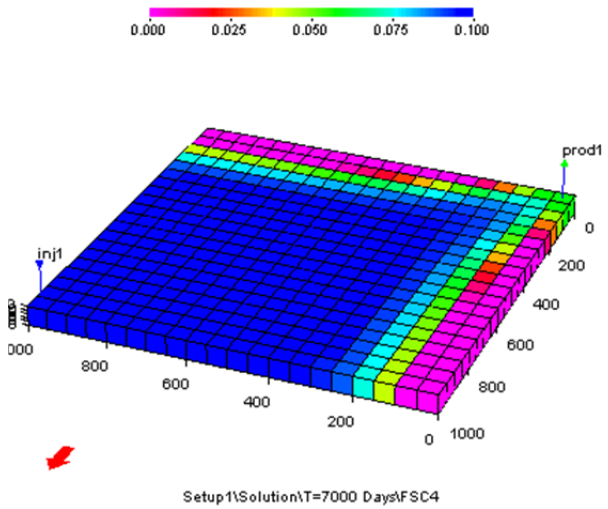

Figure 4-13 CO_3 dominates the majority of the field at almost the end of the simulation at T=7000 days (Run 4.2)

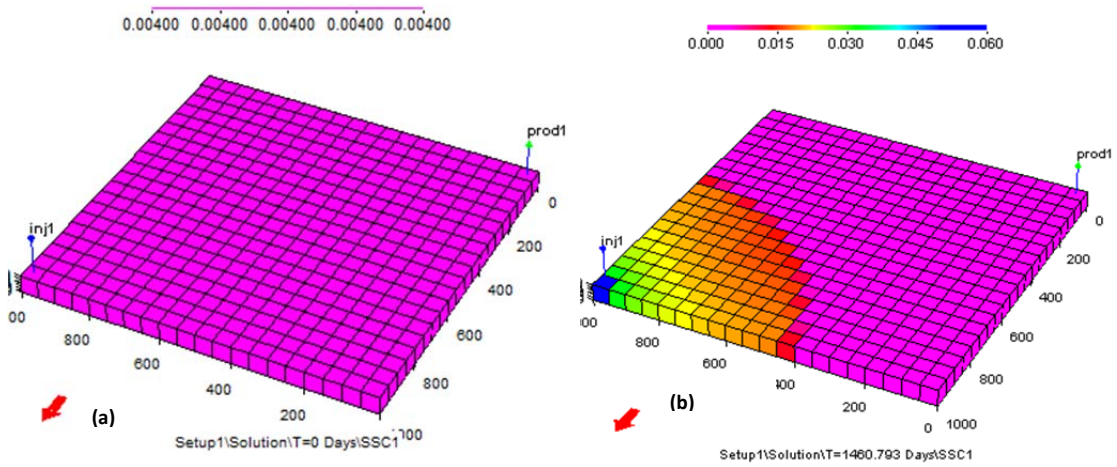

Figure 4-14 $CaCO_3$ at (a) T=0 and (b) T=1460 days. Note: we set the solid calcite to be zero, but the aqueous calcite at equilibrium is almost 0.004 mol/l from the other ions (Run 4.2)

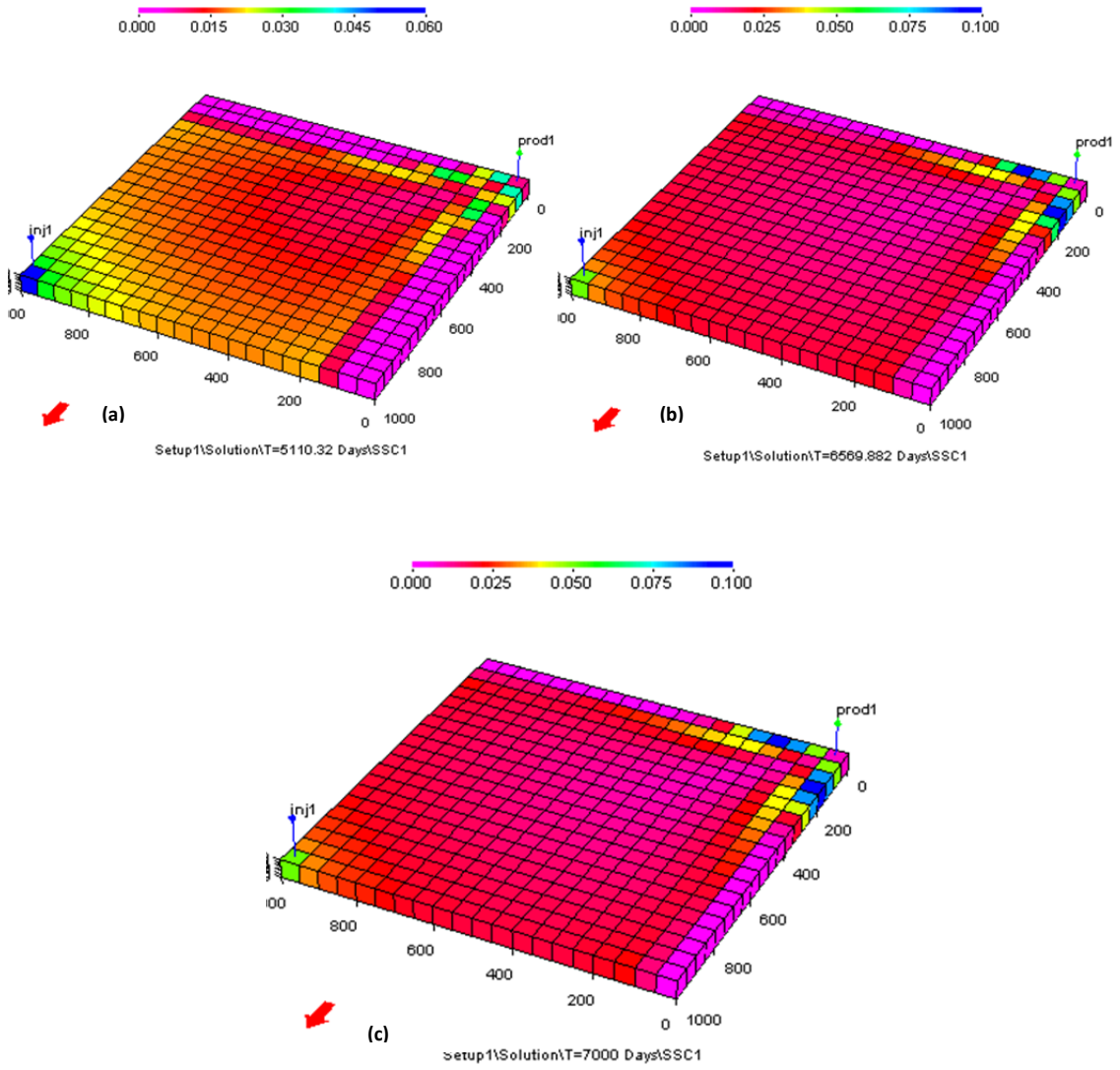

Figure 4-15 $CaCO_3$ Concentration profiles at (a) T=5110, (b) T=6569, and (c) T=7000 days. At T=5110 days, the precipitated $CaCO_3$ is more concentrated in the near-wellbore area. At 6569 days, maximum precipitation in the near-wellbore region is reached. In the remaining 500 days, calcite maintains a similar profile at the end of the simulation (T=7000 days) (Run 4.2)

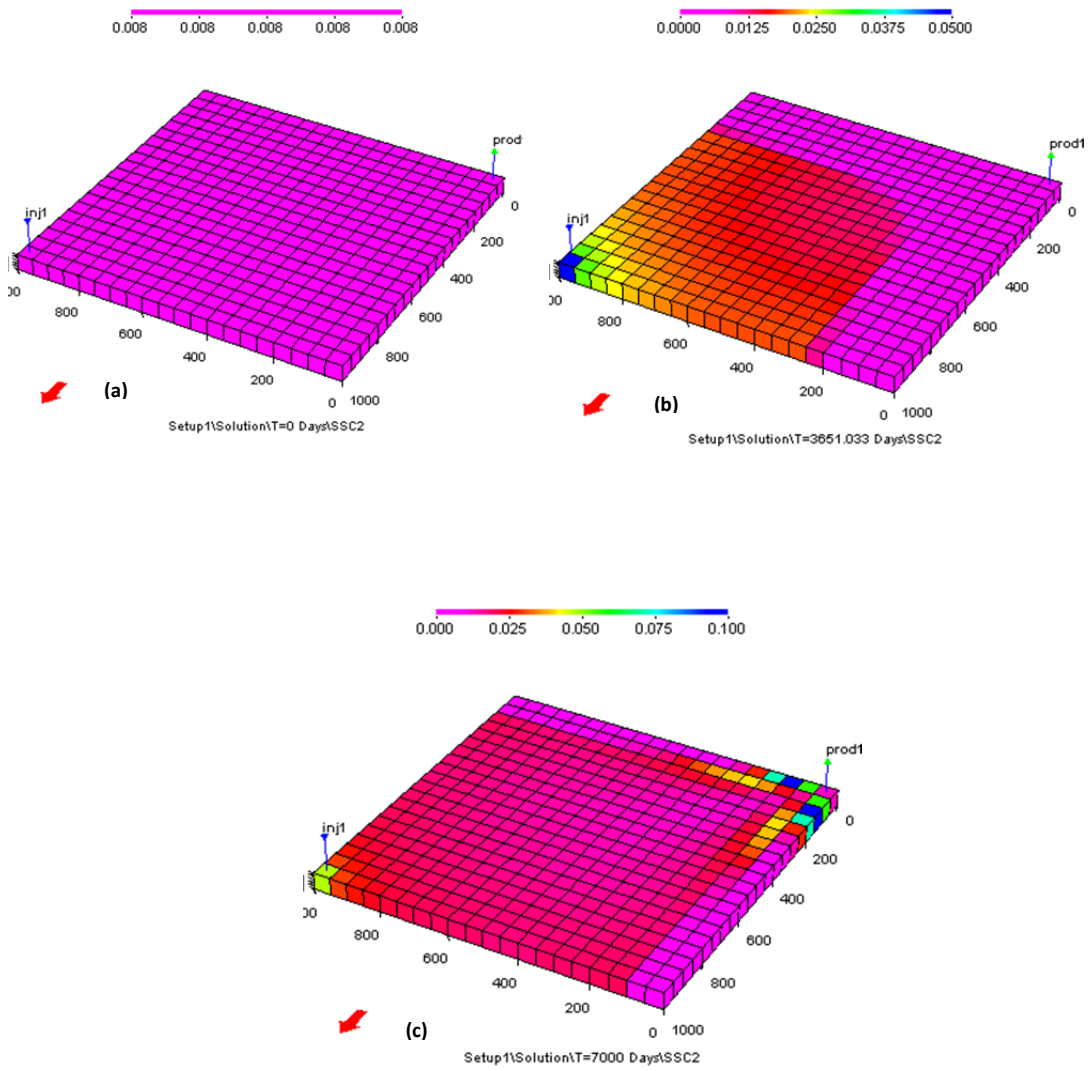

Figure 4-16 $BaSO_4$ concentration profiles at (a) T=0, (b) T=3651, and (c) T=7000 days (Run 4.2)

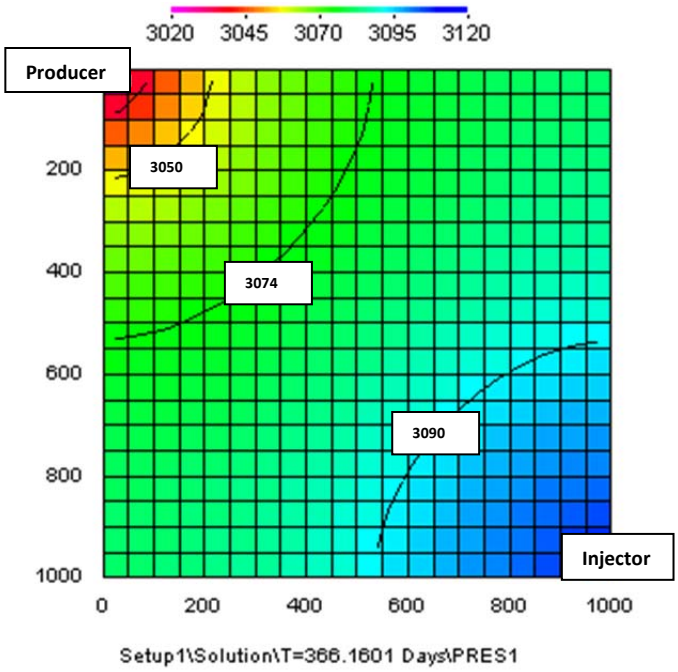

Figure 4-17 Reservoir pressure in a 2-D map (T=365 days) (in Run 4.2)

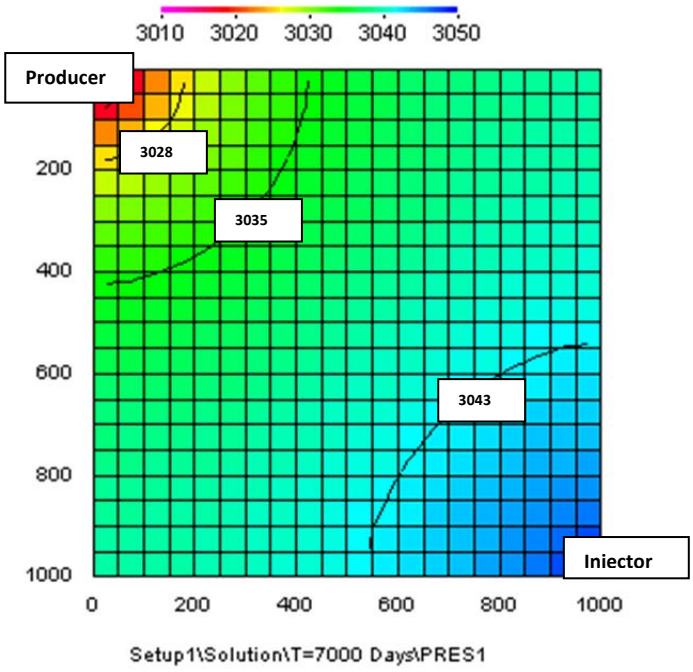

Figure 4-18 Reservoir pressure in a 2-D map at T=7000 days (Run 4.2)

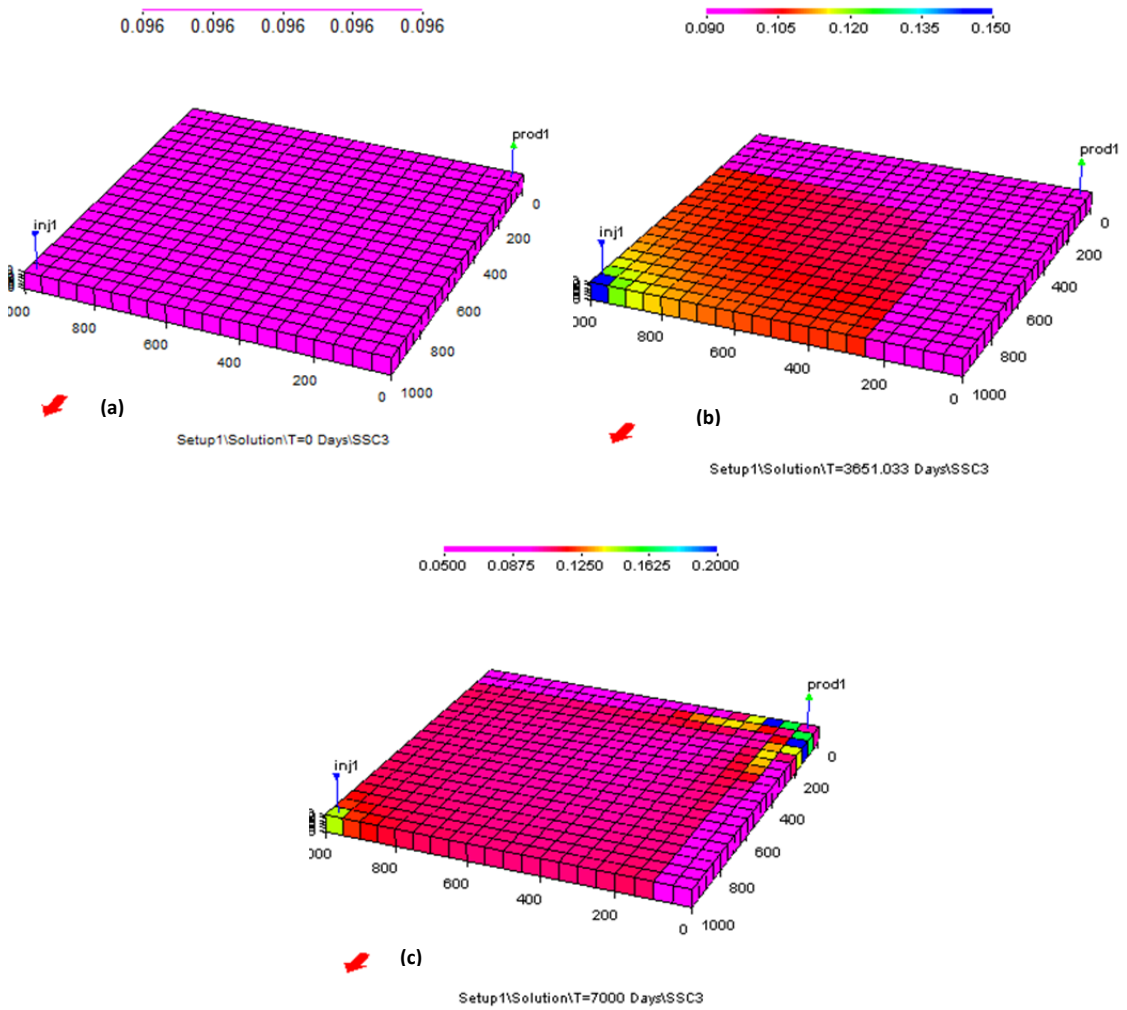

Figure 4-19 Iron sulfide profile at (a) T= 0, (b) T=3651, and (c) T=7000 days. Initially, the concentration was set to zero but equilibrium exists at 0.096 mol/l) (Run 4.3)

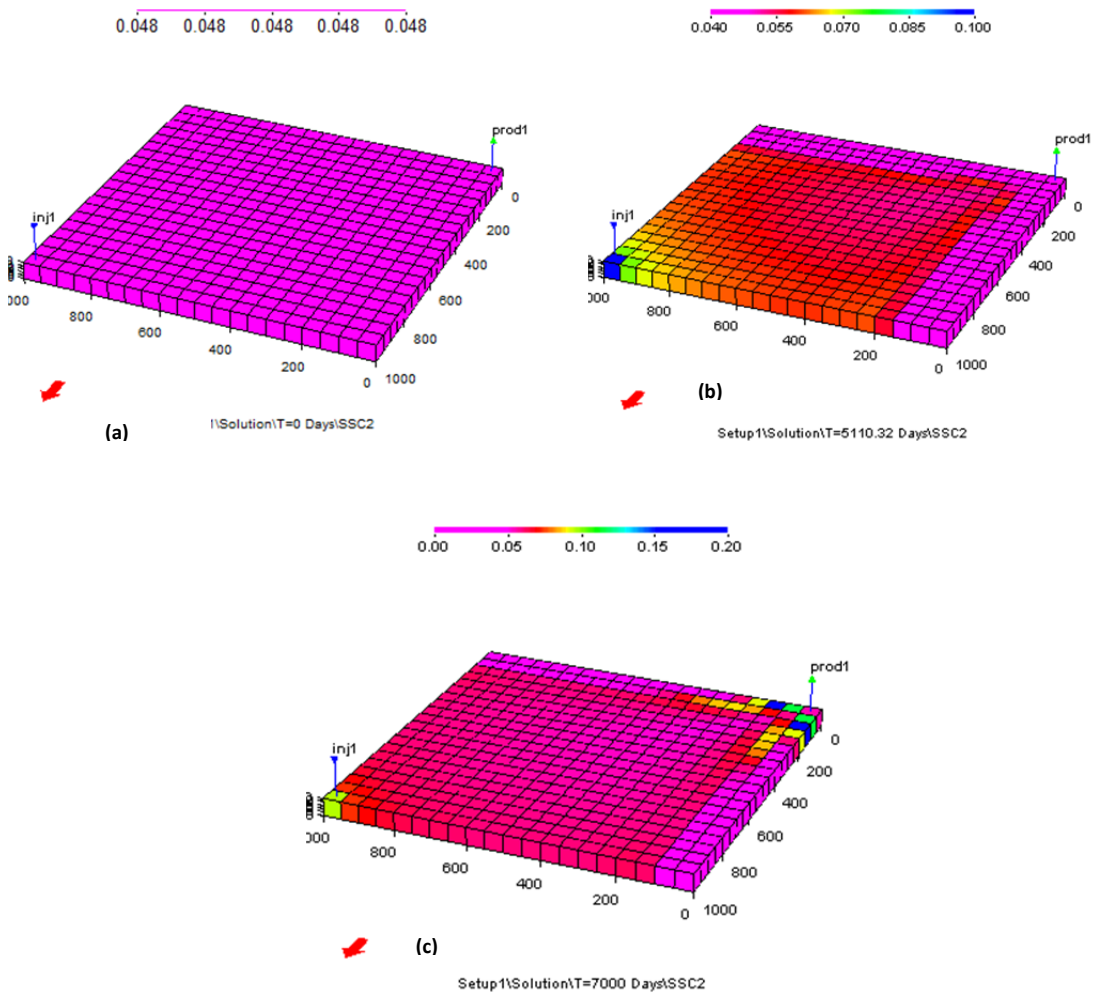

Figure 4-20 Barite at (a) T=0 , (b) T=5110 , and (c) T=7000 days (Run 4.3)

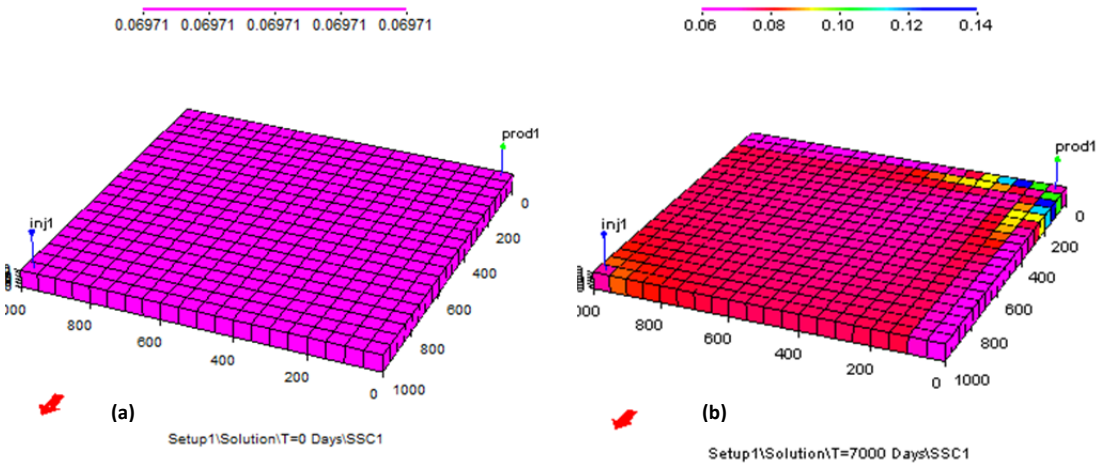

Figure 4-21 Calcite concentration profiles at (a) T=0 and (b) T=7000 days (Run 4.3)

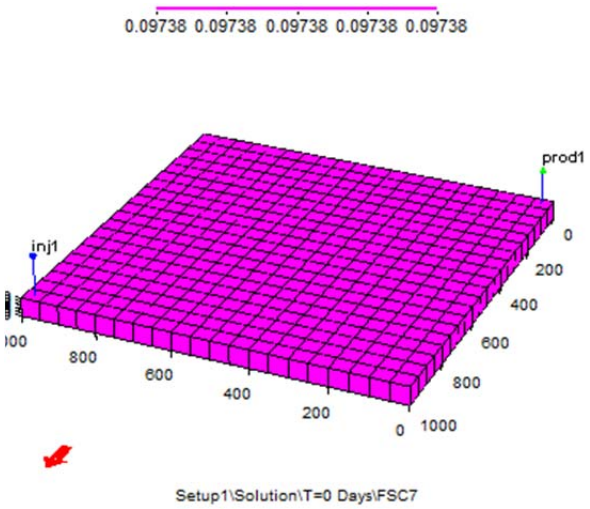

Figure 4-22 Iron [Fe^{++}] initially at equilibrium, [Fe^{++}] = 0.097 mol/l. Note: we consider that the reservoir is the iron source in this process (Run 4.3)

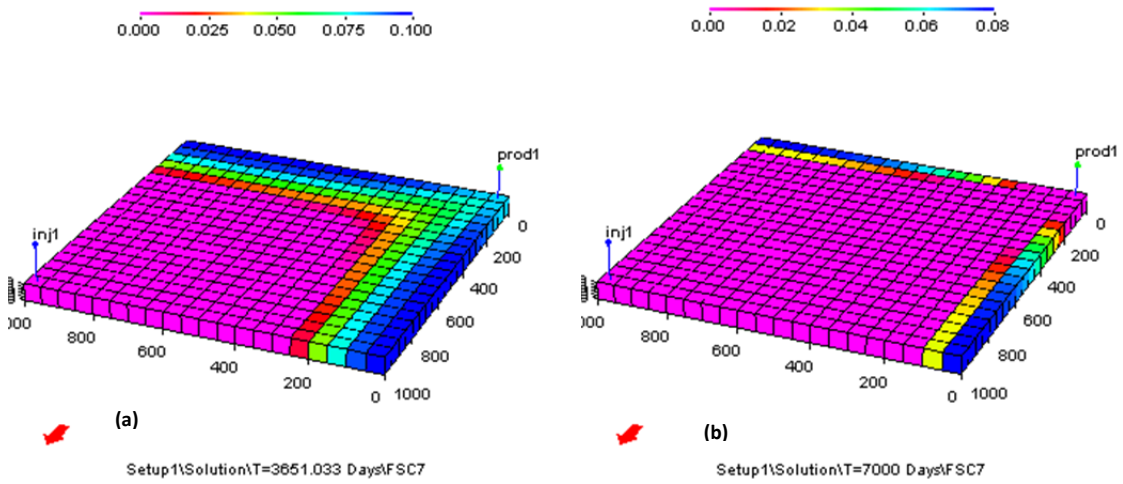

Figure 4-23 Iron [Fe^{++}] at (a) T=3651 and (b) T=7000 days (Run 4.3)

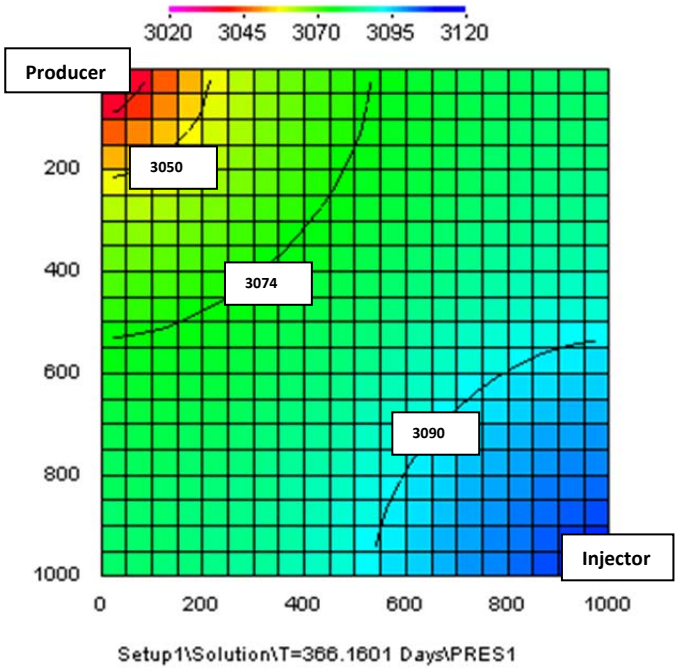

Figure 4-24 Reservoir pressure 2-D map (T=365 days) for Run 4.3

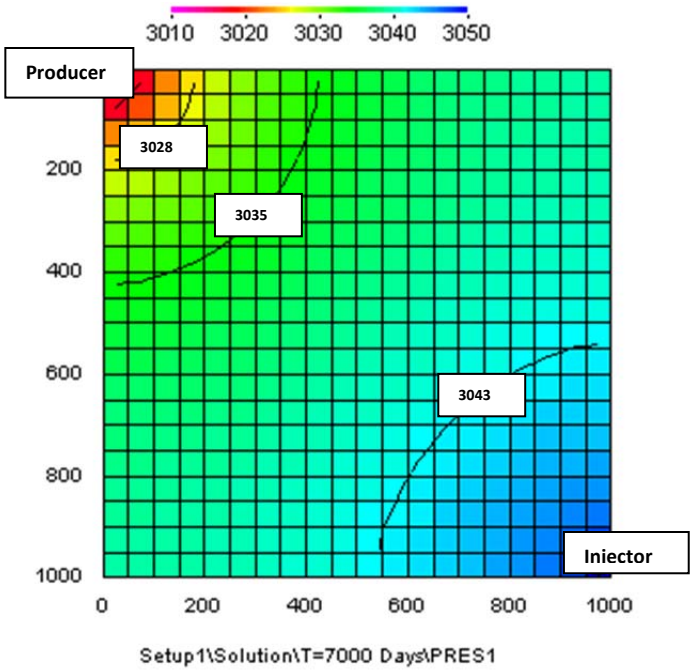

Figure 4-25 Reservoir pressure 2-D map at T=7000 days for Run 4.3

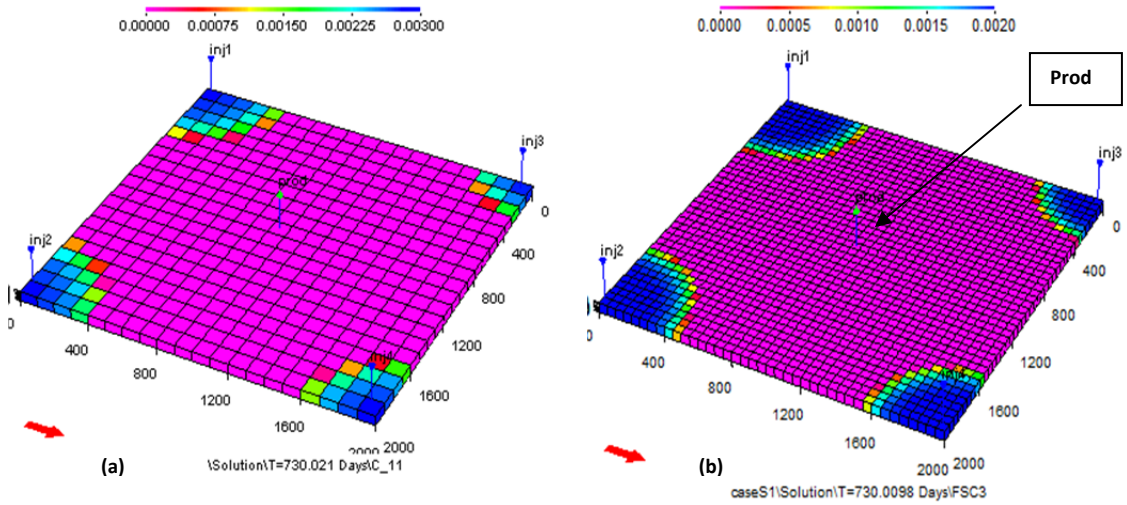

Figure 4-26 Sulfate-rich injection water front in (a) T=730 days using a 100' grid block compared to (b) T=730 days using a 50' grid block (Run 4.4)

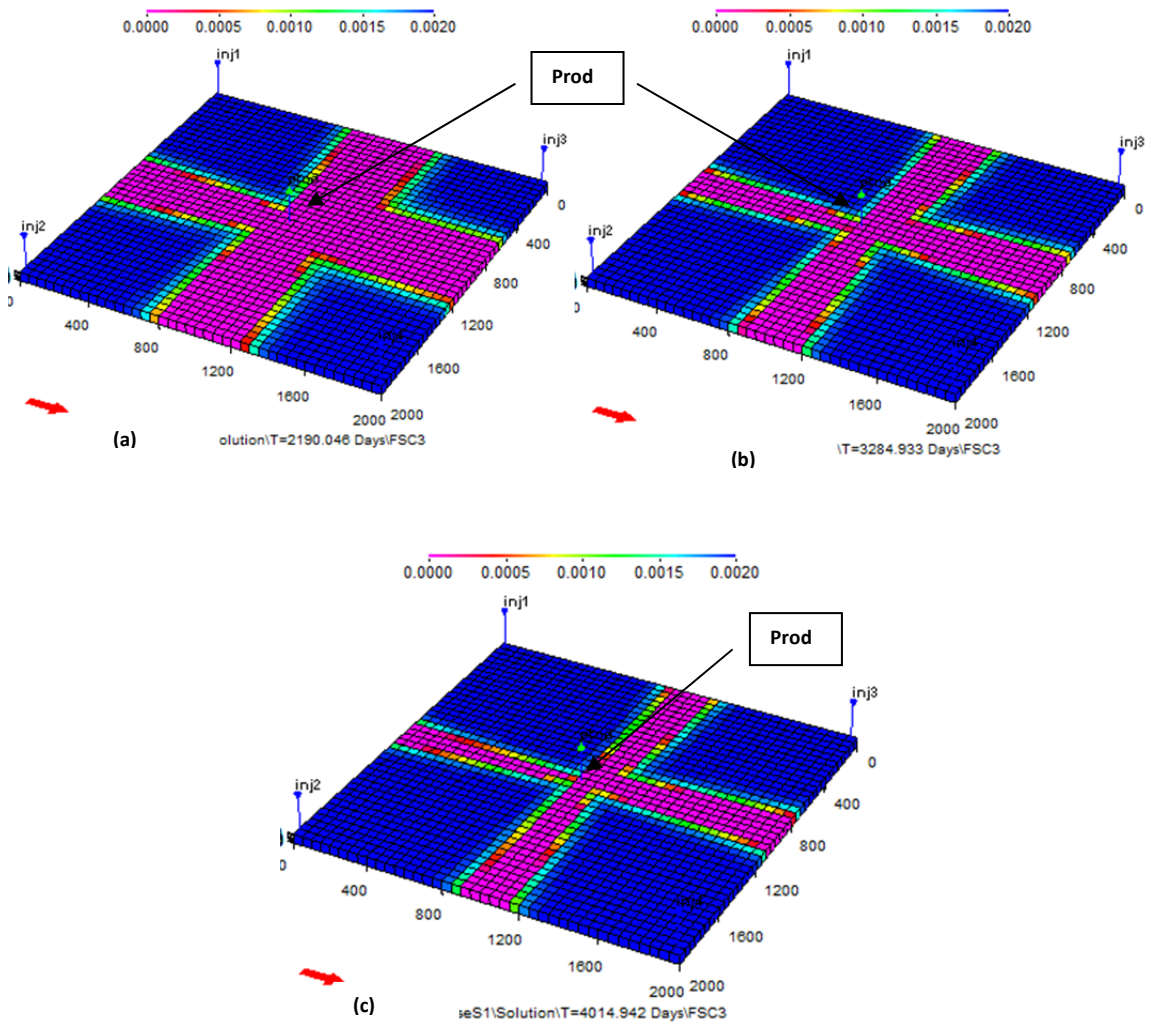

Figure 4-27 Sulfate concentration profile in the water fronts at (a) T= 2190, (b) T=3284, and (c) T=4014 days (Run 4.4)

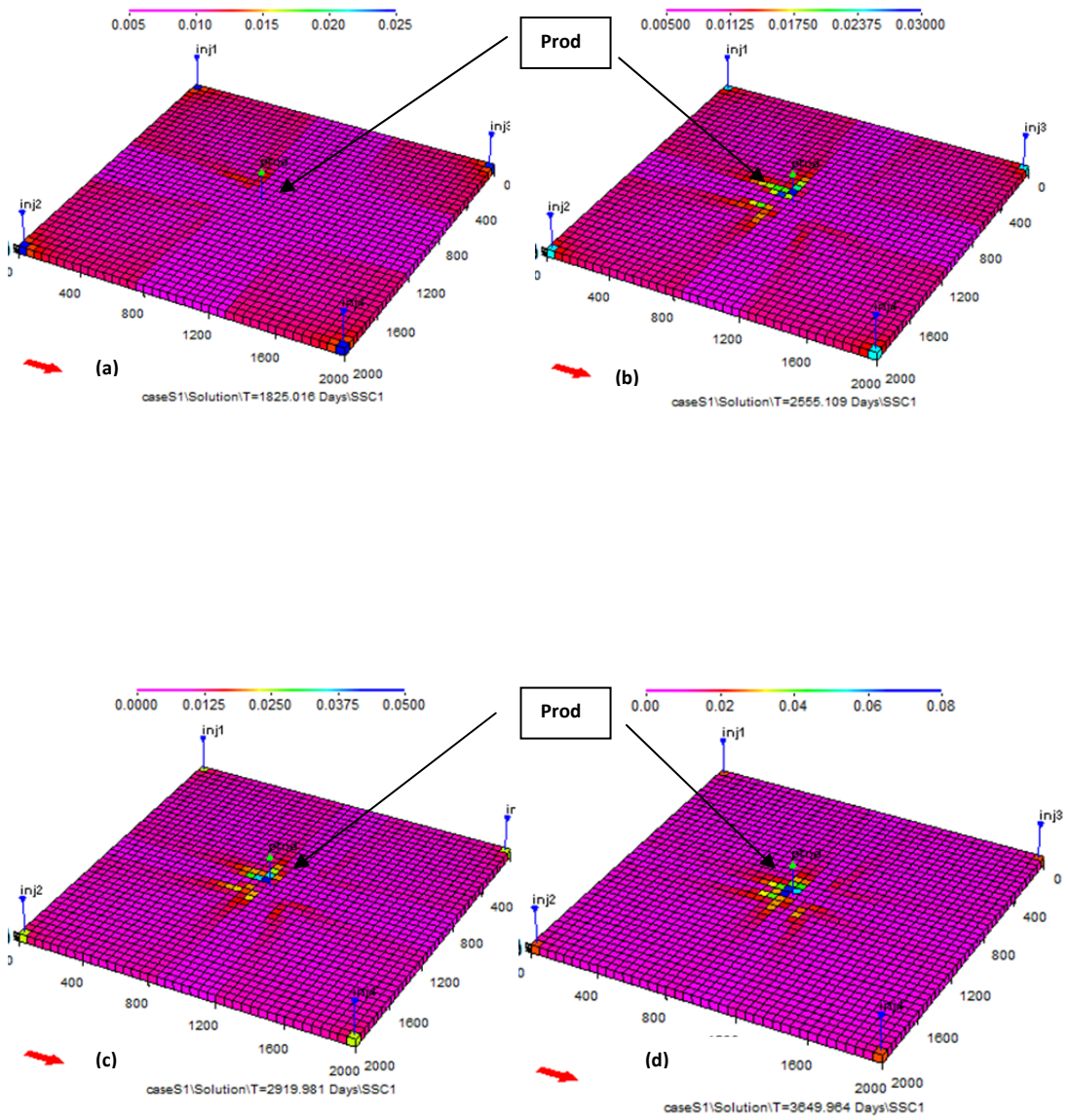

Figure 4-28 $BaSO_4$ precipitation progress at (a) T=1825, (b) T= 2555, (c) T=2919 and (d) T=3649 days (Run 4.4)

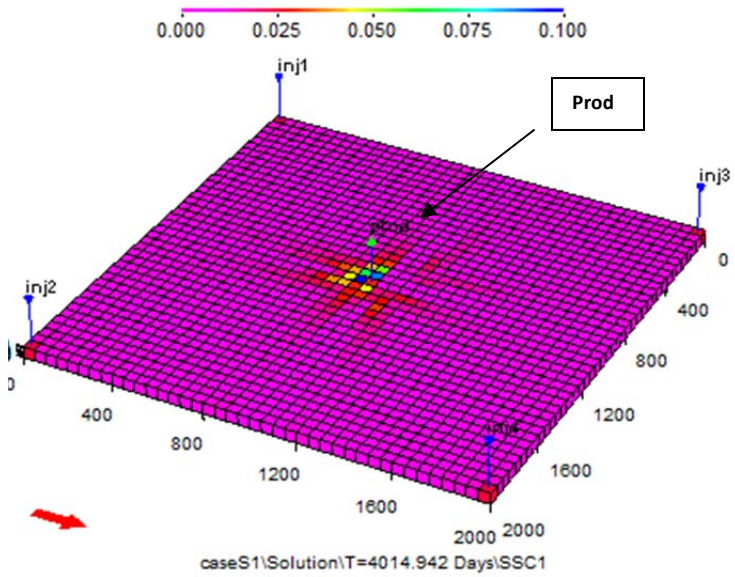

Figure 4-29 $BaSO_4$ concentration profile at T=4000 days (Run 4.4)

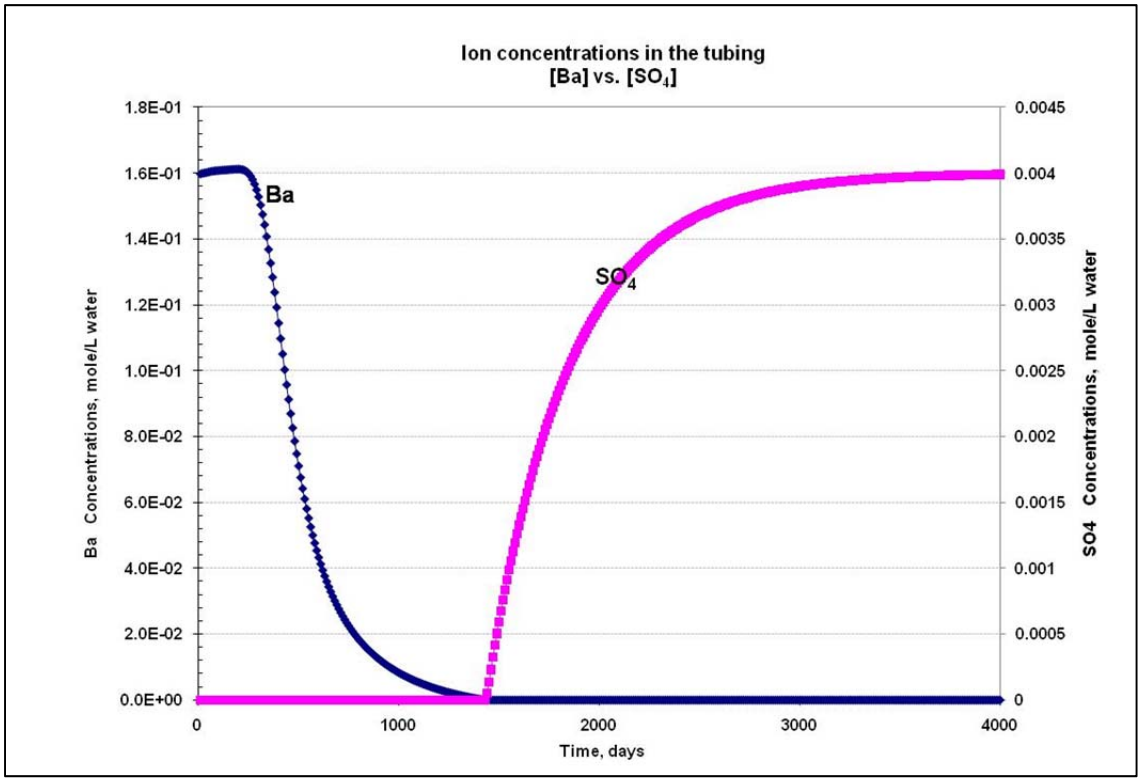

Figure 4-30 Ba and SO_4 concentration profiles in the producer well vs. time (Run 4.4)

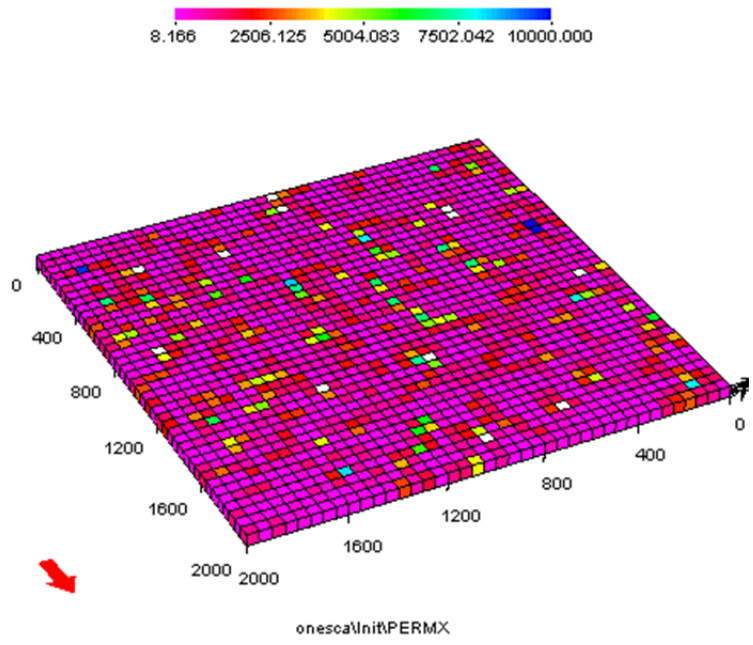

Figure 4-31 Permeability map used in Run 4.5

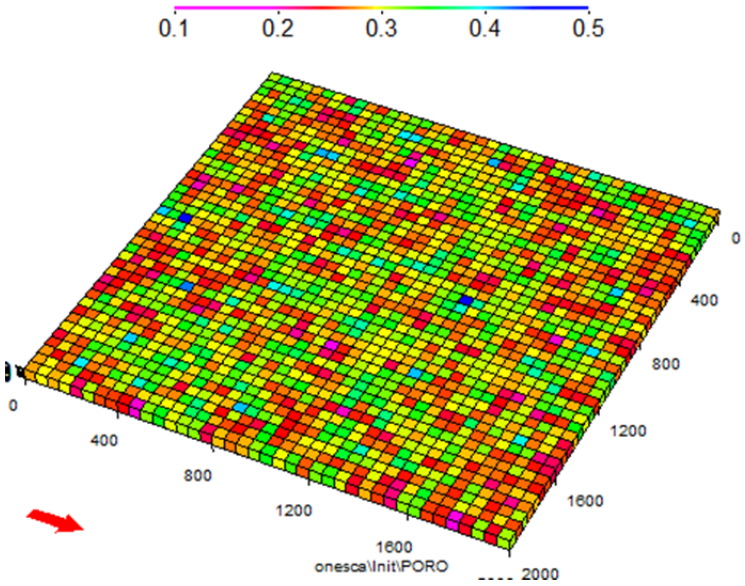

Figure 4-32 Porosity map used in Run 4.5

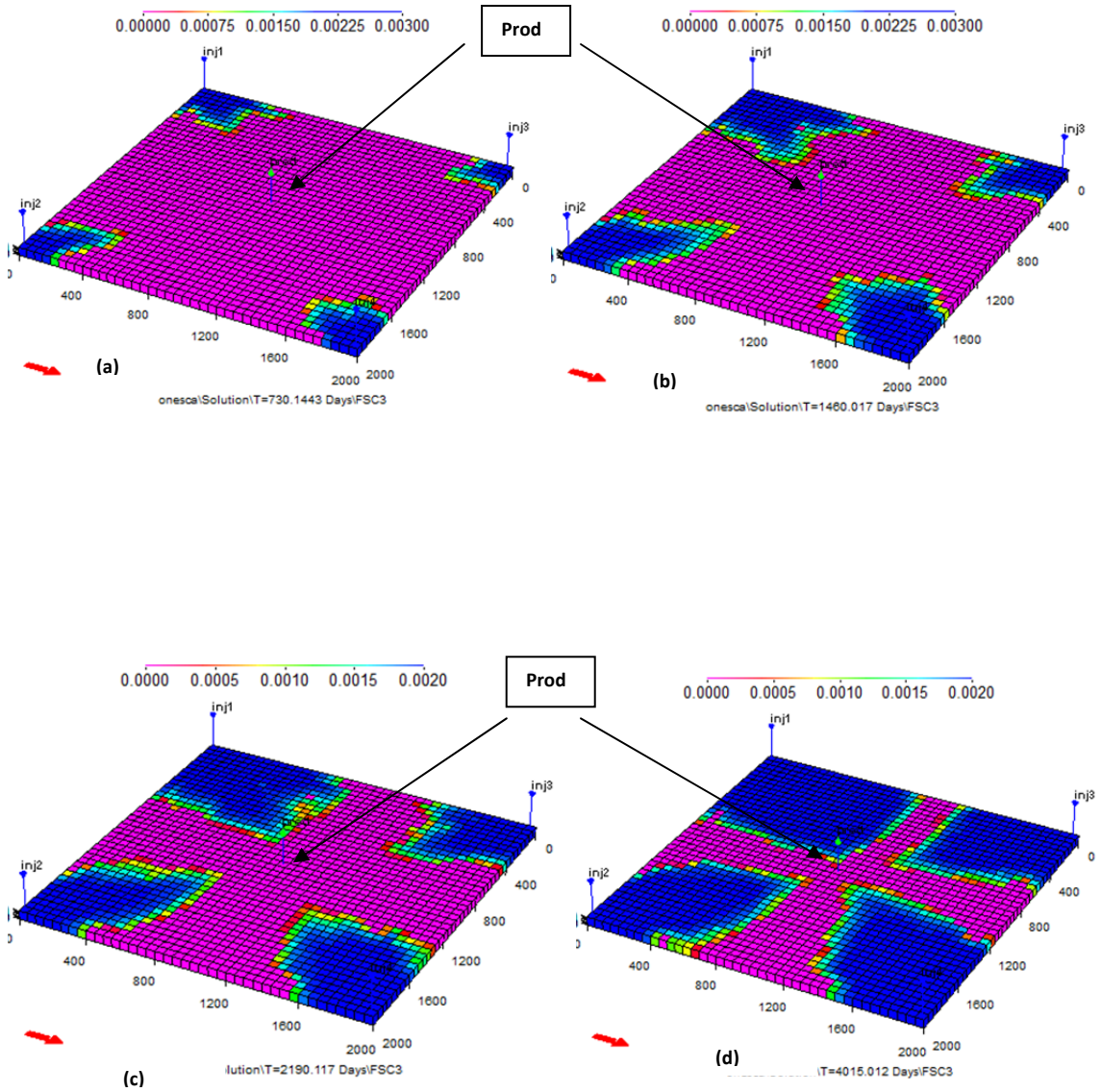

Figure 4-33 Sulfate rich injection water fronts in (a) T= 730, (b) T= 1460, (c) T=2190, and (d) T=4015 days (Run 4.5)

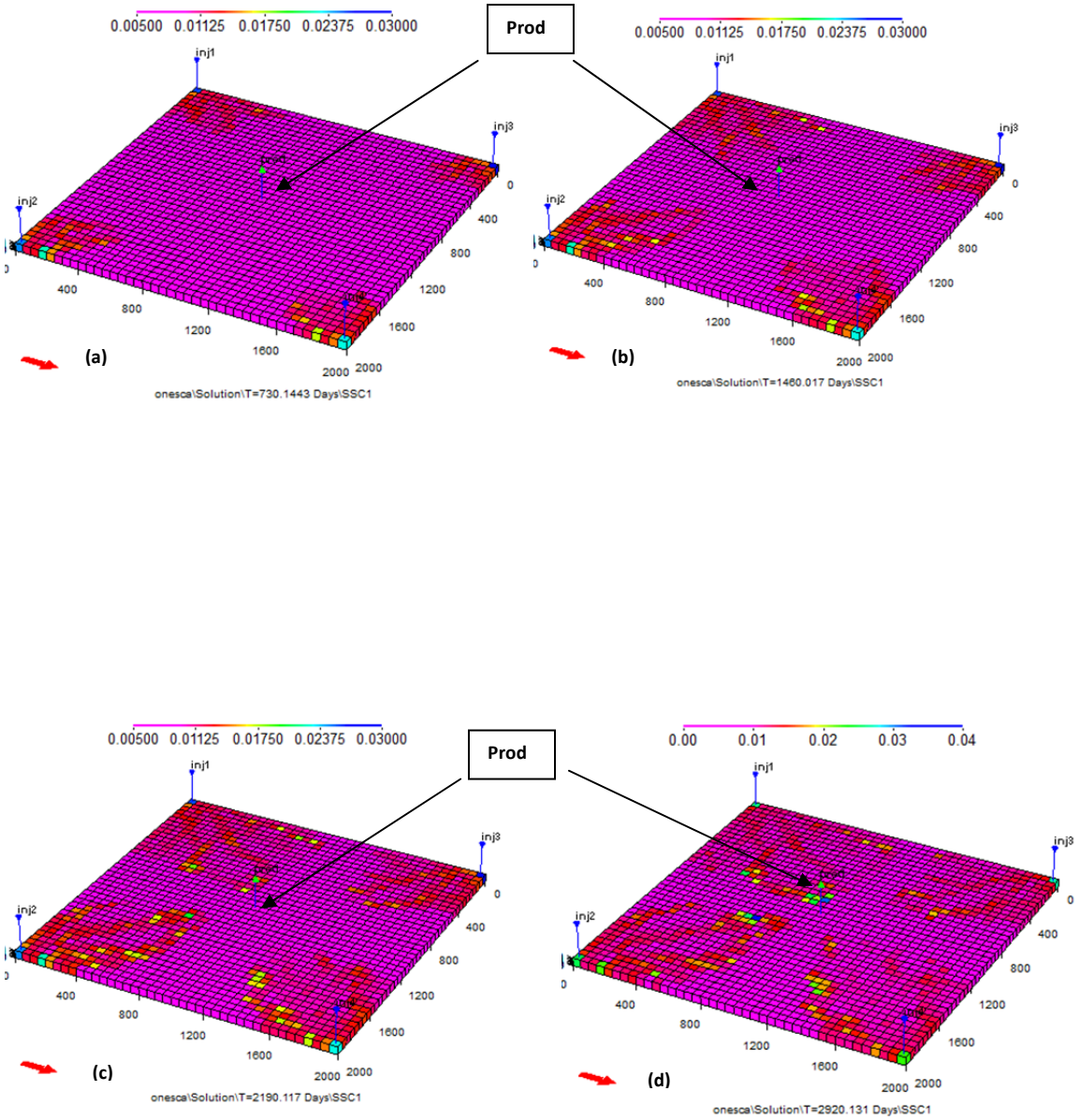

Figure 4-34 $BaSO_4$ concentration profiles in (a) T= 730, (b) T=1460, (c) T=2190, and (d) T=2920 days (Run 4.5)

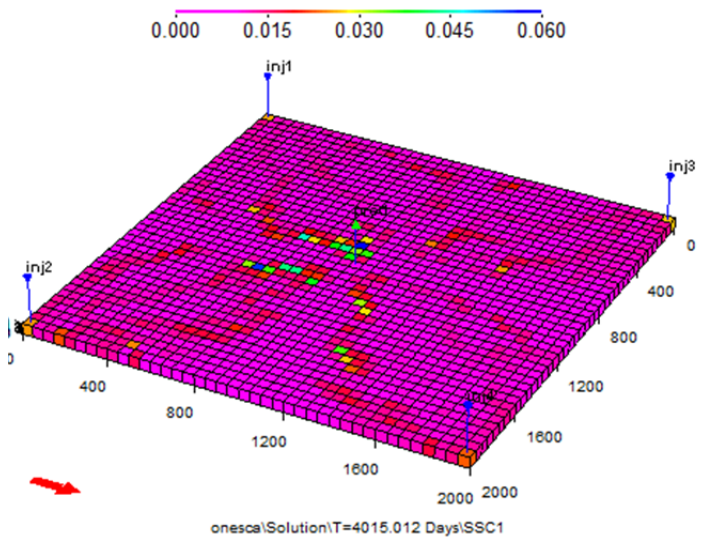

Figure 4-35 BaSO4 concentration profile in T=4000 days (Run 4.5)

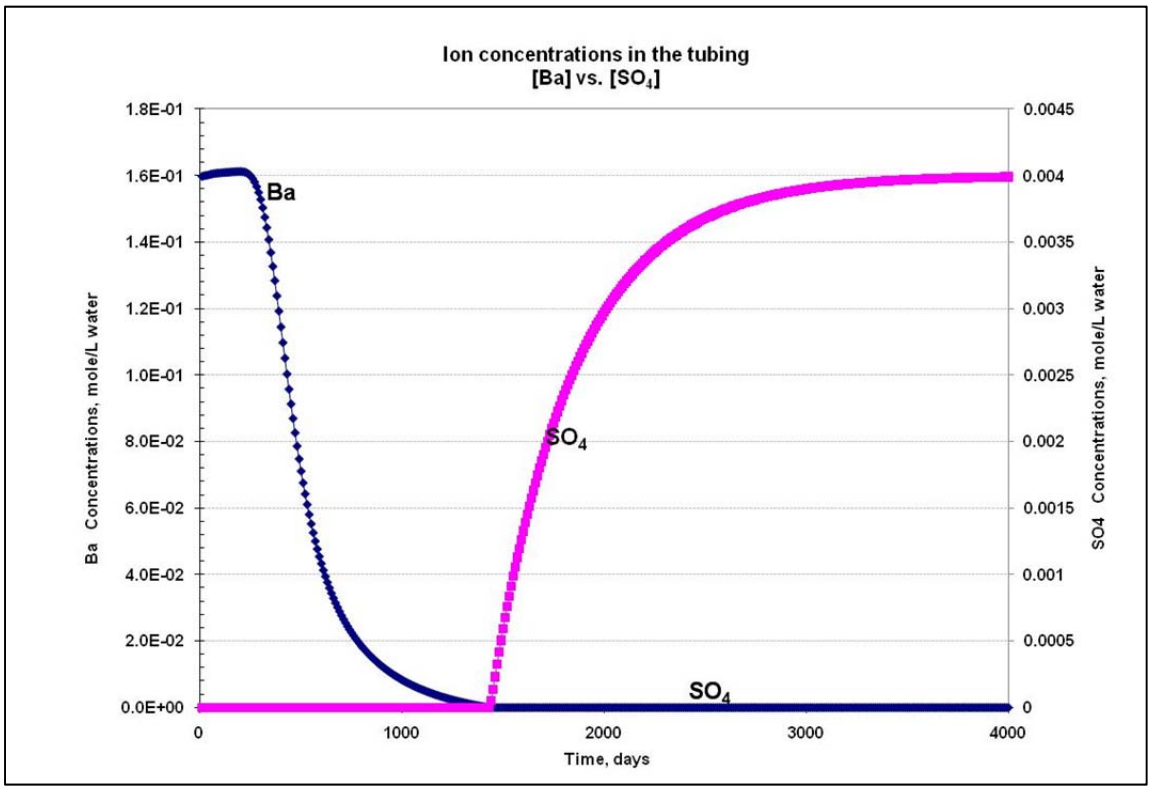

Figure 4-36 Ba and SO4 concentration profiles in the producer well vs. time (Run 4.5)

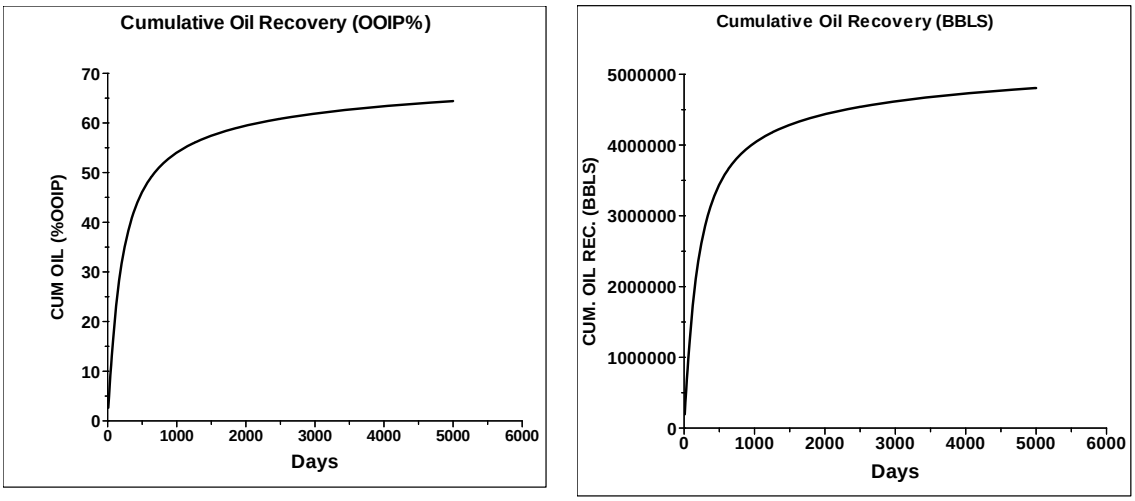

Figure 4-37 Cumulative oil recovery as a percentage of original oil in place and in bbls (Run 4.4)

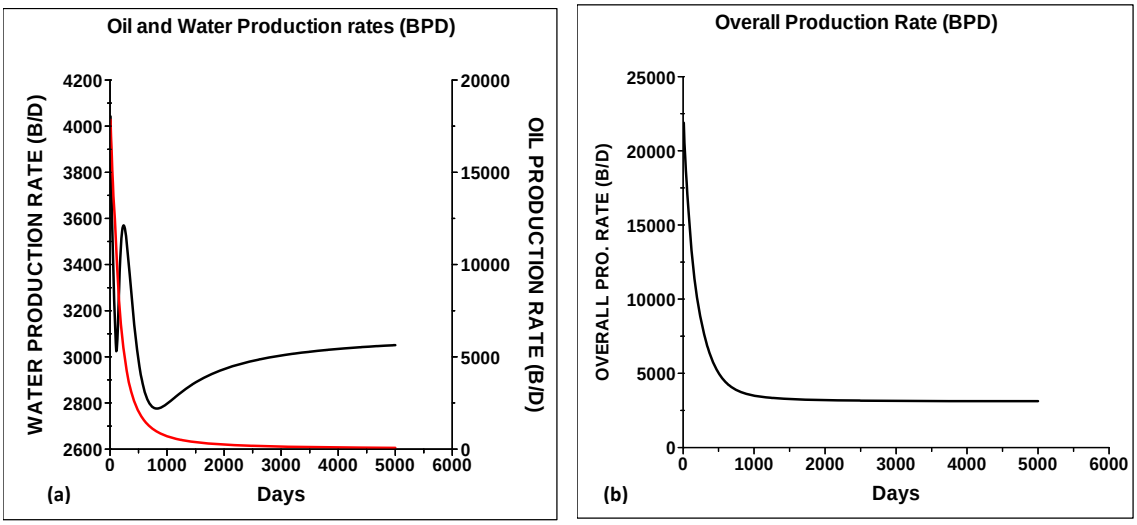

Figure 4-38 (a) Oil and water production rates and (b) Overall Production rate (Run 4.4)

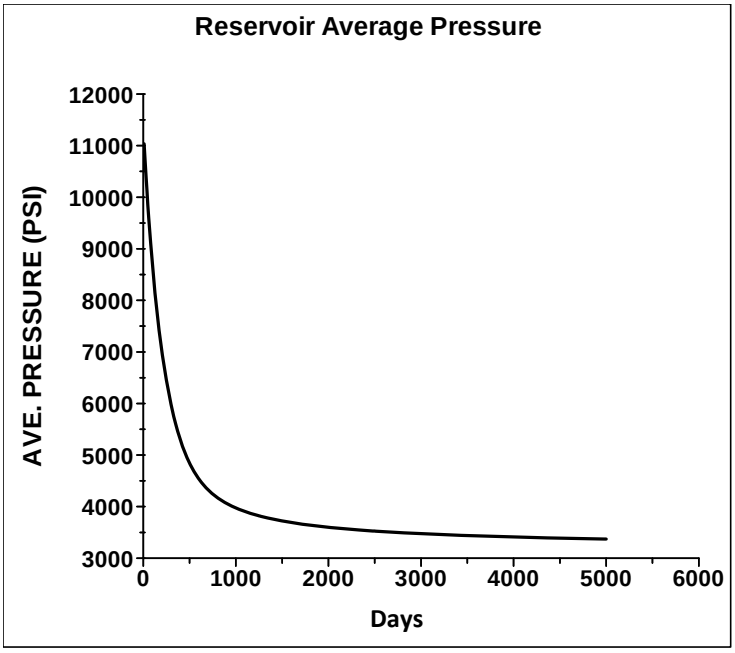

Figure 4-39 Reservoir average pressure for Run 4.4

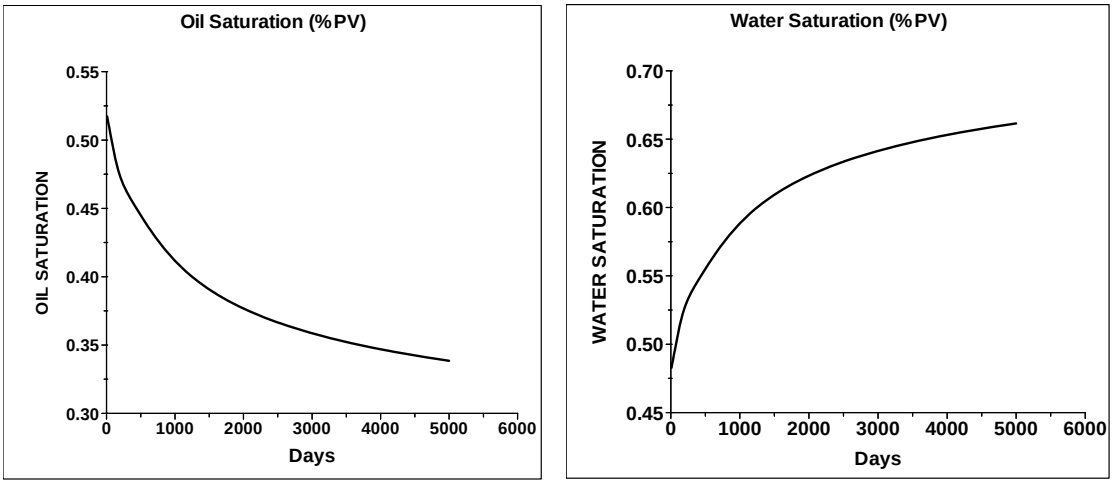

Figure 4-40 Oil and water saturation profiles for Run 4.4

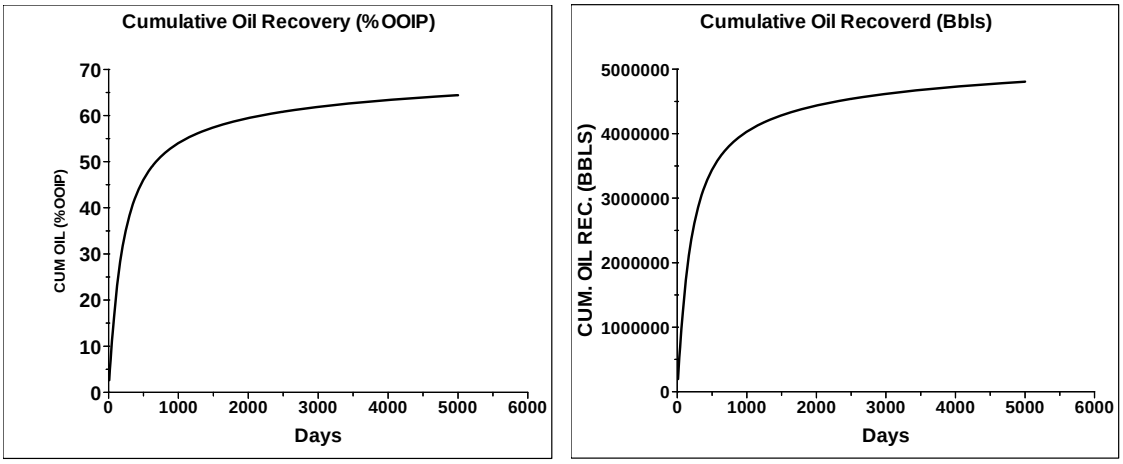

Figure 4-41 Cumulative oil recovery as a percentage of original oil in place and in bbls (Run 4.5)

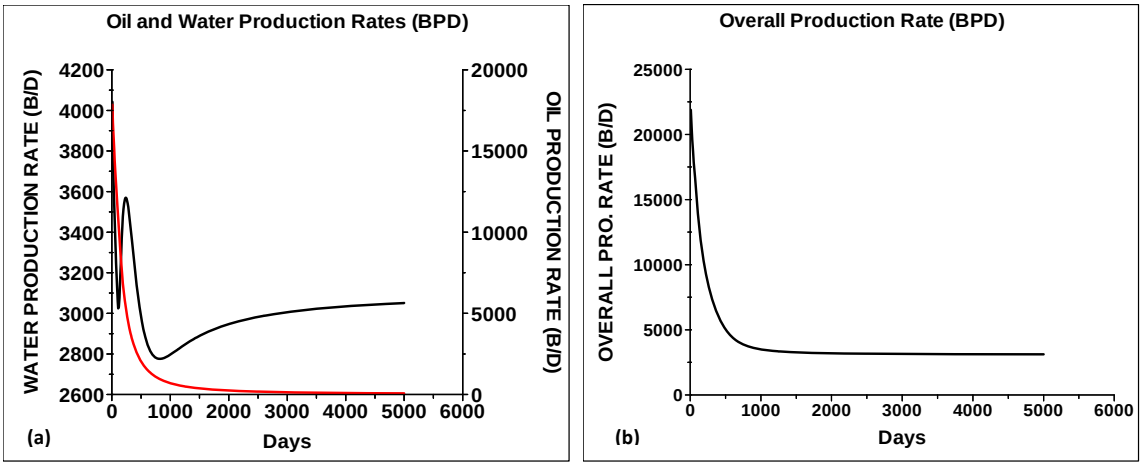

Fig. 4-42 (a) Oil and Water Production rates and (b) Overall production rate (Run 4.5)

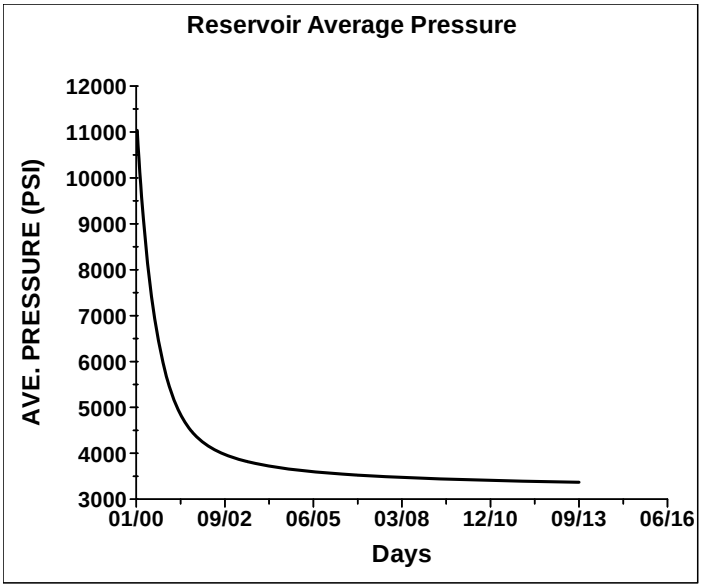

Figure 4-43 Reservoir average pressure for Run 4.5

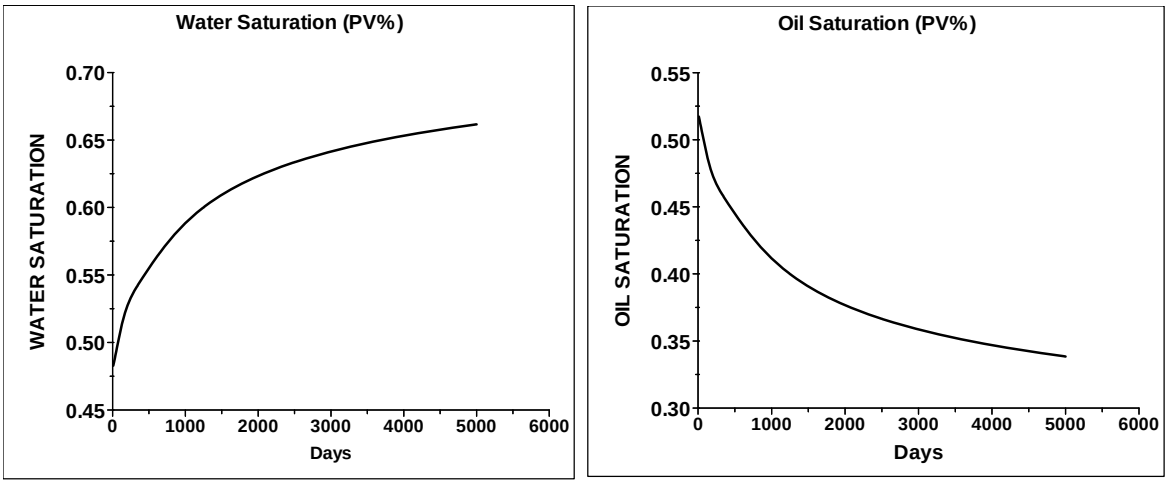

Figure 4-44 Water and oil saturation profiles for Run 4.5

Chapter 5 Remediation Simulation Runs

Hydrochloric acid has been widely used in treating calcium carbonates, but calcite may re-precipitate prematurely right after the dissolution in the acid. Following the dissolution of the metal ions, the natural tendency of calcium to bond again with carbonate is high and tends to increase as the acid is spent (as pH increases). Adding chelating solutions to the acid treatment can offset this tendency (Frenier and Ziauddin, 2008). A classic example of chelatants is Na2H2 ethylenediaminetetraacetic acid (EDTA).

5.1 Description of the EDTA Reaction with Calcite

In general, EDTA is capable of forming strong bonds with divalent cations such as calcium or barium. However, EDTA is most effective in chelating carbonate scales as opposed to sulfates, since the sulfates has a higher precipitating rate. For that reason, calcite was selected in the following simulations to show the effect of chelatants in remediating scales. According to Shaughnessy and Kline (1983), this chelating agent's structure undergoes a series of dissociation steps in which it loses four hydrogen protons to reach the fully ionized active complex. The four steps of this reaction along with their equilibrium constants are listed as follows:

$$H_4Y \rightleftarrows H^+ + H_3Y \qquad K_1 = 10^{1.7} \tag{5-1}$$

$$H_3Y \rightleftarrows H^+ + H_2Y \qquad K_2 = 10^{2.6} \tag{5-2}$$

$$H_2Y \rightleftarrows H^+ + HY \qquad K_3 = 10^{6.3} \tag{5-3}$$

$$HY \rightleftarrows H^+ + Y^{-4} \qquad K4 = 10^{10.6} \tag{5-4}$$

where (Y) denotes the EDTA compound.

The active molecule (Y^{-4}) then bonds with the dissolved Ca^{++} to form the calcium/chelate compound (CaY^{-2}). In this reaction, only one chelate molecule is needed for each calcium atom as shown below:

$$Ca^{++} + Y^{-4} \rightleftarrows CaY^{-2} \quad (5\text{-}5)$$

The equilibrium constant for this chelate molecule is 5.00×10^{10} while the aqueous $CaCO_3$ is 1.58×10^{3}, which explains the higher affinity with the EDTA. The remediation of calcite using EDTA was investigated using three different setups as shown in Sections 5.1.1, 5.1.2, 5.1.3.

5.2 Simulating Calcite Remediation with EDTA Using the Quarter 5-Spot Reservoir Model

This is a synthetic scenario to simulate the dissolution and chelating action of EDTA using a quarter 5-spot reservoir. Tables 5-1 and 5-2 list the input data used to create this case. In this simulation, we assume that the reservoir is already damaged by calcite and that EDTA is being injected at 0.025 mol/l pv (pore volume) as part of the remediation measure. The initial calcium – to – carbonate ratio in the system is 2:1 as shown in Table 5-3. The initial chloride concentration was set at 0.4 mol/l pv to create a basic environment which is favorable to deposit calcite. The metal ions usually become less soluble in basic solution (pH >7) so it is important to pay attention to the composition of the initial in-situ water. In this case, chloride as a parameter was used to adjust the acidity of the solution. Based on the calculations performed by EQBATCH, the aqueous hydrogen concentration [H^+] resulting from this setup is about 0.3×10^{-8}. Therefore, $pH = -\log[H^+] = -\log[0.3 \times 10^{-8}] = 8$, which confirms the basicity of this solution.

As shown in Figure 5-5, the calcite concentration is about 0.1 mol/l pv since the brine is in an oversaturated state. Figure 5-1 shows the calcium ion concentrations at T=0, 100, 300, 1600 days of injection and illustrates the chelating action that is taking place in the reservoir. Over time, more $CaCO_3$ is being converted to CaY^{-2} by the continuous injection of EDTA. In 300 days, 50% of the reservoir is swept and cleaned. Figure 5-1 also shows that all but small traces (0.003 mol/l) of calcite is completely removed in 1600 days.

Figure 5-2 shows that carbonate initially does not exist alone, but instead, is part of the calcite deposition. The dissolution and chelation occur concurrently as the solids are stripped of their calcium ions. This leads to leaving carbonates to build up (the concentration reaches as high as 0.03 mol/l pv). The continuous injection then pushes this carbonate toward the producer as shown in Figures 5-2 and 5-3. Figure 5-4 shows the remediation flooding, which advances in a rate analogous to the retreating front for calcium.

The overall accumulation of carbonates (as more carbonates are pushed toward the producer) means the un-swept parts of the reservoir now have enough carbonate to precipitate with calcium. This temporary premature precipitation has added to the initial calcite elevating the concentration to a maximum of 0.15 mol/l pv in the un-treated region at T=200 days, as reflected in Figure 5-5. At a larger treated area, the reservoir will be less saturated with $CaCO_3$, because more calcium is being converted into Ca-EDTA while carbonate is being produced.

5.3 Simulating Calcite Precipitation/Remediation Using a Two 5-Spot Well Spacing and a Real Geological Model

After proving the concept of remediation, another simulation is performed this time using a real geological model. A two 5-spot system, which consists of two injectors and six producers, was added to the input file. The purpose of this study is to show the effect of EDTA in a larger scale using a heterogeneous geological model. This geological section is 3,360' long in the X-direction and 27,878' in the Y-direction, using grid sizes of 210' and 263', respectively. The dimension in the Z-direction varies from 4' to 48.5'. Figures 5-6 and 5-7 show the horizontal permeability, porosity, and water saturation in a 3-D representation. Figure 5-8 shows the water saturation map and the spacing pattern for the wells. Tables 5-4 and 5-5 summarize the input data used for this geological model. Although the reservoir model resembles a real case, the well setup is synthetic. Wells were intentionally placed in the center of the field where the average water saturation is about 58%, because an abundance of ground water is preferred to create an ideal environment for in-situ calcite scaling.

Remediation simulations assume that deposition has already developed and that simulation starts once EDTA is pumped. Figure 5-9 shows the initial $CaCO_3$ precipitates in the system right before the injection (simulation) to resemble the situation in which the field has been produced for years. Table 5-6 describes the chemical composition of both formation and injection brine. Figure 5-10 shows a snapshot of calcite development without EDTA inclusion in the injection at a time of 2500 days. To confirm the effectiveness of EDTA, the simulation was repeated by injecting a treatment fluid composed of 0.025 mol/l EDTA and 0.4 mol/l sodium as shown in Figure 5-11. The treatment composition injected is similar to that given in Table 5-3.

Theoretically, the rate of removal is governed by the amount of EDTA injected and the drawdown level from the adjacent wells. The level of drawdown was controlled by setting the well–flowing pressure (Pwf) at 2500 psi for all offset producers and maintaining a high pumping rate at 4000 bpd. On the other hand, the extent of remediation is dictated by the heterogeneous permeability profile surrounding the injector. One of the observations supporting this argument can be seen in Figure 5-12 where EDTA flooding front has reached producers 1 and 2 faster than 3 and 4 (at the end of the simulation), despite that injector 1 was placed directly in the middle between the two sets of wells. The highly permeable area, separating injector 1 from both producers 1 and 2, had affected the flooding direction. The calcium and carbonate profiles at T=2500 days affirm this observation (Figures 5-12 and 5-13). The same zone is now free of calcium; however, the continuous displacement of carbonate toward producers 1 and 2 raised the concentration to 0.03 mol/l. The same observation applies to the extent of scaling as shown in Figure. 5-10. In Figure. 5-14, it can be seen that the potential risk of calcite formation has been mitigated by introducing the EDTA chemical. Figure 5-15a shows less than 45% of cumulative oil recovery (about 680,000 bbls) in the 2500 day period. The oil recovery curve is expected to plateau quickly if the run is to be extended beyond 2500 days, since the average normal oil recoveries in oil fields range between 20% and 50% of the original oil in place (OOIP). The inputs used in this case have contributed to this up normal oil recovery. As mentioned in Section 4.5, using relatively high rock and fluid compressibility values beside a small residual oil saturation will result in nearly perfect flooding and will maximize the recovery simulated by the UTCHEM. Figure 5-15b and 5-15c monitor the production rate and average pressure in the field during the injection.

Bearing in mind that the stoichiometric ratio between EDTA and Ca must be 1:1 to achieve a complete chelation, the calcium that initially exists in the reservoir is partially soluble because of the limited EDTA supply (about 0.2 mol/l Ca vs. 0.025 mol/l EDTA). Therefore, the remaining calcium is displaced forward with the carbonate explains the high solid concentrations at the front's edges (Figure. 5-11). A higher EDTA dose is also simulated to further study factors affecting the extent of the removal action.

5.4 Simulating Calcite Precipitation/Remediation (with a Higher EDTA Dose) Using a Two 5-Spot Well Spacing and a Real Geological Model

By using 0.2 mol/l of EDTA, we establish a 1:1 ratio with calcium in order to move the injection front faster. Figures 5-16 and 5-17 show results of this trial with the calcite, surrounding producers 1 and 2, is partially cleaned. Ideally, a high dose injection should yield higher oil recovery, especially with the positive impact on producers 1 and 2. However, the oil recovery numbers obtained for Run 5.3 is similar to those for Run 5.2 (Figure. 5-15a). The same applies to rates and pressure data (Figure 5-15b and 5-15c). The effect of remediation on permeability and porosity are to be explored further in section 5.4 using a modified version of UTCHEM.

One advantage for UTCHEM, that exceeds the accurate prediction of scaling, is the ability to predict the possible outcomes of a remediation operation even before the development of the field. In this case, for example, the injector could have been placed such that it delays the scaling development and optimizes any future remediation process. Similarly, the pore volume concentration of EDTA can be optimized to achieve the best possible results. Obviously, pumping high doses of EDTA would be costly.

5.5 Simulating the Effect of Precipitation/Remediation and Inhibition on Permeability and Porosity Using a Quarter 5-Spot Model

The continuous precipitation action that takes place in the formation over time will definitely lead to permeability reduction and pore plugging. Therefore, the UTCHEM simulator was modified to be able to update permeability and porosity values in each time step. A basic (quarter 5-spot) setup was used to simulate calcite formation and removal (See Tables 5-7 and 5-8 for input data). The water composition used in this scenario is identical to the composition given in Table 5-9. The field average horizontal permeability and porosity were set at 100 md and 8%, respectively. The average water saturation dropped to 0.40 compared to 0.48 used in Run 5.1.

The simulation consists of three injection stages including a normal injection of carbonate-rich water (CO_3 about 8.0 mol/l) for 400 days at 10,000 ft^3/d (2,450 bpd) followed by a shut-in period, in which the producer is used to pump EDTA treatment (about 2.5 mol/l PV) for 20 days. The simulation is concluded by resuming the normal injection period at the same rate. Figure 5-18 tracks the impact of precipitation in the near-wellbore area on the permeability and porosity maps just prior to the introduction of EDTA. It can be seen clearly that permeability has dropped to as low as 20 md. The drop in porosity was significant as it dropped to 3%. The big reduction in permeability and porosity values is justified providing that high concentrations of precipitated calcite exist in the near wellbore zone (up to 17 mol/l PV at T=400 days).

In theory, the near-wellbore zone experiences the highest level of precipitation and highest drop in permeability and porosity compared to other parts in the field, especially after seawater injection breaks through. Therefore, T=400 days was selected as the appropriate time to execute the remediation operation through the producer to help

remove the scaling around the wellbore. In order to increase the effectiveness of the treatment, chemicals were injected at 10,000 ft^3/d for 20 days. This rate is sufficient to ensure EDTA covers the critical near-wellbore zone and mitigate the risk of re-precipitation. This rate is both operationally and economically feasible. After applying the EDTA, the permeability values now back to the initial 100 md as in Figure 5-19. Also, it is worth mentioning that UTCHEM considers the formed Ca-EDTA complex as a precipitated immobile solid that cannot migrate. However, this byproduct complex has a negligible effect on the permeability and porosity. In reality, a post-flush stage or flowback period is necessary before putting the well back on the stream in order to remove any residues after the remediation.

Figure 5-19 also shows the theoretically expected behavior from permeability and porosity after the remediation. Permeability in the treated zone restores its new value (100 md) and maintains it till the end of the simulation mainly due to the shortage in calcium required for precipitation and since majority of calcium was chelated by EDTA during the remediation stage. Calcite concentration and permeability at the end of the simulation are presented in Figure 5-20.

To help evaluating the post performance of the well plus the impact of the remediation, the same run was performed again, but without the inclusion of EDTA. Cumulative oil recovery and production rate have to be looked at individually and compared to those when EDTA was not used. In terms of cumulative oil recovery, nearly a 5% difference was obtained from the comparison shown in Figure 5-21. Both curves have identical behaviors prior to applying the treatment. After the treatment, behavior starts changing in response to the new improved permeability and porosity values. Time vs. rate plots in Figure 5-22b show a nearly flat production rate after the remediation

which, may indicate that remediation managed to stop the decline in rate. When looking at Figure 5-22a, we see a nearly 50 bbls gain in oil rate when compared to the pre-treatment rate. This gain in oil rate could be attributed to the remediation slug pumped at T=400 days, and to a lesser degree, to the minimum effect of the 20-day pressure build-up period on charging the reservoir. With regard to the rates, the simulation ends with production oil rate of 50 bpd compared to 20 bpd when not including the EDTA (see Figures 5-22a and 5-24a). The relatively high average reservoir pressure at the end of the simulation (in Figure 5-25) compared to that in (Figure 5-23) may reflect the difference in the un-recovered oil volumes between the two cases or it may indicate the effect of inflicted damage caused by the calcite. For such a synthetic case with a closed-boundary reservoir plus the continuous injection and small porosity values, it is easy to reach to injection pressures as high as 12,000 psi. However, once the injected water breaks through, the pressure starts declining (Figure 5-25).

The fact that this reservoir model is small finite-acting, and has a limited oil supply, makes it unnecessary to extend the simulation time beyond 1000 days in attempt to observe any improvement in the production rate behavior for a longer time. This study could also be improved by integrating a wellbore model into the current UTCHEM version to account for scaling damage inside the well and observe the rate from the wellbore perspective. Thus, further studies are required to examine the post-remediation responses for rate and pressure to better estimate the gain in oil recovery and production rates, which is beyond the scope of this thesis.

Table 5-1: List of UTCHEM input used in Run 5.1

No. of Wells	2 (1 injector + 1 producer)
Reservoir Dimensions	1000' x1000' x50'
Grid Block Size	50'
No. of Grid Block	20 x 20 x 1
Reservoir Depth	7200'
Max. Simulation Time	4000 days
Initial Reservoir Pressure	3120 psia
Reservoir Permeability	Kx=1000 md, Ky=1000 md, Kz=250 md
Reservoir Porosity	13%
Initial Water Saturaion	48%
Rock Compressibility	0.00002757 1/psi
Reference (Stand) Pressure	3888 psia
Water Viscosity	0.65135 cp
Oil Viscosity	6.3 cp
Water Compressibility	4.7 x10-7 1/Psi
Oil Compressibility	0.00005 1/ Psi
Injection Rate	5165 ft3/d
Well flowing Pressure	3000 psi

Table 5-2: Relative permeability data used in Run 5.1

	Water	**Oil**
Residual Saturation	0.35	0.25
End Point	0.51	1
Exponent	3.5	2.5

Table 5-3: Chemical composition for formation and injection waters used in Run 5.1

Initial water composition	**C (mol/l)**
Cl	0.4
Na	0.2
Ca	0.2
CO_3	0.1
EDTA	0.0
Injected water	**C (mol/l)**
Cl	0.00
Ca	0.0
Na	0.4
CO_3	0.0
EDTA	0.025

Table 5-4: Chemical composition for formation and injection waters used in Runs 5.2 and 5.3

No. of Wells	8 (2 injectors + 6 producers)
Reservoir Dimensions	3360'x22,878'x variable
Grid Block Size	210'x263'x variable
No. of Grid Block	16 x 106 x 20
Reservoir Depth	7200'
Max. Simulation Time	2500 days
Initial Reservoir pressure	variable
Reservoir Permeability	variable
Reservoir Porosity	variable
Initial Water Saturaion	variable
Rock Compressibility	0.000004 1/psi
Reference (Stand) Pressure	3888 psia
Water Viscosity	0.65135 cp
Oil Viscosity	6.3 cp
Water Compressibility	4.7 x10-7 1/Psi
Oil Compressibility	0.00005 1/ Psi
Injection Rate	22440 ft3/d for both injectors
Well Flowing Pressure	2500 psi
Brine Salinity (C50)	3.217 mol/l PV
Divalent Cation Conc. (c60)	0.698 mol/l PV

Table 5-5: Relative permeability data used in Runs 5.2 and 5.3

	Water	**Oil**
Residual Saturation	0.35	0.25
End Point	0.51	1
Exponent	3.5	2.5

Table 5-6: Chemical composition for formation and injection waters used in Runs 5.2 and 5.3 (for the pre-treatment scenario)

Initial water composition	**C (mol/l)**
Cl	0.4
Na	0.2
Ca	0.2
CO_3	0.1
EDTA	0.0
Injected water	**C (mol/l)**
Cl	0.4
Ca	0.01
Na	0.733
CO_3	0.05
EDTA	0.0

Table 5-7: Chemical composition for formation and injection waters used in Run 5.4

No. of Wells	2 (1 injector + 1 producer)
Reservoir Dimensions	1000' x1000' x50'
Grid Block Size	50'x50'x variable
No. of Grid block	20 x 20 x 3
Reservoir Depth	7200'
Max. Simulation Time	1000 days
Initial Reservoir Pressure	3120 psi
Reservoir Permeability	Kx=100 md, Ky=100 md, Kz=250 md
Reservoir Porosity	8%
Initial Water Saturaion	40%
Rock Compressibility	0.0000275713 1/psi
Reference (Stand) Pressure	3888 psia
Water Viscosity	0.65135 cp
Oil Viscosity	6.3 cp
Water Compressibility	4.7 x10-7 1/Psi
Oil Compressibility	0.00005 1/ Psi
Injection Rate	10,000 ft3/d
Well Flowing Pressure	3000 psi
Brine Salinity (C50)	0.02 mol/l PV
Divalent Cation Conc. (c60)	0.01 mol/l PV

Table 5-8: Relative permeability data used in Run 5.4

	Water	**Oil**
Residual Saturation	0.35	0.25
End Point	0.51	1
Exponent	3.5	2.5

Table 5-9: Chemical composition for formation and injection waters used in Run 5.4

Initial water composition	**C (mol/l)**
Cl	0.2
Na	0.2
Ca	8.0
CO_3	2.0
EDTA	0.0
Injected water	**C (mol/l)**
Cl	0.4
Ca	0.0
Na	0.733
CO_3	8.0
EDTA	0.0

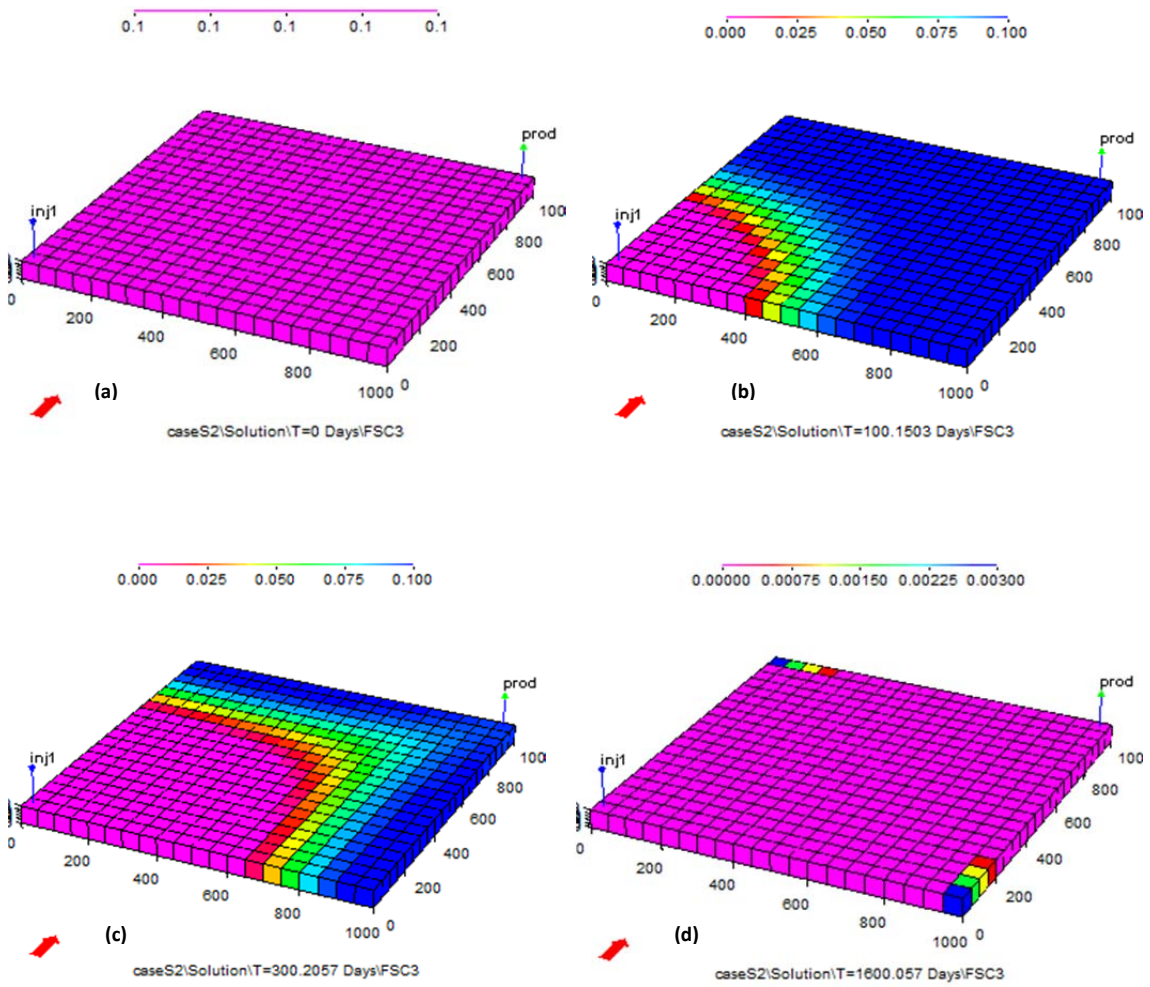

Figure 5-1 Ca^{++} concentration profiles at (a) T=0, (b) T=100, (c) T=300 and (d) T=1600 days. The snapshots describe the process of chelating calcium ions by pumping EDTA. The free calcium initially exists at 0.1 mo/l PV (Run 5.2)

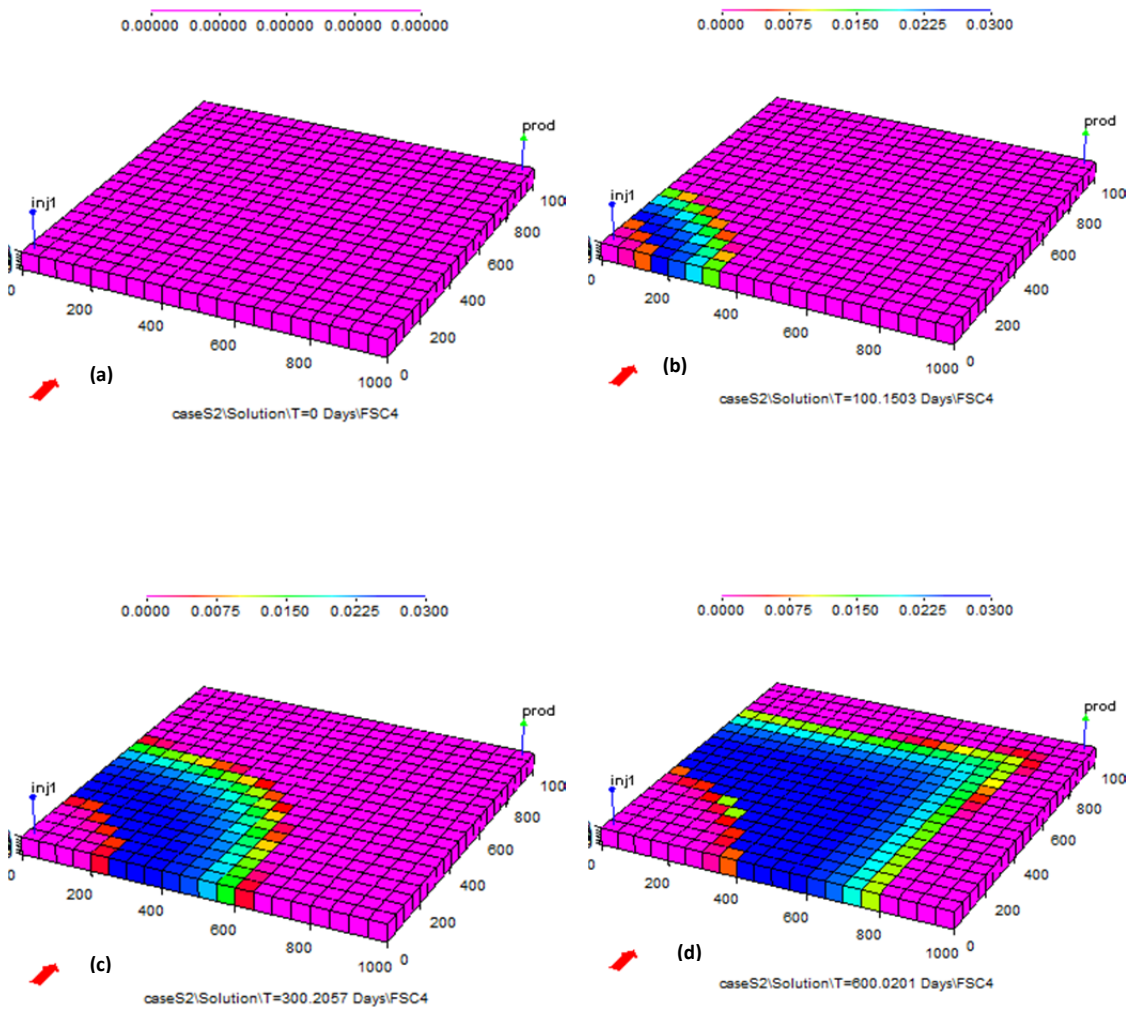

Figure 5-2 CO_3^{--} concentration profiles at (a) T=0, (b) T=100, (c) T=300, (d) T=600 days. All the carbonate in the system exists initially in the form of $CaCO_3$. The chelating process produces high quantities of carbonates with the injection of EDTA by stripping the calcium out from the calcite molecules (Run 5.2)

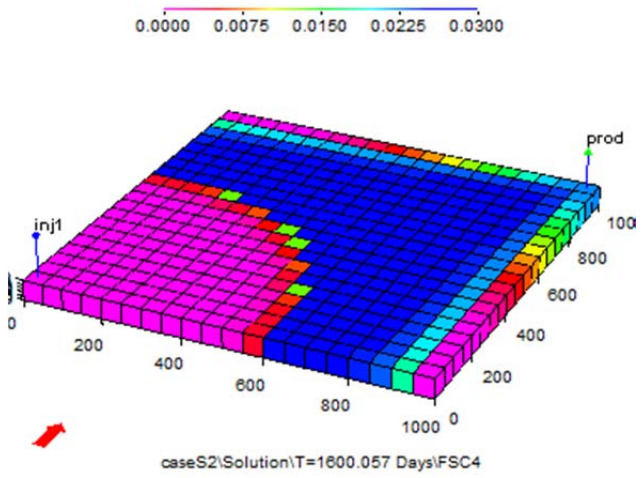

Figure 5-3 CO_3^{--} concentration profile at T=1600 days. Half of the field now is dominated by free carbonate ions as it accumulates over time (Run 5.2)

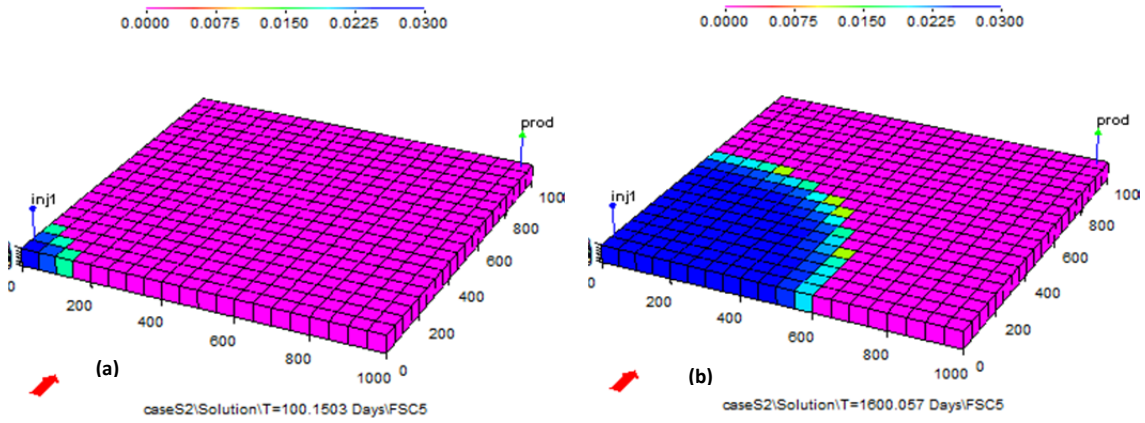

Figure 5-4 EDTA injection progress at (a) T=100 and (b) T=1600 days (Run 5.2)

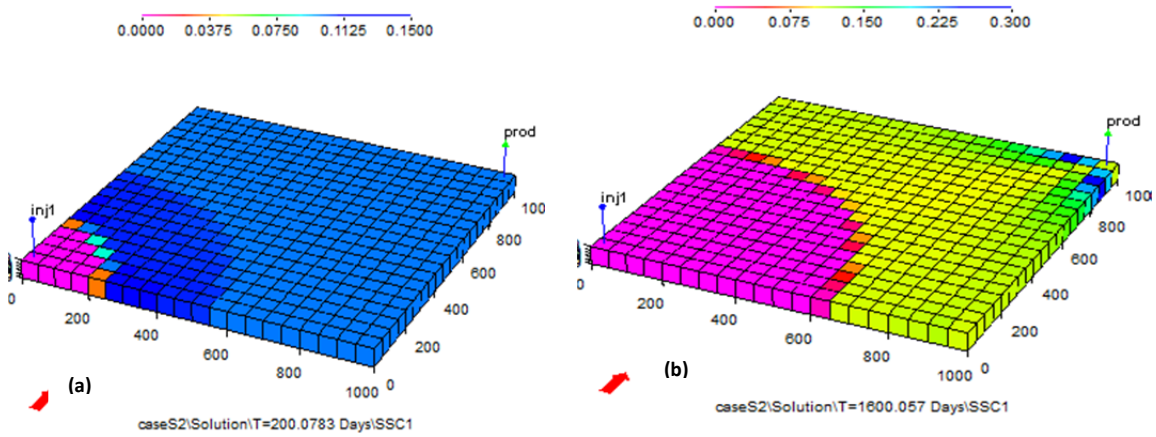

Figure 5-5 Calcite concentration profiles at (a) T=200, (b) T=1600 days. Calcite initially exists at 0.1 mol/l pv. At T= 200 days of the remediation, more carbonate is pushed toward the producer, which means the un-swept parts of the reservoir become more super-saturated with calcite (up to 0.15 mol/l pv). At T=1600 days, calcite is less (about 0.09 mol/l pv) with a larger area now treated by EDTA (Run 5.2)

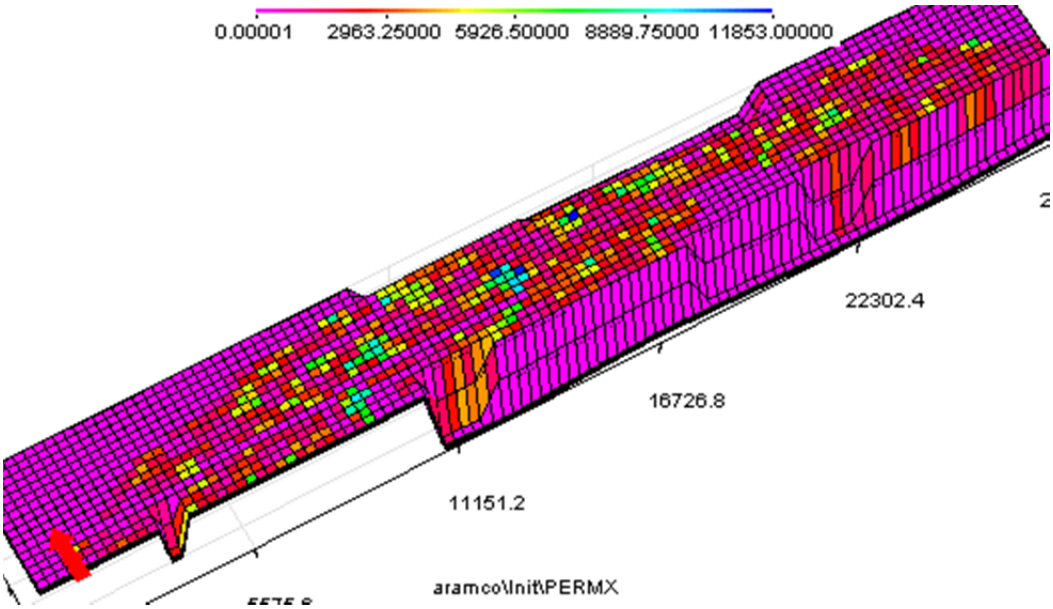

Figure 5-6 Permeability map used in Runs 5.3 and 5.4

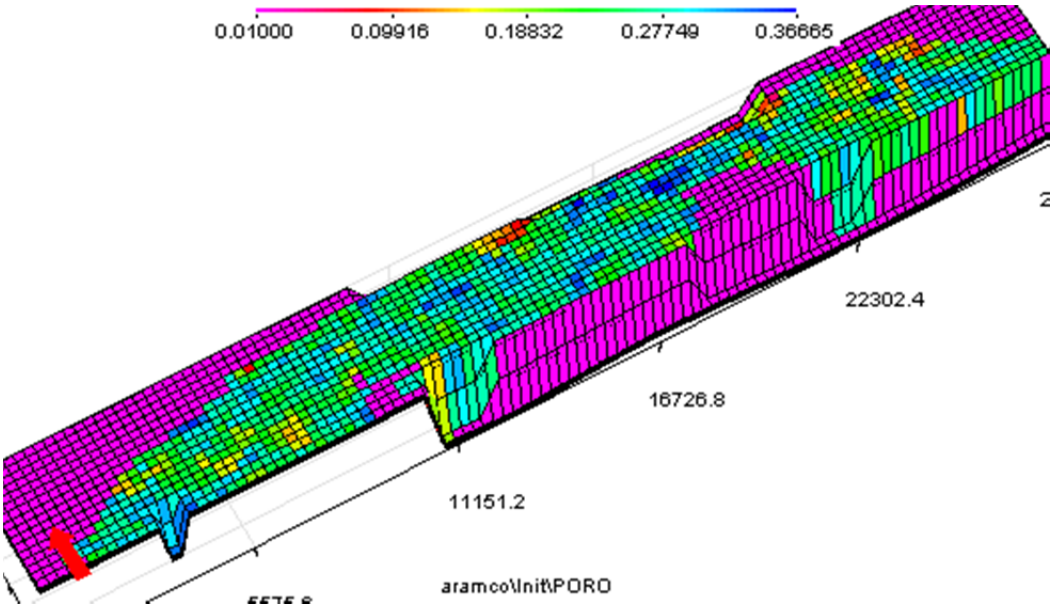

Figure 5-7: Porosity map used in Runs 5.3 and 5.4

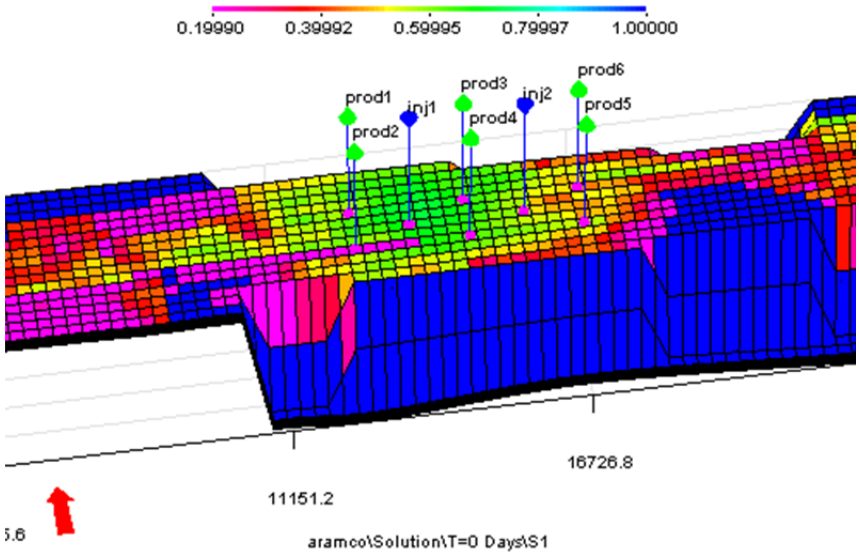

Figure 5-8 Initial water saturation map of the system (used in Runs 5.3 and 5.4)

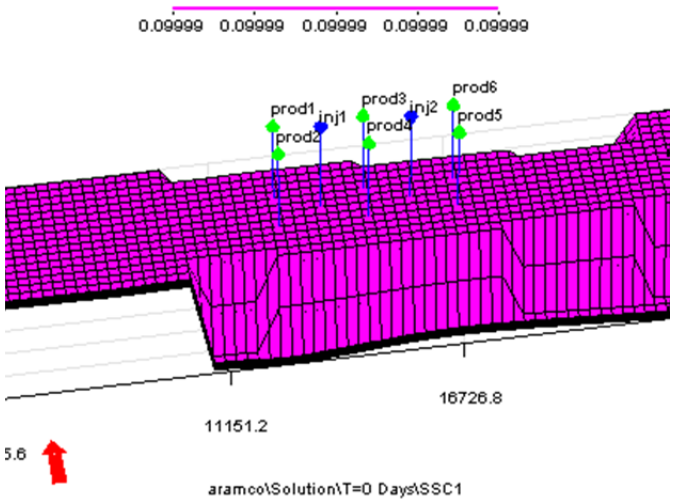

Figure 5-9 Calcite exists initially at 0.1 mol/l pv prior to remediation (Run 5.3)

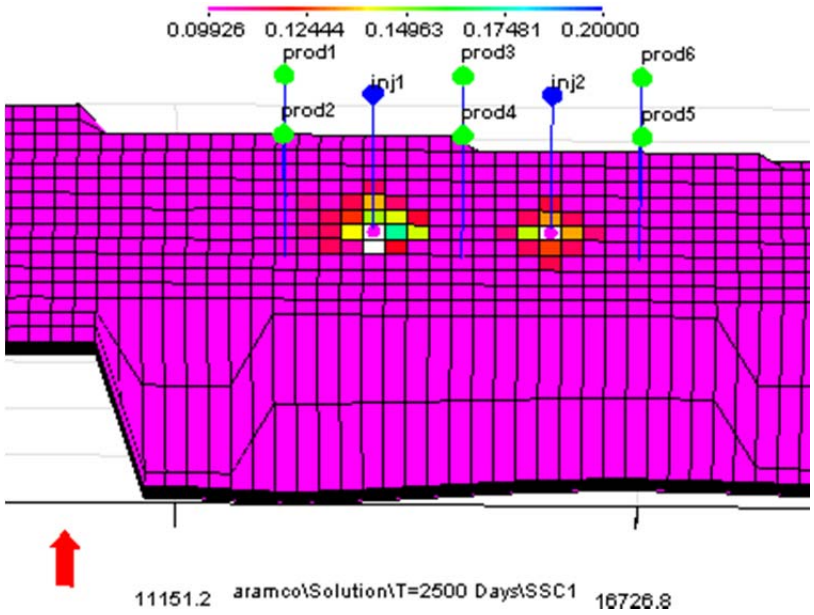

Figure 5-10 Calcite is accumulated at .12 mol/l pv in the absence of EDTA injection (Run 5.3)

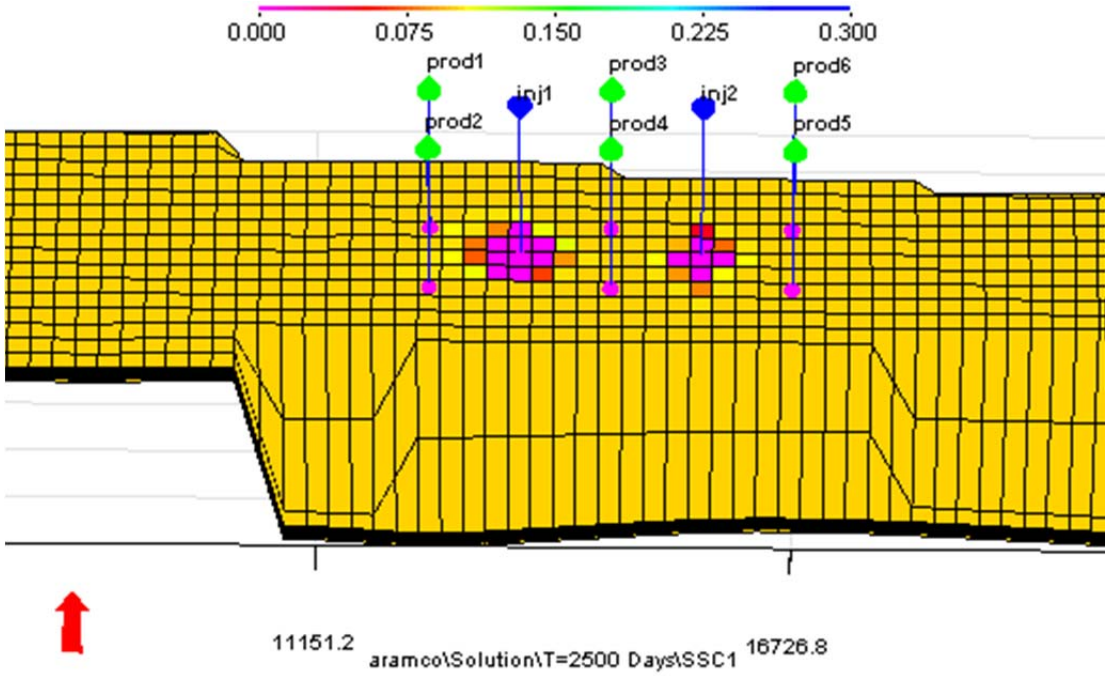

Figure 5-11 Calcite removal as EDTA is injected at 0.025 mol/l pv after 2500 days (Run 5.3)

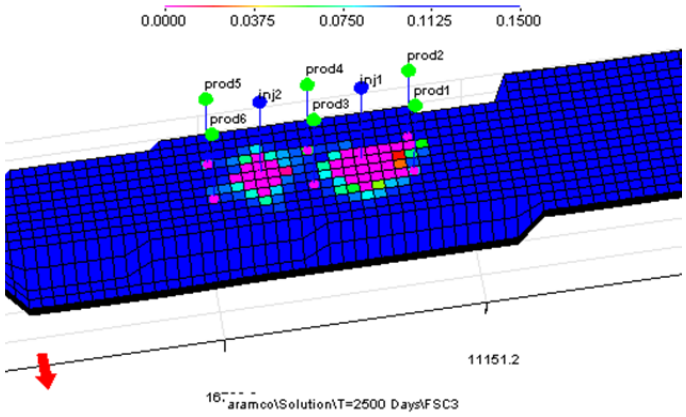

Figure 5-12 Calcium concentration at the end of the remediation (T=2500 days) for the two 5-spot spacing (Run 5.3)

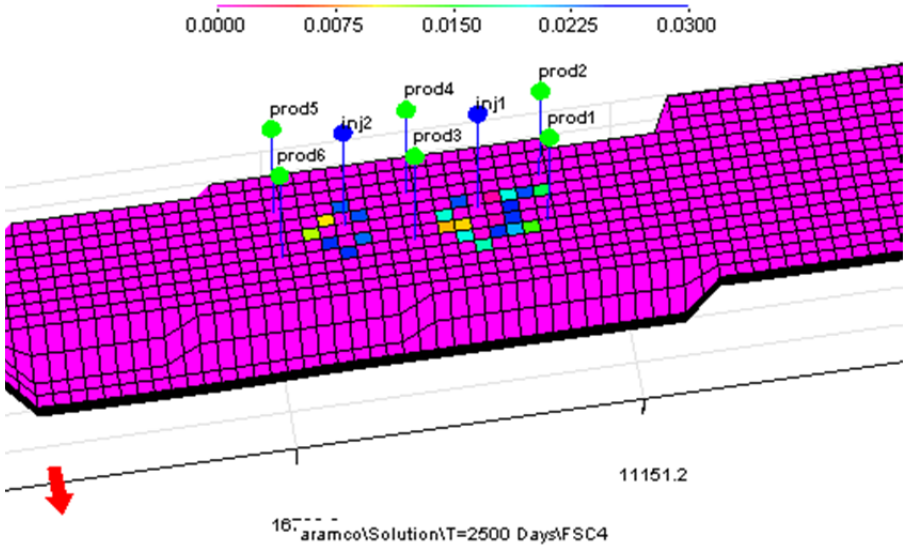

Figure 5-13 Carbonate is accumulated around the treated area at 0.03 mol/l pv after 2500 days following the successful dissolution and chelating of calcite (Run 5.3)

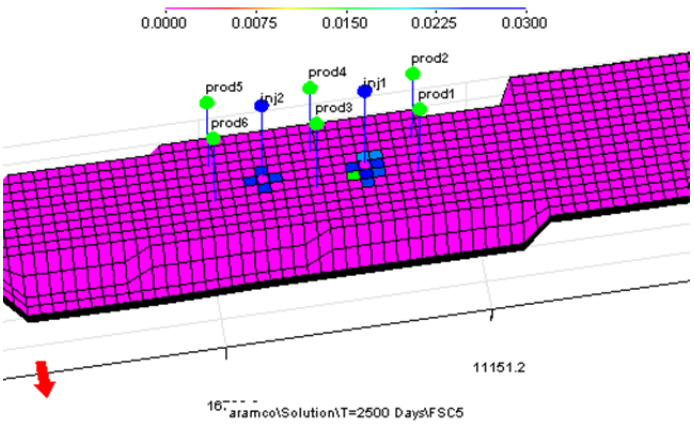

Figure 5-14 EDTA distribution in the two 5-spot reservoir at T=2500 days. EDTA is injected at a concentration of 0.1 mol/l pv with injection rate of 4000 bbls/d (Run 5.3)

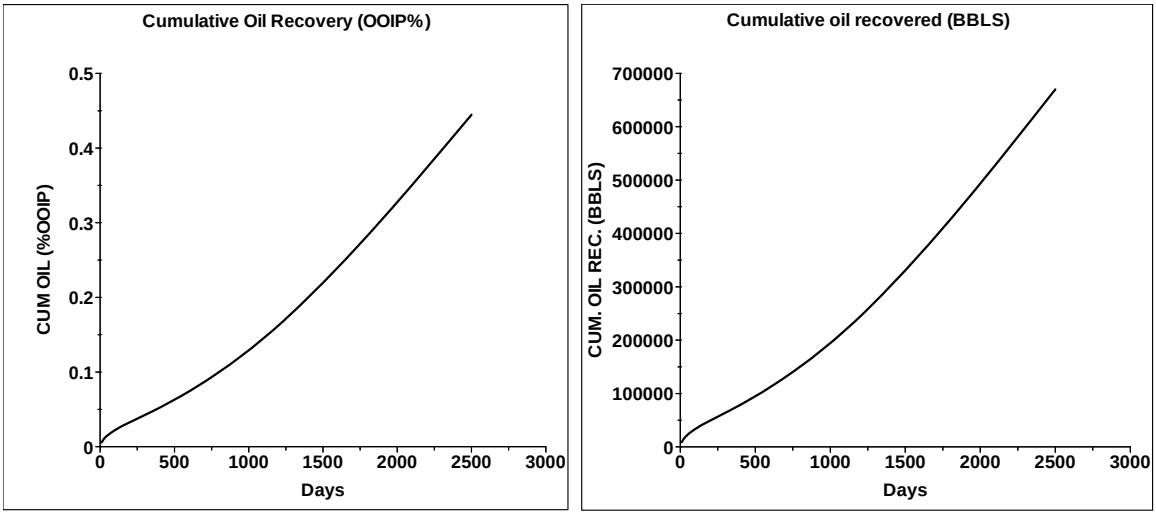

Figure 5-15 (a) Cumulative oil recovered (both as percentage of original oil in place and in bbls) vs. time (Run 5.3 and 5.4)

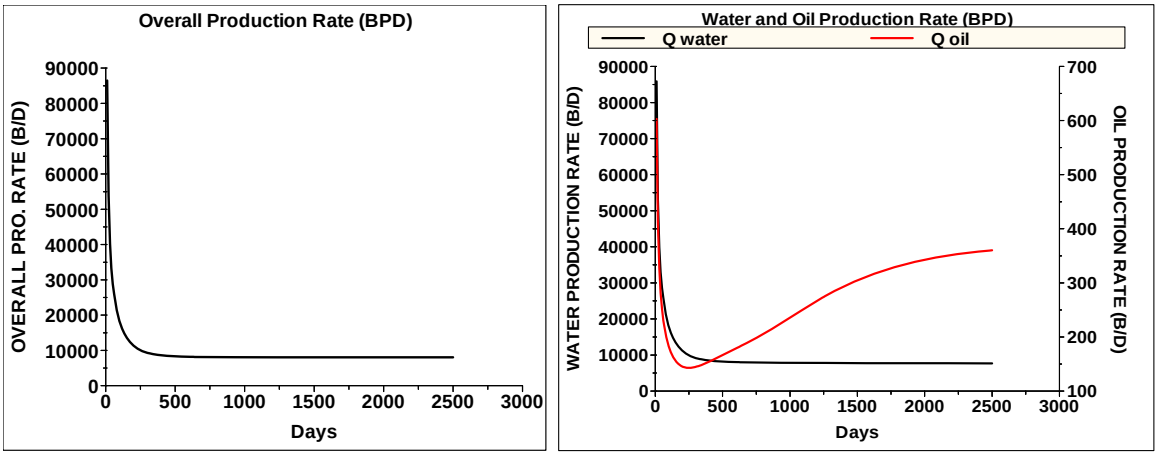

Figure 5-15 (b) Overall production rate (left) along with water and oil production rates (right) vs. time (Runs 5.3 and 5.4)

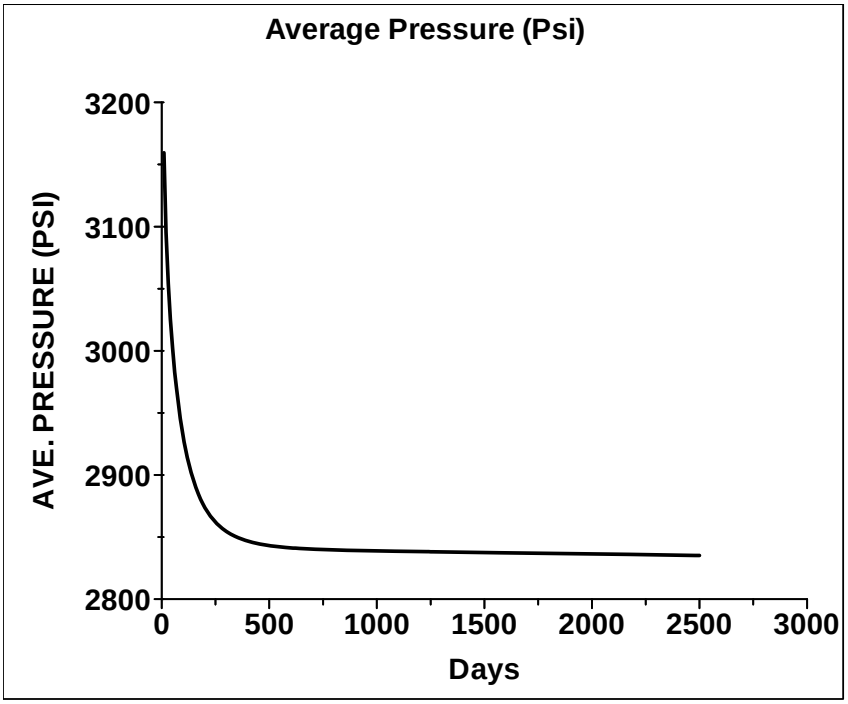

Figure 5-15 (c) Reservoir average pressure in (Psi) (Runs 5.3 and 5.4)

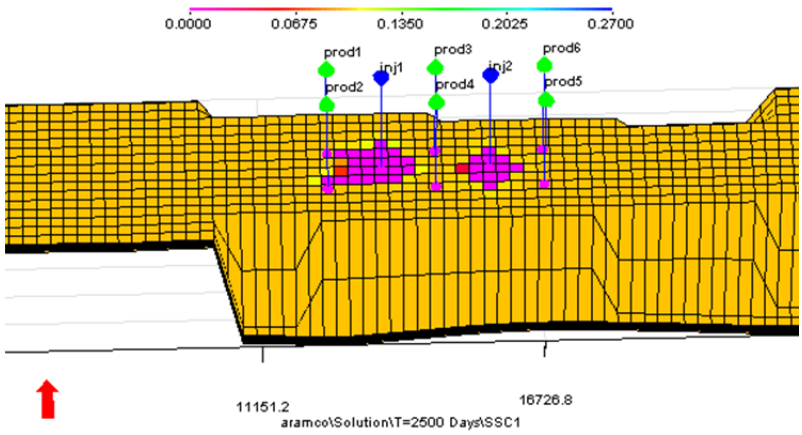

Figure 5-16 Calcite removal as EDTA is injected at 0.2 mol/l pv after 2500 days (Run 5.4)

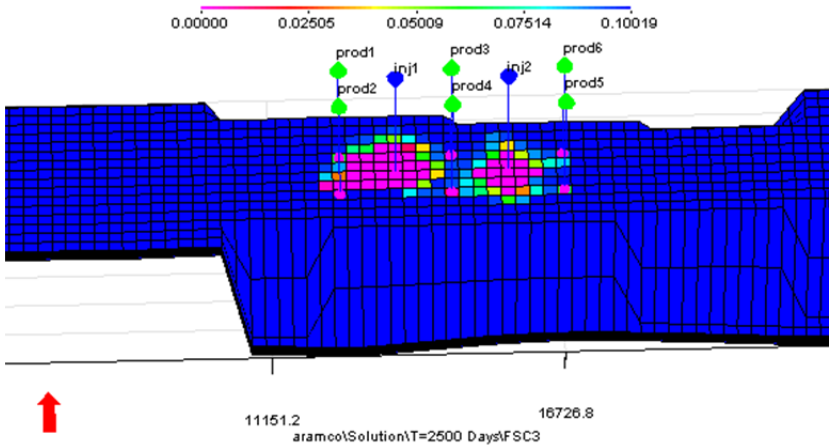

Figure 5-17 Calcium concentration at the end of the remediation (T=2500 days) as EDTA is injected at 0.2 mol/l pv (Run 5.4)

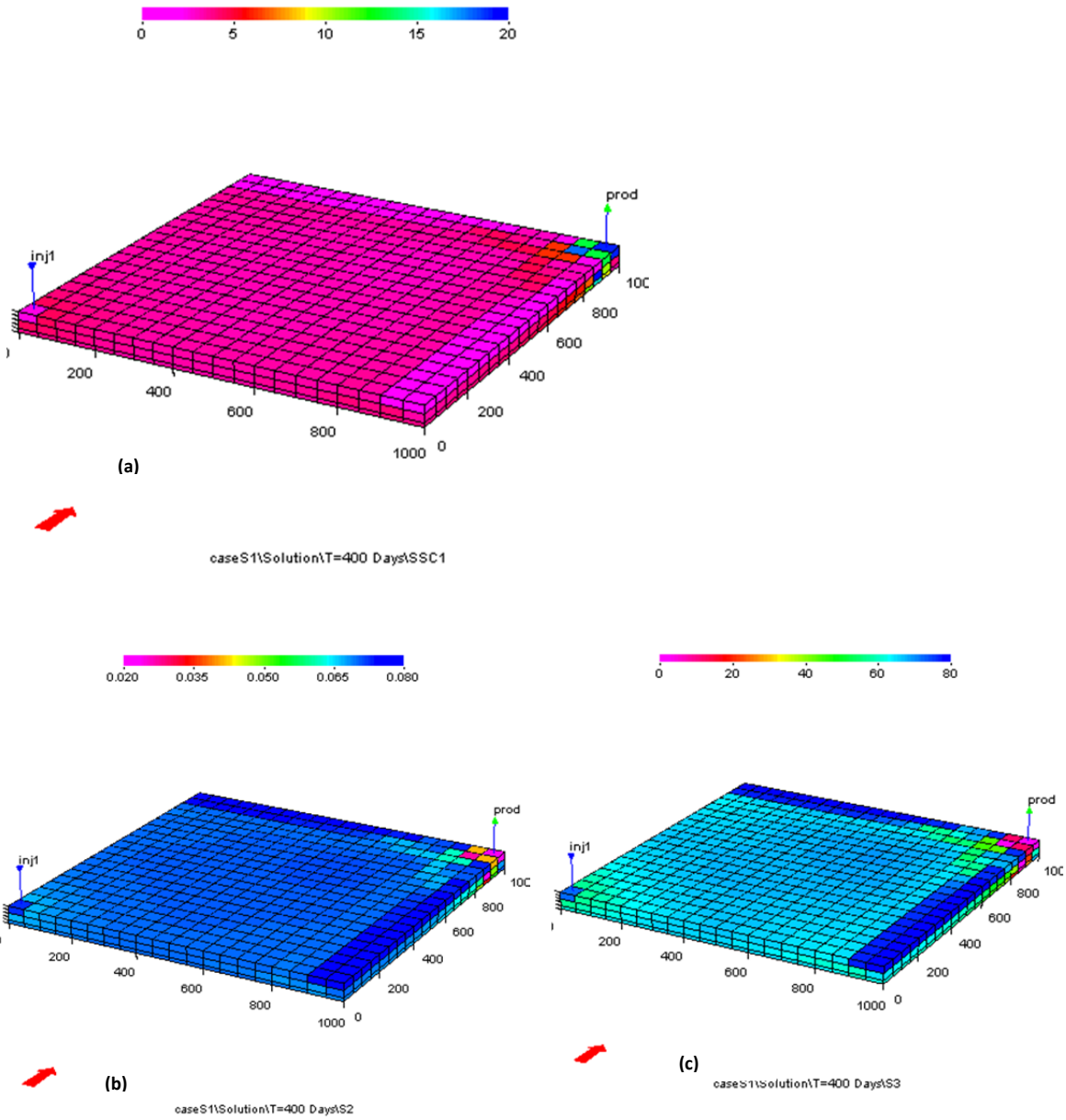

Figure 5-18 (a) shows calcite concentration (in mol/l PV) at the end of the first injection period at T=400 days. (b) shows the modified porosity map (as a percentage) and (c) shows the modified permeability map (in md) (Run 5.5)

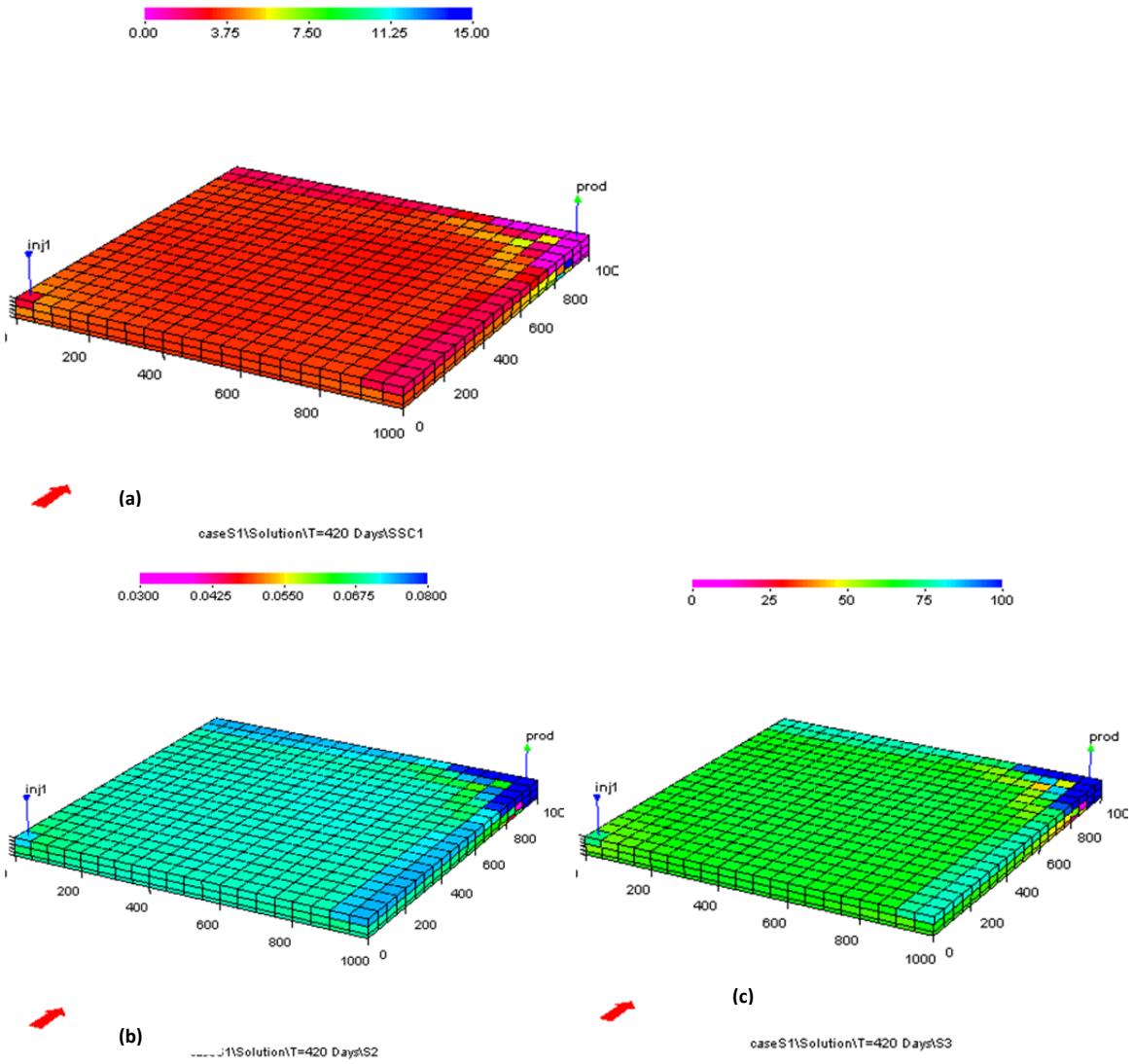

Figure 5-19 (a) calcite concentration (in mol/l PV) at T=420 days. The producer was used to inject EDTA at concentration of 2.5 mol/l at 10,000 ft^3/d rate. (b) Post-treatment porosity (as a percentage) and (c) post-treatment permeability (in md) are shown as well (Run 5.5).

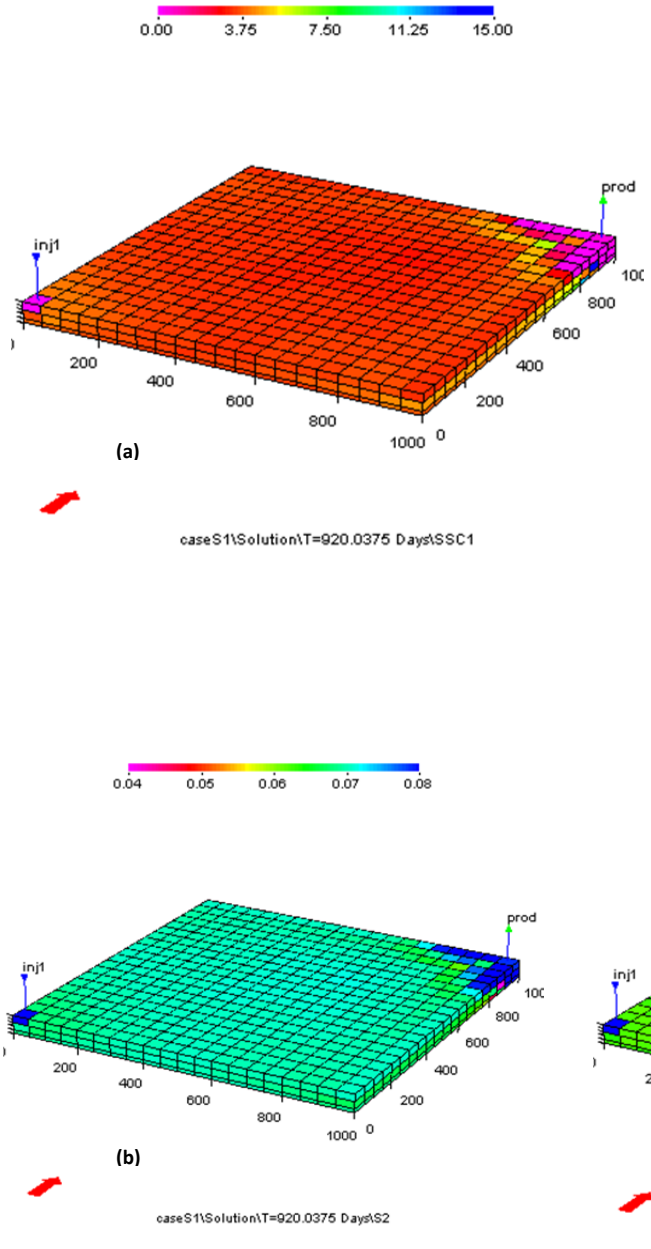

Figure 5-20 (a) calcite concentration (in mol/l PV) at T=920 days at the end of the simulation. (b) porosity map (as a percentage) at the end of the simulation and (c) permeability map (in md) at the end of the simulation (Run 5.5)

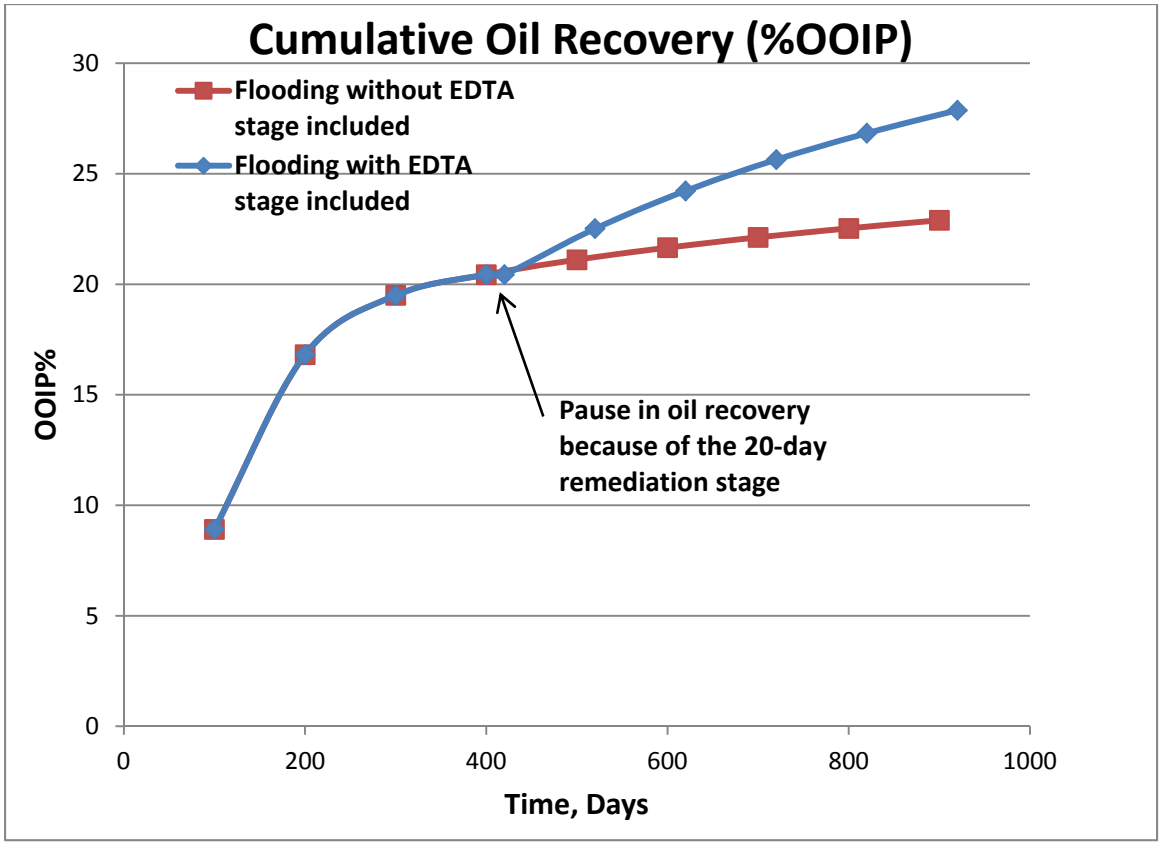

Figure 5-21 Comparison between two flooding cases one with EDTA remediation in terms of cumulative oil recovery as percentage of original oil in place. After injecting EDTA, the normal seawater injection was resumed at 10,000 ft^3/d (Run 5.5)

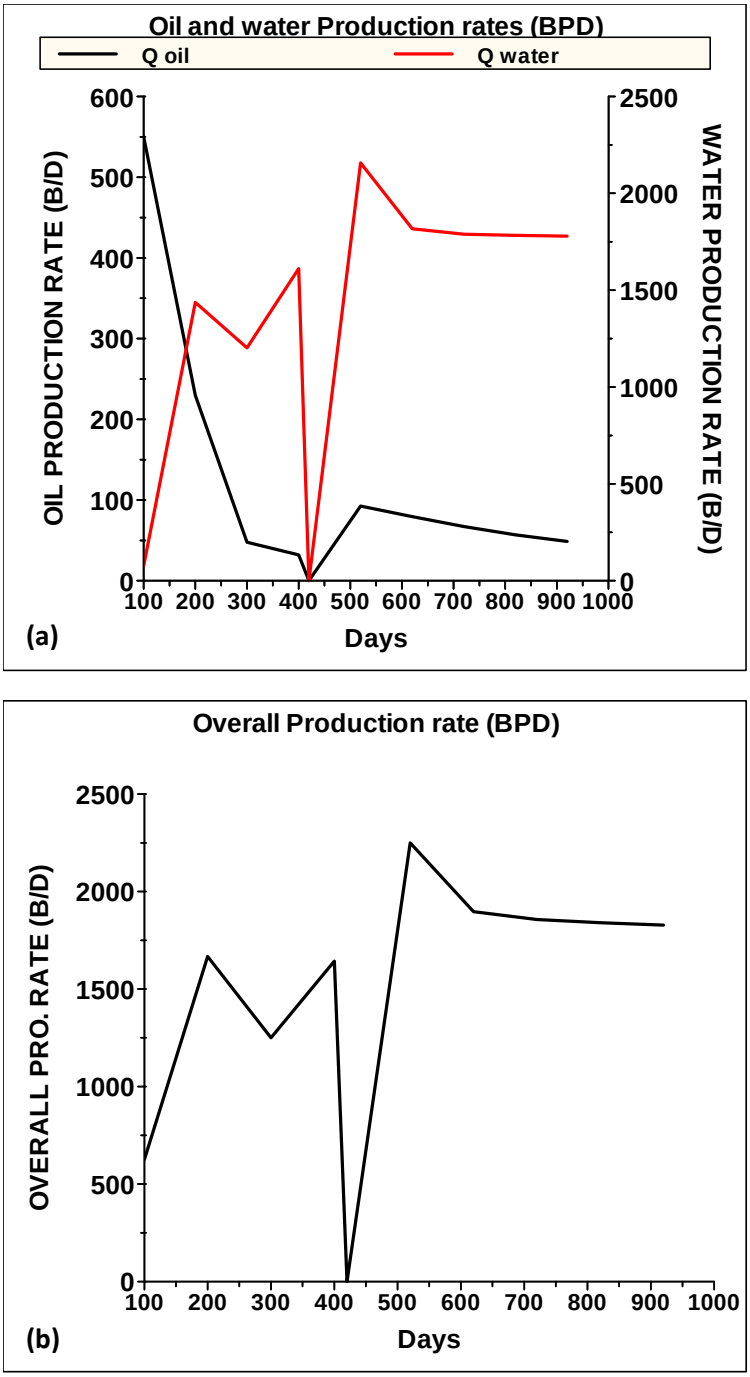

Figure 5-22 (a) Water and oil production rates separately for 900 days. (b) Overall production rate profile for 900 days. The sudden drop in rate represents the shut-in period (remediation) which lasted for 20 days (Run 5.5)

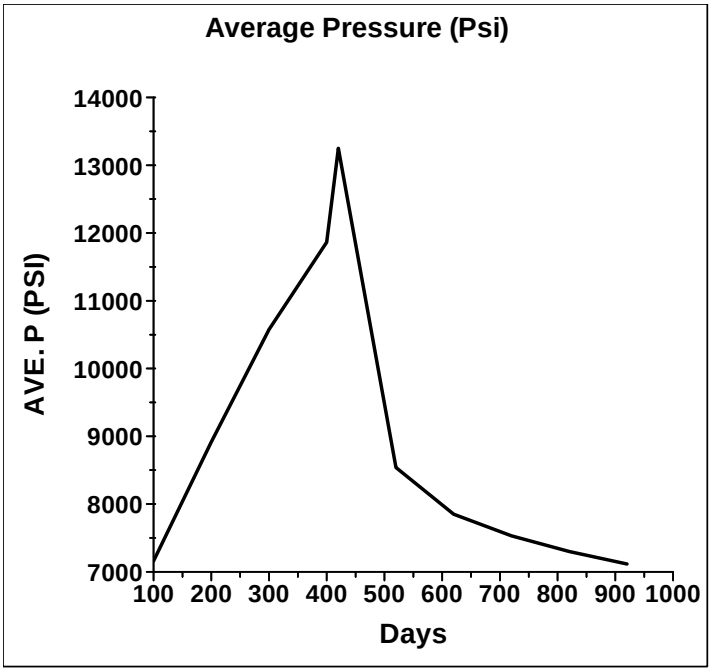

Figure 5-23 Reservoir average pressure for the flooding case with EDTA (psi). The EDTA is pumped at T=400 days for 20 days causing a brief spike in pressure. Pressure at the end of the simulation is 7000 psi (Run 5.5)

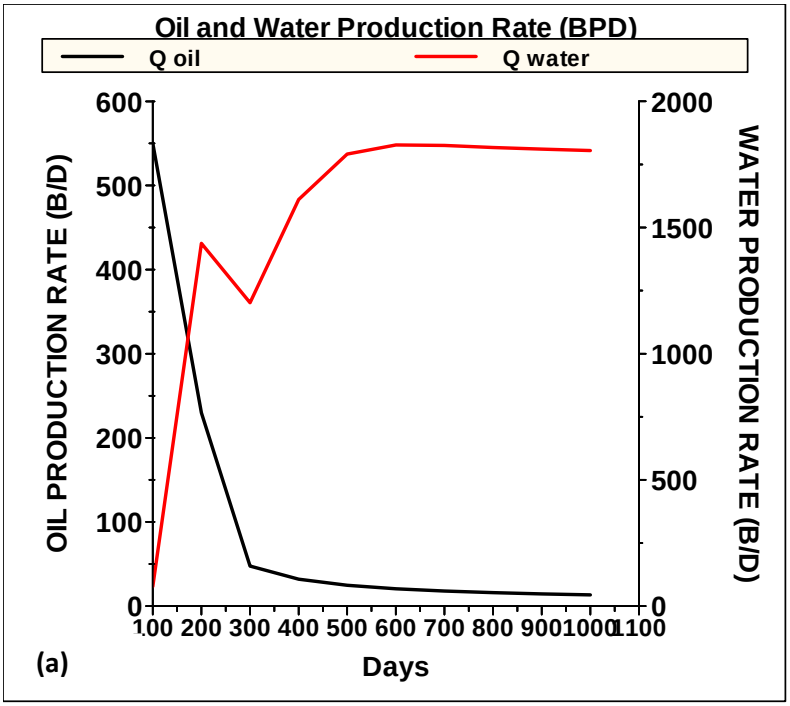

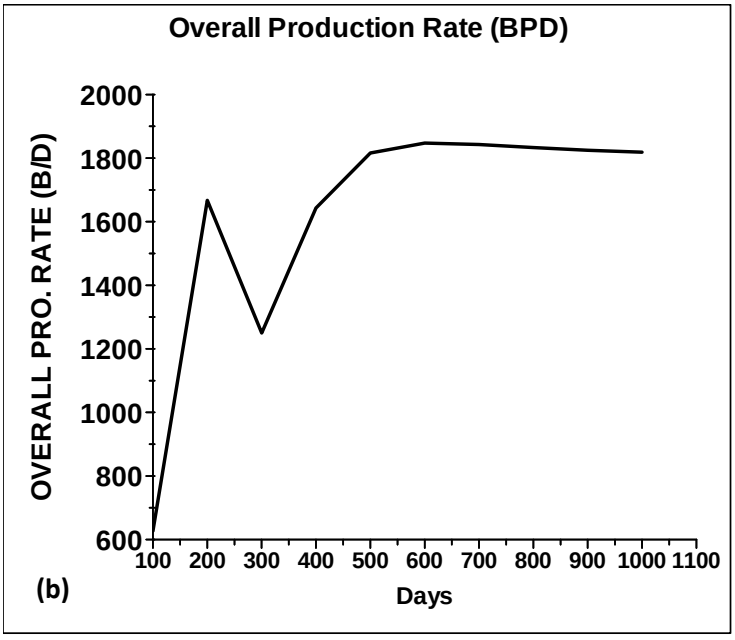

Figure 5-24 (a) water and oil production rate profiles for 1000 days without EDTA treatment. (b) Overall production rate profile for 1000 days without EDTA treatment (Run 5.5)

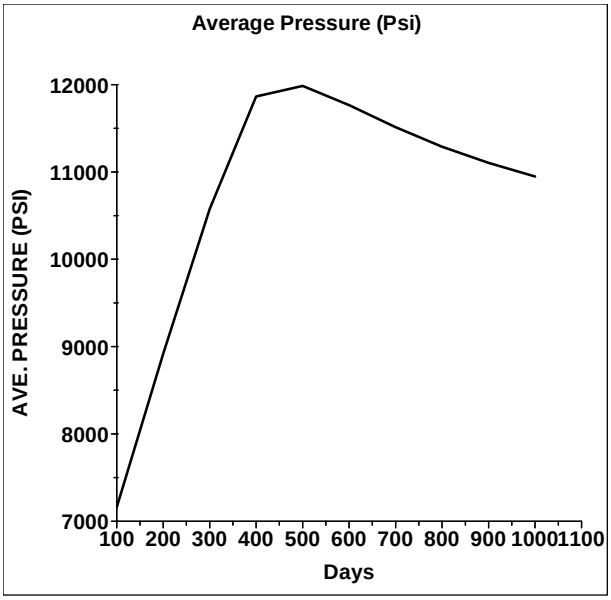

Figure 5-25 Reservoir average pressure for the flooding case without EDTA (psi) (Run 5.5)

Chapter 6 Summary, Conclusions, and Recommendations

6.1 Summary and Conclusions

In this study, we reviewed the inorganic scales commonly found in the reservoir such as carbonates, sulfates, and iron oxides. We discussed the formation and inhibition mechanisms along with the factors affecting them. Then, we highlighted the effect of pH, temperature and cations/anions impurities on the effectiveness of both nucleation and crystal growth retarders. A listing of the common inhibitors' placement methods concluded the literature survey section.

Subsequently, by using the compositional simulator (UTCHEM), we were able to carry out several case studies with the objective to monitor the precipitation as well as the distribution of solids in an oil field. We were able to simulate more than one type of scales simultaneously using calcite, barite, and iron sulfide as examples. The model is only able to simulate scales resulting from mixing incompatible brines. Then, we investigated the effect of heterogeneity on the distribution and quantity of the barite precipitates using a 5-spot reservoir model with four injectors and a producer. An entire chapter was dedicated to simulating the remediation effect on permeability and porosity. The chelatant (EDTA) reactions with calcite was used solely in this chapter to explain the concept of chelating and to carry out the rest of the case studies. The findings of the study are summarized as follows:

- Low amounts of precipitates develop at the mixing zone between the injected water and the formation water.
- The injection front shape is controlled by the level of drawdown by the producer well as well as by the pressure effect from the boundaries.

- Most of the simulated deposition is taking place in the near-wellbore region. The remaining cation supply in the system (after the initial breakthrough of injection water) determines the quantity forming in that area.
- In terms of performance, a small difference is detected when comparing the homogeneous and heterogeneous reservoir. In this case, where both reservoirs share the same average porosity and permeability, a small amount of oil is recovered in the homogenous case compared to the heterogeneous case.
- The impact of the heterogeneity on the distribution of the solids is much pronounced than the impact on the oil recovery. The solid volume in the near-wellbore region is higher in the homogenous reservoir than in the heterogeneous one.
- High oil recoveries are obtained when using the synthetic 5-spot, finite-boundary reservoir model. Values within the normal range can be achieved by decreasing the rock and fluid compressibility values or increasing the residual oil saturation.
- The speed and extent of the remediation is controlled by the amount injected, injector placement, and heterogeneity of the reservoir.
- The gain in oil recovery after the remediation placement was significant, which can be attributed to the restoration of the original permeability and porosity values (removing the skin damage).

This study has shown that the simulator used in this study can be an important tool to accurately predict how long it will take for the mineral scales to impact the production from offset wells. Additionally, the simulator can predict the effectiveness of remediation/inhibition prior to the pump out. The flow model can also estimate when it is appropriate to re-inject these stimulating chemicals as well as to optimize the volumes

needed. This thesis is comprehensive in terms of predicting the precipitation and dissolution of inorganic scales.

6.2 Recommendations

The following recommendations are made to further enhance UTCHEM capabilities:

- **The effect of fine migration.** The simulator assumes in-situ deposition once the fluid is saturated with scaling ions. In addition, the model does not allow for scaling particles' movement in the pores. The inclusion of these features is important as it may affect the scaling distribution inside the reservoir.
- **The effect of permeability reduction.** Each grid block is assigned a permeability value that should change constantly over time, because of the in-situ deposition as well as the migrating fines. Although this effect was recently incorporated in UTCHEM, further testing is required.
- **The effect of including gases in the model.** The model does not support systems with extremely compressible fluids such as gases, which makes the model limited to oil fields.
- **The effect of changing the pH level on the precipitation of carbonate scales.** Generally, carbonate scale precipitation is very sensitive to fluctuations in pH levels. Generally, the dissolution/evolution of CO_2 gases in/from particular brine affects the pH level significantly. The model only deals with scales, formed by mixing incompatible waters, and does not consider the role of CO_2 and pH in forming carbonates. The simulator should be extended to include such effects.
- **The effect of changing temperature.** Some sulfate scales are very sensitive to temperature fluctuations as their solubility and formation rate change as a function of temperature. As a consequence, solubility products should be treated as variables that change as a function of temperature, rather than fixed constants.

The model should also be able to determine whether or not the reactions are in a state of equilibrium, instead of assuming they always attain equilibrium. The simulator's capabilities could be expanded to handle additional grid blocks, and thus, simulate large-scale reservoirs. The results generated by the geochemical model should be compared to those obtained from the other existing geochemical software. Also, further studies are necessary to compare the results generated by UTCHEM with the measured data from the oil fields.

References

Bhuyan, D. 1989. “Development of an Alkaline/Surfactant/ Polymer Compositional Reservoir Simulator,” Ph.D. dissertation, The University of Texas at Austin.

Bourne, H. M. et. al. 1995. “A Novel Scale Inhibitor Delivery System for Horizontal and Problem Wells,” Presented at the IBC Scale Conference, Aberdeen.

Claassen, J. 1989. “Scale in Khuff Gas/Condensate Wells,” Champions Chemicals, Inc.

Crabtree, M. et al. 1999. “Fighting Scale-Removal and Prevention,” Schlumberger Oilfield Review. Autumn 30 – 45.

Delshad, M. and Pope, G. 2003. “Effect of Dispersion on Transport and Precipitation of Barium and Sulfate in Oil Reservoirs,” SPE 80253 presented at the International Symposium on Oilfield Scale, Houston, 5 – 8 February.

Ford, W., Walker, M. Halterman, and Parker, D. L. and et al. 1992. "Removing a Typical Iron Sulfide Scale: The Scientific Approach," Paper SPE 24327. SPE Rocky Mountain Regional Meeting, Casper, Wyoming, 18 – 21 May.

Franco, C. et al. 2009. “Analysis of Deposition Mechanism of Mineral Scales Precipitating in the Sandface and Production Strings of Gas-Condensate Wells,” SPE 120410. 2009 SPE Middle East Oil and Gas Show and Conference, Bahrain, 15 – 18 March.

Frenier, W. 2002. “Scale Control Slides. Sugar Land, Texas: Schlumberger Well Services”.

Frenier, W., Ziauddin, M. "Formation, Removal, and Inhibition of Inorganic Scale in the Oilfield Environment," SPE Book. 2008. 59 – 85.

Graham, G. M et al. 1998. “Scale Inhibitor Selection for Continuous and Download Squeeze Application in HP/HT Conditions,” Paper SPE 49197 Presented at the SPE Annual Technical Conference and Exhibition held in New Orleans, Louisiana, 27 – 30 September.

Graham, G. M. and Mackay, E. J. 2004. “A Background to Inorganic Scaling-Mechanism Formation and Control. Short Course,” 2004 SPE Formation Damage Symposium, Lafayette, Louisiana, 17 February.

Holtz, M. H. 2002. "Residual Gas Saturation to Aquifer Influx: A Calculation Method for 3D Computer Reservoir Construction," Paper SPE 75502 Presented at the Gas Technology Symposium Calgary, Alberta, Canada, April 30 – May 2.

Kahrwad, K. S., Sorbie, K. S. and Boak, L.S. 2009. “Coupled Adsorption/ Precipitation of Scale Inhibitors: Experimental Results and Modeling,” SPE Paper 114018 was accepted for presentation at the SPE International Oilfield Scale Conference, Aberdeen, 28 – 29 May 2008.

Kerver J. K, Heilhecker J. K. 1969. “Scale Inhibition by the Squeeze Technique,” The Journal of Canadian Petroleum: January-March, 1969. Presented at the 19th Annual Technical Meeting of The Petroleum Society of CIM, Calgary, May, 1968.

Langmuir, D. 1997. “Aqueous Environmental Geochemistry,” Englewood Cliffs, New Jersey: Prentice Hall.

Meyers, K.O. 1984. “Method for Scale Removal and Scale Inhibition in a Well Penetrating a Subterranean Formation,” U.S. Patent No. 4,485,874.

Miller, M. 1999. “San Andres Formation Inhibitor in Frac Fluid. Sugar Land, Texas: Schlumberger Technology Corporation".

Nancollas, G.H., White, W., Tsai, F., and Maslow, L. 1979. "The Kinetics and Mechanism of Formation of Calcium Sulfate Scale Minerals: The Influence of Inhibitors," *Corrosion* 35 (7): 304 – 308.

Nasr El-Din, H. A., Al-Saiari, H. A. and Al-Hajji, H. H. 2004. “A Single-Stage Acid Treatment to Remove and Mitigate Calcium Carbonate Scale in Sandstone and Carbonate Reservoirs,” Paper SPE 87454 Presented at the International Symposium on Oilfield Scale, Aberdeen, 26 – 27 May.

Przybylinski, J. L. 2001. "Iron Sulfide Scale Deposit Formation and Prevention Under Anaerobic Conditions Typically Found in the Oil Field," Paper SPE 65030 Presented at the SPE International Symposium on Oilfield Chemistry, Houston, 13 – 16 February. DOI:10.2118/35822-MS.

Ramastad, K., Tydal, T., Askvik, K. M., and Fotland, P. 2004. "Predicting Carbonate Scale in Oil Producers From High-Temperature Reservoirs," *SPEJ* 10 (4): 363 – 373: DOI:10.2118/87430-PA.

Shaughnessy, C.M. and Kline, W.E. "EDTA Removes Formation Damage at Prudhoe Bay," *Journal of Petroleum Technology*. October 1983. 1783 - 1791.

Smith, P.S., Clement, Jr. C. C., and Rojas, A. M. 2000. "Combined Scale Removal and Scale Inhibition Treatments," Paper SPE 60222 Presented at the International Symposium on Oilfield Scale, Aberdeen, 26 – 27 January.

Sorbie, K.S. and Laing, N, 2004. "How Scale Inhibitors Work: Mechanism of Selected Barium Sulfate Scale Inhibitors Across a Wild Range of Temperatures," Paper SPE 87470 Presented at the International Symposium on Oilfield Scale, Aberdeen, 26 – 27 May. DOI: 102118/87470-MS.

Talbot J. and Talbot, D. 1997. "Corrosion Science and Technology," Boca Raton, Florida: CRC Press.

Tantayakom et al. 2005a. "Kinetic Study of Scale Inhibitor Precipitation Squeeze Treatment," Crystal Growth Design 5(1): 329 – 335.

Thomson, M. B., Fu, G., Watson, M. A., and Kan, A. T. 2002. "Mechanisms of Mineral Scale Inhibition," Paper SPE 74656 Presented at the International Symposium on Oilfield Scale, Aberdeen, 30 – 31 January. DOI: 10.2118/74656-MS.

Tomson et al. 2006. "Scale Formation and Prevention in the Presence of Hydrate Inhibitors," Paper SPE 80255 Presented at the International Symposium on Oilfield Scale, Houston, 5 – 8 February 2003.